5-2009

# Design, construction, and experimentation of a heat pipe augmented solar wall.

Nicholas E. Chmielewski
*University of Louisville*

# DESIGN, CONSTRUCTION, AND EXPERIMENTATION OF A HEAT PIPE AUGMENTED SOLAR WALL

By

Nicholas E. Chmielewski
B.S., University of Louisville, 2008

A Thesis
Submitted to the Faculty of the
Speed Scientific School of the University of Louisville
In Partial Fulfillment of the Requirements
For the Degree

MASTERS OF ENGINEERING

Department of Mechanical Engineering
University of Louisville
Louisville, KY

May 2009

DESIGN, CONSTRUCTION, AND EXPERIMENTATION

OF A

HEAT PIPE AUGMENTED SOLAR WALL

Submitted by: _____

Nicholas E. Chmielewski

A Thesis Approved on

_____

by the Following Thesis Committee:

_____

Thesis Director, Dr. Michael Keith Sharp

_____

Dr. Ellen Brehob

_____

Dr. Eric Berson

# ACKNOWLEDGEMENTS

I would like to gratefully and sincerely thank my advisor and mentor Dr. Keith Sharp for his advice, assistance, and direction during my studies and work at the University of Louisville. I have learned much through my work with him and greatly appreciate the diligence, commitment, and excellence he upholds for his work, and am grateful for his friendship during my studies. I also wish to thank Dr. Ellen Brehob and Dr. Eric Berson for their comments and suggestions on this thesis.

I would like to thank my parents, John and Chris Chmielewski, for their encouragement and support for me during my challenges at the University of Louisville, as well as the invaluable hands-on help that John volunteered into the late hours during construction of the experimental model. I would also like to thank my sisters Melissa and Rebekah, and Jennifer and Ganesh Nayakwadi for their words of encouragement and understanding during my studies. I would also like to thank Lauren Monk and her family for their presence and involvement in my life. I don’t think she will ever know how much I appreciate her friendship and the beauty of her spirit.

I would also like to thank John Jones for his ever-present assistance during the design and construction of the unit, as well as Cam Metcalf, Don Douglass, John Thompson, and Dr. William Hnat for their involvement and input during my thesis work. I wish to thank the Department of Energy, the University of Louisville, and the Kentucky Rural Energy Consortium for their financial support of the research.

Most importantly I would like to thank my Lord and Savior Jesus Christ for his perfect grace and sacrifice, and for giving me the talent, resources, and strength for my accomplishments. I praise Him for the joy he gives me and the passion he has given me for life and the engineering discipline.

# ABSTRACT

The heat pipe augmented solar wall operates much more efficiently for domestic air heating than alternative passive solar technologies. The thermal diode effect of heat pipes reduces the insulating losses of the unit during nighttime and adverse solar conditions. The exceptionally high conductivity of heat pipes allows for much greater heat gains, and significantly reduces the response time of the unit. The response time is also reduced by a smaller thermal mass of preheating components, which allows the system to passively alternate between insulating and heating conditions much more quickly. By separating the thermal mass of the system from external cold temperatures through the use of insulation and heat pipes, the insulation values of the unit are larger than that of other passive devices.

A heat pipe augmented solar wall was designed with emphasis on thermal efficiency and mass manufacturing techniques. Design drafts, solid models, and assembly and production instructions were created to assist and spur future production of these units. Detailed consumer and producer economic analysis of the unit was also performed. The cost of the approximately four foot wide by seven foot tall domestic heating unit to

be produced, shipped, and installed is projected to be $1580 with current tax credits. Economic analysis yielded a payback period of 14 years and a 30 year return on investment of 130% based on Louisville, KY weather and East Central United States utilities.

A full-scale experimental heat pipe augmented solar wall was constructed as close as possible to the mass production design and was installed in a classroom at the University of Louisville. The unit was tested under actual weather conditions from April 1 – 21, 2009. Weather conditions for testing included clear, cloudy, rainy, and snowing and outside temperatures ranged from 4 – 24 degrees Celsius. Efficiency of the experimental unit ranged from approximately 60 - 75% under various solar radiation and ambient temperature values, all of which by necessity were at a high incidence angle. Efficiencies upwards of 80% are estimated for peak solar insolation conditions and low incidence angle.

TABLE OF CONTENTS

LIST OF TABLES

LIST OF FIGURES

# I. INTRODUCTION

## A. Energy Demand and Global Climate Change

World energy demand was drastically increased by the industrial revolution in the early 19th century. Before this event, gross domestic product was relatively stable for all nations and the energy demand per capita was very small. With the advent of mechanical power in the form of the steam engine replacing a great number of previously manual labor jobs, the world began to experience production and consumption levels never before seen. Though the steam engine was used in factories since the 1700's, increased efficiency greatly enlarged its applications, and land and sea transportation began to be revolutionized by the early 1800's. Coupled with the development of the internal combustion engine in the late nineteenth and early twentieth century, these power generation devices provided for the production and mechanization of a previously unseen number of products. Through the use of technology and these new energy devices, a crew of 10-50 men is now able to produce 25 times the power output of an ancient working force of men and draft animals in excess of 100,000. We find that the power output

potential per capita in the last millennium increased by six orders of magnitude [Vanek 2008].

The introduction of alternating current and modern electricity in the late nineteenth century began to create much larger energy demands, starting with industry and working its way to the household. With modern electricity brought directly into the home, a great number of inventions emerged that continued to increase energy demand, including such devices as the light bulb, electrical oven, refrigerator, and television. With the introduction of the modern gas-expansion refrigeration cycle, energy demands again continued to rise at an alarming rate.

Factories and homes used to supply their energy demands individually with predominantly biomass fuels. Exponentially higher energy demands created the possibility for centralized power plants, which were powered largely by fossil fuels such as coal and petroleum products. Until the advent of emissions testing and standards, power plants remained largely unchecked until such events as the Great Smog of 1952 in London began to gain the attention of the general public. Large municipal areas began to implement committees to investigate and regulate chemical and biological hazard conditions in these areas. However, due to the vast majority of these emissions being the result of prosperous industrial endeavors, the steam and internal combustion engine continued to emit massive amounts of harmful particulates into the atmosphere. Coal-based power plants also continued to release unprecedented volumes of harmful particulates into the atmosphere.

Although emissions standards have been increased in recent years, hydrocarbon fuels still remain a staple for energy production. Coal-burning power plants are the least carbon efficient power stations in use. That is, they emit the greatest amount of harmful carbon byproducts per energy produced compared to other energy production methods. However, they still produce 47% of the United States' power plants' electrical power, with other fossil fuels accounting for another 21% [EIA 2008]. The United States, with about 5% of the world population, consumes approximately 25% of the world's production of energy [Tester, *et al*. 2005]. Although gas combustion power plants and nuclear power plants have higher efficiencies and lower levels of carbon dioxide, nitrous oxides, and trace elements per energy produced, they still contribute negatively to environmental conditions. As shown in Figure 1.1, world energy production, which underwent slow growth through the nineteenth century, has increased tenfold over the last fifty years. It is predicted that world energy demand will triple within the next thirty years [Dahl and McDonald 1998]. It should be noted that although world energy production has increased tenfold, the energy production per capita has only tripled. This reflects the large concentrations of energy production and consumption in industrial and modern populations, while much of the world lagged in the industrial revolution. However, as emerging economies begin rapid development up to the modern standards of leading nations, their energy production also vastly increases. This trend is most visible in China's economic and energy demand from 2002 to 2004 increasing by 40% [Vanek and Albright 2008].

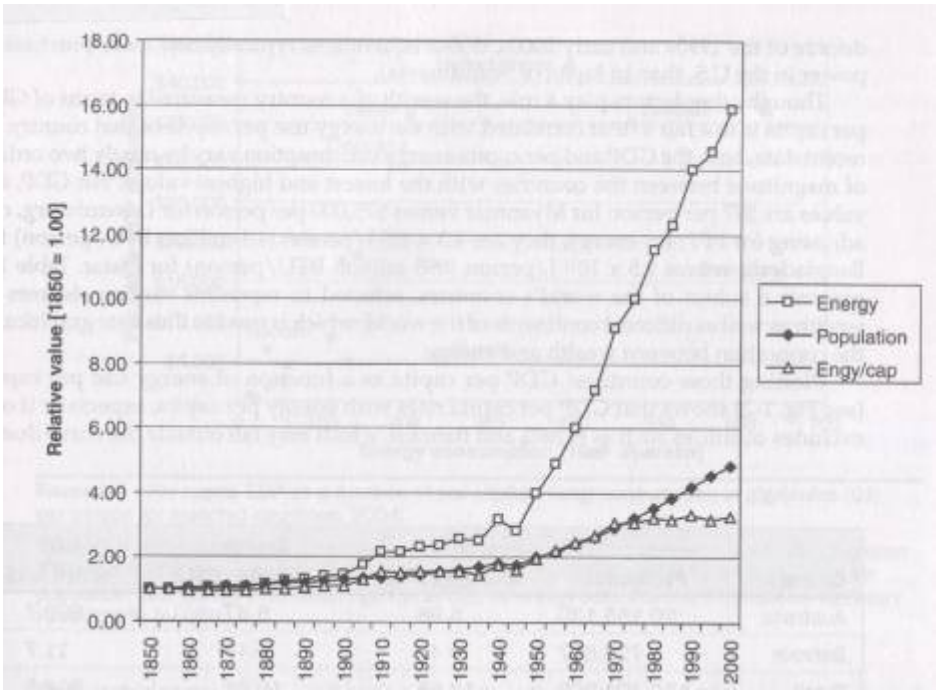


*Figure 1.1 - Relative growth in world population, world energy production, and average energy production per capita 1850-2000, indexed to 1850 = 1, [Vanek 2008]*

Peak oil production in the United States in 1970 and 1973 also points to a greater need for alternative sources of energy to offset the rise in cost of fossil fuels associated with supply and demand [Tester, *et al*. 2005]. According to the law of supply and demand, the price of oil products will continue to increase, and we have seen these trends strongly in the last decade. It is also important to note the desperate state of dependence our economy has on these products. 69.3% of United States energy production in 2007 was generated by fossil fuels. These levels of dependence in the United States and similar dependence in international economies pose a large threat to economic stability without alternative energy production methods. In 2007, renewable energy sources accounted for a total of 9.3% of energy production, with hydroelectrical applications at 7.0% and other renewable including solar, geothermal, wind, biomass, and various other methods totaling

2.3% of total energy production. World production of sustainable resources, not including hydroelectrical, has increased by 7.9% annually over the last decade, and is anticipated to continue to grow strongly. The United States accounted for 27% of production, Germany 12%, and Japan and Spain both accounted for 6% each of sustainable energy production. The average world emissions of carbon dioxide from fossil fuels has increased annually by 2.5% over the last decade. Non-hydroelectric renewable energy sources are projected to meet 33% of these rising energy demands over the next 20 years. [EIA 2008].

With the concentration of power output for greater populations of people, dependence on this production raises concerns for the possibility of production shutdowns. Modern economies and populations would now incur serious hazards if long-term failure of these power grids occurs. Food and water distribution systems would be inoperable, and biological concerns would begin to be raised for human waste, disease control, and food spoilage. Modern communications would also halt, creating great losses in the nation's economy. These massive energy concentrations and dependencies are a liability not only to a nation's function but also national security, with communications, security monitoring systems, and defense system grids inoperable. It should be noted that the most stable and efficient form of energy production is at an on-location and on-demand basis, rather than the centralized power production today which leads to dependency, population congestion, and the inherent biological and economic risks previously mentioned. When coupled with the climate and health concerns of hydrocarbon fuel consumption, energy production alternatives are increasingly attractive.

The negative combustion byproducts of fossil fuels include carbon monoxide and dioxide, nitrous oxides, sulfur oxides, unburned hydrocarbons, particulate matter, and

smoke. Harmful effects of these emissions include biological disease (often respiratory related), acid rain from sulfuric matter, cancer from ozone depletion, and the climate changes due to deposition of these gases into the atmosphere. One of the most alarming of these emissions is the study of the effect of carbon dioxide and its effects on the atmosphere. Carbon dioxide is recognized as the second most abundant of greenhouse gases on earth, which contribute to the developing global environmental phenomenon known as global warming. Although there is much debate on the actual rate of increase of the earth's temperature, it is conclusive that over the last century we are experiencing average temperature increases which exceed normal short term cyclical temperature variations. These trends, when studied along with the greenhouse gas trends in the past century, have alarming implications for our environment. It should also be noted that although nuclear power production does not emit greenhouse gas emissions, radiation byproducts and waste pose other concerns for future generations. Again, large-scale energy production units, although industrially viable, are inferior to local sustainable energy production units which are much more beneficial to the environment.

Carbon dioxide emissions, when understood as detrimental to the ecology and climate of the planet, show alarming trends over the past two centuries. Figure 1.2 shows the carbon emissions from fossil fuels, and Figure 1.3 shows a sample increase of carbon dioxide since the mid twentieth century. Though these levels seem to be relatively low, their concentrations have increased by greater than 35%, and show signs of exponential growth trends. It should also be noted that the response time of the environment to return to sustainable carbon emissions levels is estimated on the order of a decade or more, which increases our need for immediate action.

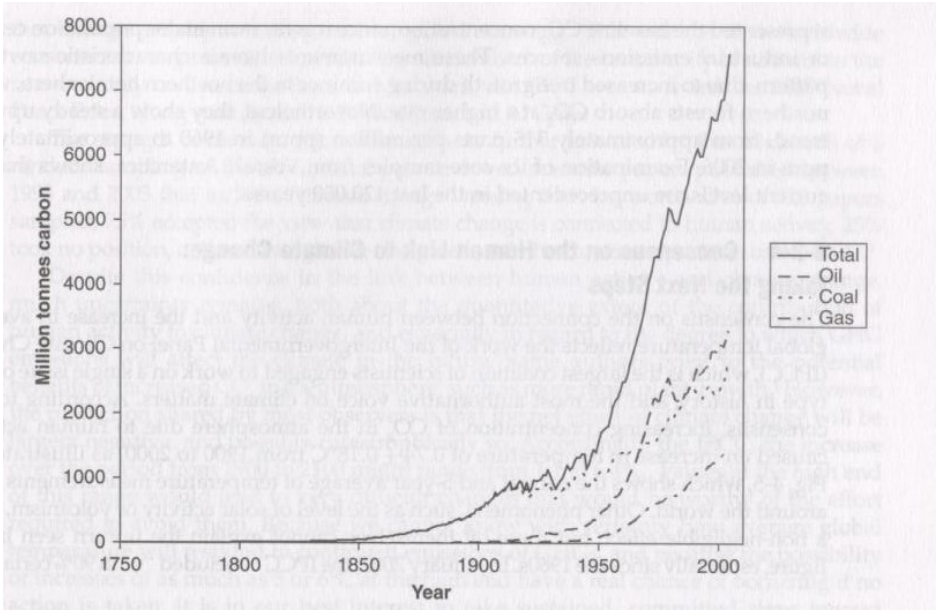


*Figure 1.2 – Carbon emissions related to fossil fuel use in tonnes carbon, 1750-2000, [Vanek 2008]*

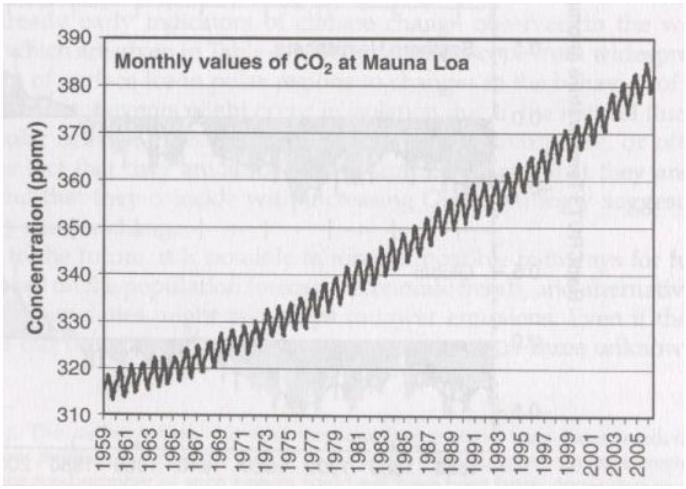


*Figure 1.3 – Concentration of $CO_2$ in the atmosphere in parts per million, 1957-2006, [Vanek 2008]*

The Intergovernmental Panel on Climate Change has been recognized as the largest coalition of scientists addressing these global implications, and is viewed as the

authority on global warming trends, data, and concerns. The IPCC has shown that carbon dioxide emissions in the last century has raised the global temperature by 0.74+-0.18 °C. This number, though at first seems small, is startlingly large in light of the sensitivity of global air currents, polar ice cap melting rates, oceanic salinity and the undersea currents associated with them, and potential of bringing on the next ice age is in the range of a couple degrees Celsius. Computer simulations for the next century predict another 2-6 °C temperature increase [Tester, *et al*. 2005].

The increase of global temperature by this magnitude would have very significant effects. The rise in sea level resulting from the possible melting of polar ice caps is significant, and is increased as pressure is released from the crust of the earth and expansion occurs. Very small changes in the salinity balance of seawater can drastically effect the underwater oceanic currents which are a key contributor to the thermal equilibrium of current weather patterns and distribution.

Other notable deterrents to the increasing trend of fossil fuel-based energy production are the aesthetic effects on the areas of mining, the availability and longevity of these resources, and the negative effects and costs incurred in the transportation of these resources. Although on a short term basis these seem to have a small overall effect on the planet, current energy production trends and predictions, if not curbed by alternative energy sources, will quickly deplete the planet's resources and quite possibly endanger the survival of future generations.

## B. Sustainable Energy Resources

More solar energy strikes the earth's surface in an hour than the amount of energy consumed by the world population in a year. 0.15% of the surface area of the United States in solar panels would produce all of the nation's energy demand. Potential wind energy in the United States is also in excess of our current demands [National Renewable Energy Laboratory]. Other renewable energy sources also show promising volumes of yet untapped availability.

Scientific research and engineering have been shown to only have about 25% weight for energy development decisions, while the remaining factors include politicians, public opinion, media, and legislations [Twidell and Weir 2006]. This explains the trend of much of the world moving towards nuclear energy in the past decades, while the United States lagged behind significantly, largely due to legislation and public opinion. It is clear by the energy trends of the United States when compared to the trends of the rest of the world that public opinion and short-term economics have large precedence over engineering projections for energy. The seminal report by the World Commission on Environment and Development in 1987 [DESA 1999] gave the public a new perspective and appreciation for the global effects that modernization and consumption of natural resources has on our environment and future generations. The concept and methodology of sustainable development became a much greater part of design and economic considerations after these publications. Sustainable development also takes into account the variability of energy, resources, and population across the globe and its effects on the environment, economy, and people within the scope of benefit and detriment of the changes.

Improvements in the efficiencies of production will also contribute to a decrease in carbon emissions. However, on a global basis, carbon dioxide emission per gigajoule of energy produced was only reduced by 6% from 1980 to 2004, revealing that alternative solutions for energy production must be promoted in order to reverse global greenhouse gas levels [Vanek and Albright 2008]. It has been shown that the increasing trends of global energy production may not be able to be immediately curbed through the implementation of greater efficiency in systems and production. Current resource estimates for fossil fuels, nuclear energy, and sustainable resources remain optimistic. Nuclear energy resources and the remaining reserves of fossil fuels can be coupled with the development of sustainable energy resources to bring the levels of these greenhouse gases brought back to non-harmful concentrations within the atmosphere. The area within these three technologies that has the greatest potential to offset net carbon dioxide output is in the use of existing sustainable resources for energy, such as wind, geothermal, hydroelectrical, and solar power. These resources, whose technologies have been growing much more quickly through research and awareness of detrimental energy production byproducts and their effects, will help sustain our environment and economies for the next generations.

## C. Passive Solar Research and its Impact on Domestic Heating

Solar energy flux in the form of radiation is received outside the earth's atmosphere at about 1367 $W/m^2$, or what is known as the Solar Constant. The energy is either absorbed by the surface it contacts and converted into thermal energy or reflected

back to its surroundings. This constant energy source has been taken advantage of by photovoltaic applications, and active and passive water and air conditioning systems. Photovoltaic applications are valuable for their production of electricity and thus great variability of end use. However, the efficiency losses associated with the photon energy band of the photovoltaic surface alone account for greater than 53% of the insolation (solar radiation) on the panel [Twidell and Weir 2006]. Other smaller efficiency losses, coupled with the expensive manufacturing methods of traditional silicon-based photovoltaic cells, greatly limit their economic payoff for domestic uses.

Thermal solar technologies, which involve the conversion of solar radiation directly into heat, have achieved insolation to heat conversion efficiencies greater than 90%. These greater efficiencies, coupled with the relatively affordable materials necessary for construction of equipment, make solar thermal technology much more viable as a sustainable energy solution. The development and research of active and passive solar water heating panels has been extensive and continues to have increasing frequency in building installations. Space heating, ventilation, air conditioning, and lighting comprise an estimated 40% of total energy demand, and 70% of electrical energy. Alternatives for space heating will reduce energy consumption, as well as decrease the carbon dioxide output for residential purposes.

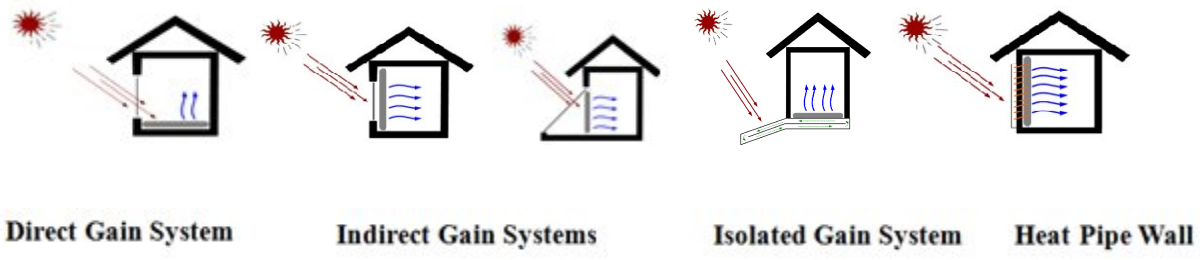


*Figure 1.4 - Passive Solar Technologies*

Passive solar technology for space heating consists of the three main system designs shown in Figure 1.4. The first and most common method of design for solar energy gains is the direct gain system. Direct gain systems consist of sun-facing exposed windows and skylights in buildings which allow the sun's rays to directly pass through a glazing and be absorbed by the environment to be heated. These systems, although allowing almost all of the energy flux through during heating hours, have large heat losses due to a lack of insulation during night and non-solar heating conditions. It may also be noted that these systems, because of their direct method of heat transfer, have fast heating response times when compared to other solar methods. Thermal masses can be taken advantage of to receive and absorb the energy, with absorption coefficients recommended to be greater than 80%, and this large thermal mass helps dissipate the heat more evenly and longer throughout the day.

The next type of heating system is the indirect gain system, which consists of a glazing unit on a solar facing wall which is separated from the dwelling environment by a thermal mass which absorbs the sunlight during the day, heats up, and slowly gives off heat throughout the day. Most typical indirect gain systems are greenhouses or Trombe walls. This system has the advantage of curbing significant temperature swings due to the thermal mass. However, because of the greater insulation properties of the thermal mass, which is the heat transfer unit, much of the heat absorbed does not make it into the heated room before it is lost during nightly conditions. Both direct and indirect system efficiencies can be significantly increased by the use of nighttime insulation. However, passive automatic systems have yet to be designed, and daily manual installation and removal of insulation on each unit during changing solar conditions is tedious.

The other main type of passive domestic heating system is the isolated gain system. This system usually consists of a receiving unit with a heat exchanging fluid on a slope next to the heated space. As the sun heats the air or fluid within the secondary space, the heat is transferred by natural convection, or thermosyphoning, into the dwelling place. These systems have the advantage of significantly reduced losses since the thermosyphon effect only creates natural flow when heat is being transferred into the heating space. This is achieved since the receiving area is below the heating area. However, since the fluid within the isolated gain system is only driven by the buoyant forces in the fluid from temperature changes, the circulation of these systems is limited. In a heat pipe, circulation is much greater due to the phase change of the working fluid. Research has concluded that the use of heat pipes is a substantial solution for the relatively low flowrates involved in single phase thermosyphoning for isolated gain systems.

The heat pipe augmented solar wall is a type of isolated gain system which greatly increases the insulation value of the solar heating device with the advantage of the “thermal diode” phenomenon in heat transfer with heat pipes. The system also eliminates the need for solar-facing slopes next to a residence in order to take advantage of a thermosyphon effect. These units perform similar to ground-based isolated gain collection units but can be installed in any solar-facing wall. The increased insulation value of these systems and their ability for installation in any building with solar exposure makes them much more likely to have the greatest impact on the building heating market.

## D. Heat Pipe Operation and History

A diagram of a heat pipe is shown in Figure 1.5.

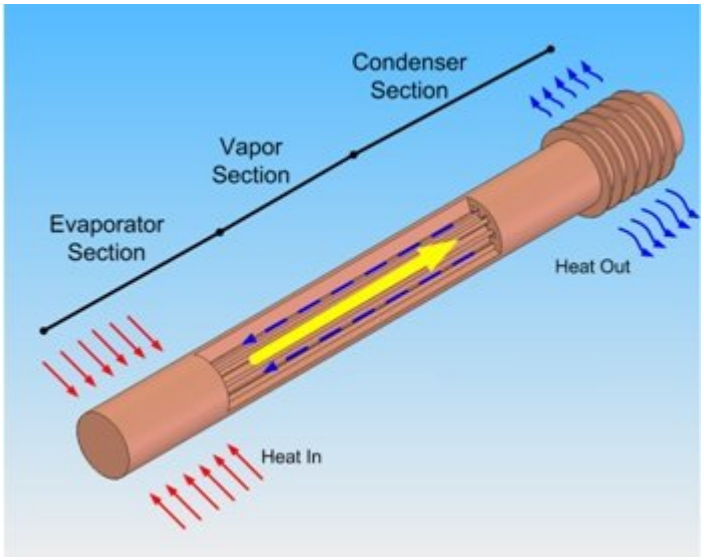


*Figure 1.5 - Diagram of Heat Pipe*

Heat pipes are thermal transfer devices that involve an evaporator, condenser, and often an adiabatic section (vapor section in Figure 1.5). Heat pipes usually work at a vacuum, with a phase change fluid chosen according to the operating temperatures of the heat pipe. When heat is transferred into the evaporator section, the fluid is boiled. The vapor then rises or circulates to the condenser end of the heat pipe, where heat is lost due to the lower temperature at this location, and the vapor returns to its liquid state. The liquid is driven back to the evaporator section by gravity (in a gravity assisted heat pipe), inertia (in a rotating heat pipe), or by capillary action through a wicking structure (in wicking heat pipes). In a gravity assisted heat pipe (a heat pipe oriented at an angle), the lower end is the evaporator and the upper end is the condenser. When the evaporator end is hotter than the condenser, high thermal conductivity is achieved through circulation.

When the evaporator end is colder than the condenser, the fluid remains liquid in the evaporator section and does not circulate. This leads to good thermal resistance to heat flow in the undesired direction, and is referred to as the thermal diode effect. Also, since energy is absorbed primarily as latent heat, the heat pipe operates with very small temperature gradients along its length. This leads to very high thermal conductance properties, and values 700 times greater than copper have been achieved [Dunn 1994]. This thermal diode effect makes heat pipes very suitable for a solar application where the absorber and thermal mass need to be separated by an insulator to ensure minimal heat losses at night, but where maximum heat transfer from the absorber to the thermal mass are desired.

The thermosyphon, or the "Perkins heating device," was invented in 1831 by Angier Perkins. The difference between a heat pipe and a thermosyphon is that a thermosyphon is single phase, while a heat pipe involves two-phase heat transfer. This two-phase heat transfer method was invented by and introduced by R. S. Gaugler in 1942, who was awarded a patent for his device [Gaugler 1944]. Grover was awarded a patent with the United States Atomic Energy Commision for his very similar device in 1963, in which it was first named a "heat pipe" [Grover 1990]. Further development of the device was researched by Cotter and Cheung at Los Alamos Laboratories in the 1960's for their applications in the cooling and isothermal needs of electronic devices in space applications [Cheung 1968, Cotter 1965]. Feldman, Eastman, and Katzoff had several publications in 1967 and 1968 that investigated alternative applications of the heat pipe and also variations including flexible, flat plate, and arterial designs. Since the late sixties and early seventies, heat pipes have become more common in electronic

devices where rapid cooling is necessary. The technology and applications of heat pipes continues to broaden today.

The heat transfer of heat pipes has several limiting factors. The viscosity of the working fluid slows heat transfer in the heat pipe at low temperatures due the friction between the rising vapor and the falling condensed liquid. The sonic limit applies to heat pipes at high temperatures when the compressibility of working fluids at the exit of the evaporator section begins to cause choking conditions. Entrainment of the working fluid occurs when the rising vapor exerts enough viscous force on the liquid in the heat pipe to carry it up to the evaporator end, leaving little or no liquid in the condenser section. The boiling limit within a heat pipe occurs when the nucleate vapor creation within the liquid creates a large enough volume in the evaporator to restrain the condensed fluid from reaching the evaporator heat flux location. A capillary limit applies to heat pipes with a wicking structure, which occurs when the wicking structure cannot overcome the pressure gradient across the heat pipe to return the fluid to the evaporator section. This pressure gradient results from the density changes with temperature variation and with dynamic pressures resulting from vapor flow. Burnout occurs under very high heat fluxes when the conditions within the heat pipe cause all of the fluid to exist in the vapor state, creating much lower thermal conductivity. Both the capillary limit and burnout conditions do not apply for the heat pipes used in the experimental model. For normal operating conditions of the experimental unit, these limiting factors should not be reached except in the case of failure of a certain component.

## E. Literature Survey

Solar selective coatings have greatly increased the efficiencies of modern solar thermal devices. Mar performed analysis on optical coatings for flat plate solar collectors [Mar 1974]. Testing was performed on silica saturated fluosilicic acid solutions for antireflective coatings on glass and Tedlar glazings, and reflective losses were reduced from 8 percent to 2 and 0.8 for single and double coatings, respectively. These coatings, however, return to performances of unetched glass if not cleaned every six months. Coatings for absorber plates were also investigated, and black chrome was concluded to offer the best combination of optical performance, cost, and durability. Painted absorber coatings were also investigated and showed promise with further research.

The development of single and two-phase heat transfer devices has been quite extensive. Trefethen studied the effects of slight inclinations on fluid filled parallel plates [Trefethen 1970]. Faunce performed testing in vertical solar collectors and various heat transfer rates, and also incorporated testing of multiphase thermal storage methods [Faunce 1978]. Muramoto implemented heat pipes in various solar collector designs and Trombe walls, proving the economic viability of heat pipe augmented systems for residential heating [Muramoto 1985]. Bairamov and Toilev performed analysis on thermosyphon versus heat pipe systems, and reported a 10-11 degree increase in water tank temperature for the two-phase heat transfer device [Bairamov and Toilev 1981]. Saman investigated the use of heat pipes to reduce heating load within walls [Saman 1989]. The use of heat pipes in evacuated collectors for active applications was also evaluated [Riffat 2005].

Corliss performed an extensive study of heat pipe augmented passive solar devices with various heat pipe materials and fluids and unit configurations. His main tests consisted of a six piece heat transfer configuration, with each piece consisting of a heat pipe mounted within the groove of a selectively coated absorber, a thermal mass consisting of plastic water tanks separated from the absorber by a layer of insulation. The heat pipes were mounted with an angle of 5 degrees and used Freon 21 as the working fluid. This unit was created to be modular and weight supporting, with installations most likely in new home construction. Simulations and real weather tests were performed for various climate conditions, with simulation locations for four differing climate conditions: Madison, WI; Phoenix, AZ; Albuquerque, NM; and Columbus, OH. Simulations showed increased solar gains for all locations over other standard passive solar devices. Corliss concluded that a modular design would be most cost effective and have the greatest impact in the energy market, and recommended detailed design studies for the most economical design [Corliss 1979]. Van Dijik performed comparable economic, performance, and manufacturing optimization on a heat pipe wall with an additional layer of insulation between the thermal mass and the heated space to help regulate heat transfer between the two [Van Dijik 1983].

Susheela and Sharp designed and investigated a similar system which could be installed on existing homes without the demolition required for modular units [Susheela and Sharp 2001]. The absorber portion was mounted on a solar facing wall, with plastic water tanks as the thermal mass on the other side of the wall. A hole was drilled in the existing wall for the adiabatic section of the heat pipes, connecting the absorber and water tanks. The heat pipes used had a 5 degree angle and were made from copper pipe

with 1 inch inner diameter, with DuPont SUVA-124 (chlorotetrafluoroethane) as the working fluid and a stainless steel wire wicking structure. Experiments were performed outdoors, and produced superior heating data for comparable passive solar units. Computer simulations were also performed to model the performance of the unit.

Albanese directly followed Susheela and Sharp's recommendations for improvements on their design, and developed computer simulations for similar heat pipe systems for permanent modular units [Albanese 2008]. Computer simulations were run for a large number of variations in system parameters, including glazing characteristics, selective surfaces, absorber thicknesses, insulation properties, and the number and material of heat pipes. The resulting solar fractions were followed with economic considerations and recommendations for production of the design of a unit with emphasis on manufacture. Various heat pipe fluid fill levels were also tested for optimum conductance values. A finned condenser section of the heat pipe was also determined to increase the solar fraction less than 0.5%. A small-scale prototype was built and tested under laboratory conditions. Albanese recommended full scale testing in realistic weather conditions, especially the relatively cloudy and cold conditions in Louisville, KY. This prototype could also be tested for overheating performance during summer months when heat transfer into the home is undesirable.

## F. Research Goals

This research focuses on the design of a modular heat pipe augmented solar wall for cost effectiveness and on experimental testing of a full-scale model in actual weather conditions. The specific goals of the project are:

- Design a heat pipe augmented solar wall with emphasis on mass production methods and cost-efficiency.
- Build a full-scale experimental modular unit and test under actual weather conditions, with emphasis on the prototype unit being as close as possible to mass manufactured unit for performance prediction accuracy.
- Conduct performance analysis of the experimental model including component thermal resistances, conductivities, and overall system efficiency with emphasis on design optimization from results.
- Give design considerations for further research which may impact the performance/cost of the unit.
- Analyze overheating characteristics and performance and provide design suggestions for overheating prevention.
- Prepare economic analysis of the unit including manufacturing cost per unit, future fuel cost analysis, life cycle cost analysis, and payback period with emphasis on preparation for production startup and marketability.

- Prepare manufacturing drafts, solid models, and construction details as well as assembly and packaging instructions for mass production of unit.

Production of the full-scale prototype and testing under weather conditions will generate valuable data for a startup production company to market the unit. Extensive analysis of system performance through experimentation will give valuable insight for improvements and overall efficiency of the mass manufactured unit. The location of the unit in a university classroom will positively impact public opinion and policy on sustainable energy and specifically the viability of solar technology in any climate. Mass production and public use of the heat pipe augmented solar wall will have a positive and lasting effect on the energy production methods and ideologies of the 21$^{st}$ century, as well as begin to stabilize the climate changes associated with non-renewable energy resources.

# II. METHODS

## A. Design Considerations

The Heat Pipe Augmented Solar Wall had several governing considerations for the design phase. These are as follows:

1. Competitive Cost/Benefit ratio and payoff time to encourage release into market.

2. Simplicity of design to accommodate modern manufacturing methods and facilitate possible future repairs or modifications.

3. Thermal efficiency, both in heat gains and in insulation properties under various operating conditions.

4. Maximum possible working life of unit.

5. Aesthetic design that will not deter architects and builders from its inclusion in their designs.

6. Standard installation size to allow for current construction methods to be used.

7. Design unit to be light and simple enough so as not to require specialized equipment or personnel for installation.

The most important factor in attracting buyers, builders, and designers in order to make an environmental impact is cost. The unit must be viewed as beneficial to the worth of a home or office construction. In order to ensure the best payoff times and cost/benefit ratios, the unit must be designed in a manner that will facilitate its production. The ability to mass produce these units gives the greatest benefit to a company because of the economies of scale. The unit was designed accordingly, with a minimal number of fasteners, and with the least complications involved in its assembly. Another important factor in cost/benefit ratios is, of course, the thermal efficiency of the complete unit. Greater thermal gains during the heating season and lesser insulation losses at night both lead to higher economic viability.

The working life of the unit also greatly affects its impact on the market, and a stable long-term performance prediction gives the unit much credibility. This is accomplished through the use of components that eliminate concerns for corrosion, mechanical wear, and deformation from stresses induced during operating conditions.

An emphasis during design on the aesthetic value of the unit will increase its implementation in standard building constructions. This was accomplished through the use of an anti-reflective surface on the glazing, which not only increased the thermal efficiency of the unit, but also helped to hide the mechanical components directly behind the glazing which would be less attractive to an architect or designer. Aesthetic value was also emphasized for the unit's rear cover, which led to the use of a dark screen that

shadowed the inner features while still allowing maximum heat transfer from the thermal mass (plastic water tanks). Another feature that makes the unit more attractive to designers is the design of the unit to have equivalent dimensions of a standard entry doorway. By using currently-existing construction codes and installation methods, inclusion of these units does not require additional engineering time or training for construction crews.

Finally, the unit was designed for simple installation by professionals or homeowners. The unit has no hookups, requires little except a screwdriver and a water hose for start-up, and needs no specialized training or assistance for installation. Great emphasis was also placed on the unit's ability to be installed from the inside of a building, and on the unit being light enough for transport and installation to be made without the need for lifting equipment, which would result in extra installation cost. This was accomplished by designing the water tanks to be filled once the unit was installed in place, reducing installation weight by 67%.

A lack of emphasis on any of these factors would result in a much smaller response in the building sector and limit the renewable energy impact of the unit. As is the case in all designs, some design factors must be given precedence over others since there must be compromises in design. The greatest emphasis in this design was placed on thermal efficiency and ability for mass-production. The unit's influence on sustainable energy practices relies most heavily on these two factors. In accordance with the emphasis on the unit's market impact, design drafts have been prepared to facilitate mass production and are available in Appendix I. Solid model assembly and construction files

have also been created and are included in Appendix II and on the included CD in Appendix III.

## B. Construction of Experimental Model

### 1. Description of the Heat Pipe Augmented Solar Wall

An experimental model was constructed to test the performance characteristics of the heat pipe augmented solar wall designed for mass production. The design consisted of five individual heating units each consisting of an absorber plate clamped to a heat pipe. The heat pipes were mounted at 5 degrees and consisted of an evaporator, adiabatic, and condenser section. The adiabatic section of the heat pipe was run through a layer of thermal insulation and then was placed within a water tank which acted as a thermal mass. An aluminum frame was built to support the absorbers, heat pipes, and water tanks, and the five heating units were enclosed within an aluminum sheet metal skin with a glazing on the front of the unit. The rear of the unit consisted of a screen facing on the heated face which allowed the thermal mass to slowly give off heat to the space.

Each of the five heating units was designed to be as close to identical as possible. However, geometric efficiency and aesthetic considerations of the heat pipe system resulted in two of the five total heating units being designed with slight modifications. These modified heating units were at the top and bottom of the model. Descriptions of the experimental model and its construction apply to all of the heating units, and modifications of the two heating units will be addressed when applicable.

## 2. Construction of the Heat Pipe Augmented Solar Wall

Drafts and solid model views of the unit are shown in Appendices I and II. A sheet metal skin 2.09 m x 1.25 m x 0.394 m (82-1/4 inches x 49-1/4 inches x 15-1/2 inches) was constructed to interface the outer edges of the unit with the wall in which it was placed and to seal around a glass glazing on the front of the unit. The glazing consisted of 0.00318 m (1/8 inch) thick low-iron glass with an anti-reflective coating. The glazing was 2.06 m x 1.22 m (81-1/8 inches x 48 inches), and was mounted to a 0.0191 m (3/4 inch) mounting flange formed into the sheet metal skin. The glazing edges were protected with a silicone rubber extrusion and were clamped into place using a front mounting flange along the outer edge of the unit. The front mounting flange was attached to the sheet metal skin using standard aluminum sheet metal screws, and the sheet metal skin was attached to the supporting frame of the unit with closed-end self-sealing aluminum rivets. The sheet metal screws, rivets, and mounting seams were all sealed with construction-grade silicone to ensure no air or rain leakage during inclement weather conditions.

The absorber plates of the unit consisted of 0.00635 m (1/4 inch) thick aluminum which were coated with a solar selective surface. The selective surface consisted of a nickel substrate applied directly to the raw aluminum followed by a black chrome coating. Both of these coatings were applied by an electroplating process. The absorber plates were formed with a semi-circle groove in them to mate as close as possible to the heat pipes for maximum heat conduction. This was achieved through the design of a female die used in conjunction with a hydraulic press. The absorbers had 0.0670 m (2-3/4 inches) slots cut out of the groove section to allow for the larger diameter of the heat pipe

elbows and 0.0381 m (1-1/2 inches) slots cut out for the end caps. The outside edges of the absorber plates were mounted to the support frame with aluminum screws and plastic spacers. These plastic spacers insulated the absorber plates from the aluminum frame and ensured maximum heat transfer to the heat pipes. The receiving side of the absorber plates was mounted 0.0254 m (1 inch) from the rear face of the glazing to ensure minimum local convection heat transfer from the absorber.

The receiving face of the absorber plates was 1.17 m (46 inches) wide. The total absorber receiving surface of the unit was 2.007 m (79 inches) tall with a 0.00635 m (1/4 inch) gap between each plate, resulting in 2.30 $m^2$ (3562 $inches^2$) of receiver surface area. The plates were mounted at a 5 degree angle from the horizontal with the heat pipes, and were cut at 5 degrees on each side accordingly. Each absorber plate had a height of 0.368 m (14-1/2 inches), with the heat pipe groove centered to allow for even heat conduction from the upper and lower portion of the absorber. Since the front face of the experimental model was rectangular, the absorber plates corresponding to the upper and lower heating units were modified to have horizontal edges instead of the angled edges of the middle three. The absorber plates for each of the five heating units required further modification due to size limitations of the nickel-substrate coating tanks. The five absorber plates were cut in half, resulting in ten total absorber plates. The absorber plates were cut perpendicular to the thermal conduction path to the heat pipe, resulting in no change to the thermal behavior of the experimental model. The full absorber plate assembly is shown in Figure 2.1 at a horizontal orientation during construction, with the upper portion of the experimental model to the left. The cut of the absorber plates may be noted along the center of each absorber plate section.

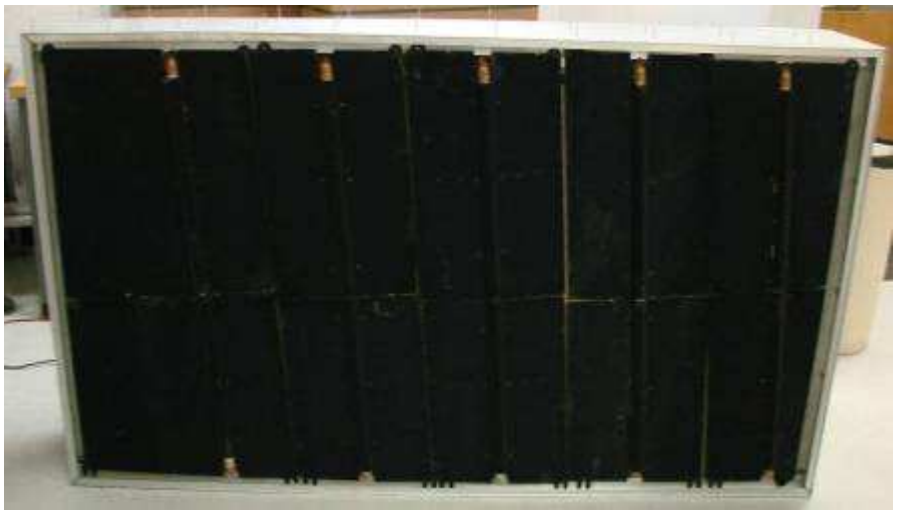

*Figure 2.1 - Absorber plate assembly at horizontal orientation during assembly (upper portion on the left)*

The heat pipes were constructed from 0.0254 m (1 inch) inner diameter and 0.0286 m (1-1/8 inch) outer diameter copper pipes. The heat pipes consisted of a 1.16 m (45-3/4 inches) evaporator, a 0.229 m (9 inch) adiabatic section, and a 1.09 m (43 inches) condenser section. All sections of the heat pipe were mounted at 5 degrees from the horizontal. To achieve this, the copper elbows which were soldered to the copper pipe were heated and bent to achieve an angle slightly greater than 90 degrees. The pipes were then soldered at their corresponding perpendicular planar orientations. Copper end caps were soldered at the end of the evaporator and condenser sections. The heat pipe construction used is shown in Figure 2.2.

*Figure 2.2 - Heat pipe construction.*

A valve fitting was necessary for the filling of the heat pipes. This feature was achieved by drilling a small hole in the adiabatic section of the heat pipe and using a punch to expand the hole. This formed a female slot in which a 0.00635 m (1/4 inch) outer diameter copper pipe was soldered. The smaller diameter copper pipe was then soldered to a butterfly valve. The filling feature of the heat pipe is shown in Figure 2.3.

*Figure 2.3 - Filling feature of the Heat Pipe.*

Filling of the heat pipes was achieved using a charging system consisting of a vacuum pump, refrigerant tank, vacuum gauge, and several control valves. The fully-constructed heat pipe was washed and connected to the charging system with a threaded

butterfly valve fitting. The entire charging system was drawn to a vacuum of 648 mm (25.5 inches) of mercury with the vacuum pump. Once the adequate vacuum level was achieved, the pump was closed off from the system and the heat pipe was charged with fluid through manipulation of the control valves. The heat pipes were filled with DuPont SUVA-124 refrigerant corresponding to previous research [Susheela 2001, Albanese 2009]. The amount of refrigerant added was monitored by a scale which the heat pipe rested on during the charging process. The amount of refrigerant added was 957 g (2.11 pounds). This amount corresponded to a 120% filling volume of the evaporator section with liquid refrigerant at 1.36 g/cm$^3$ (0.0491 lb/in$^3$) as recommended by previous research [Albanese 2009]. A diagram of the heat pipe filling apparatus is shown in Figure 2.4.

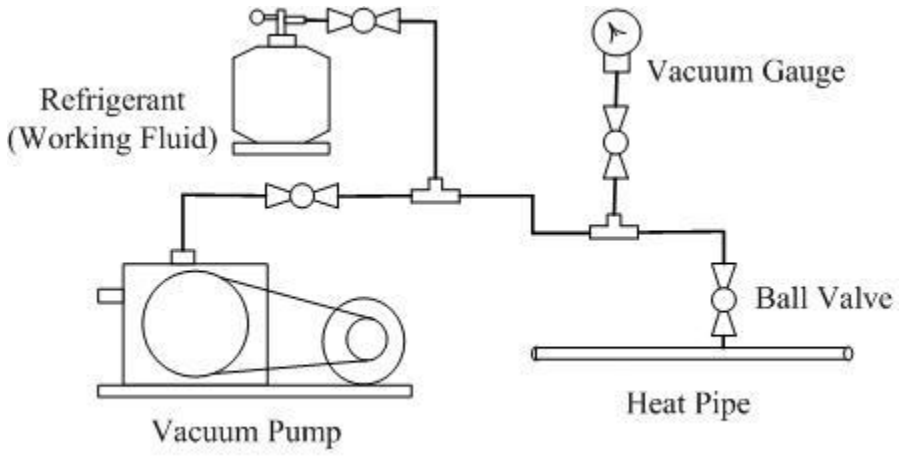


*Figure 2.4 – Heat Pipe Charging Apparatus [Albanese 2008]*

The heat pipes were assembled to the absorber plates using 0.00318 m (1/4 inch) thick aluminum clamps 1.09 m x 0.102 m (43 inches x 4 inches) which were formed with the female press die. Holes were drilled through the absorber plates and clamps, through which a screw, nut, and washer were used to achieve the tightest assembly possible

between the absorber plates and the heat pipe. A thermal paste was used in the groove to enhance heat transfer between the heat pipes and absorbers where very small air gaps would otherwise act as an insulator. Flat black paint was used on the aluminum screws and on the inside of the holes drilled to ensure no moisture penetration between the electroplated layers, which would lead to breakdown of the coating over time.

Plastic water tanks 1.11 m x 0.356 m x 0.203 m (43-1/2 inches x 14 inches x 8 inches) were used as a thermal mass. The tanks were threaded with a 0.0318 m (1-1/4 inches) female NPT fitting to allow for the heat pipe entrance and water seal. The tanks had two threaded access caps, one on top which was utilized for instrumentation installation and the other on the side for filling of the tank once installation was complete. The filling cap was mounted at an angle at the top of one side of the tank to allow for the maximum amount of thermal mass (water). This necessitated a cutout in the bottom of the tank for filling up of the tanks after installation. Total tank capacity when installed was 65.1 liters (17.2 gallons) per tank. The plastic water tank used is shown in Figure 2.5, and a side view of the female fitting and fill-up cap are shown in Figure 2.6.

*Figure 2.5 – Plastic Water Tank used for Thermal Mass*

*Figure 2.6 - Female Fitting and Fill-up Cap on the side of the Water Tank*

Bushings were machined to mate the heat pipes to the female fitting of the plastic tanks. These consisted of a 0.0318 m (1-1/4 inches) male threaded NPT yellow brass bushing machined to a 0.0320 m (1.26 inch) inner diameter. A water-tight seal was achieved between the water tank and heat pipe with this bushing. Epoxy was applied between the heat pipe and the bushing, and gasket thread sealant was applied to the threaded fittings to ensure no leaks. The brass fitting used is shown in Figure 2.7, and the completed and sealed joint is shown in Figure 2.8.

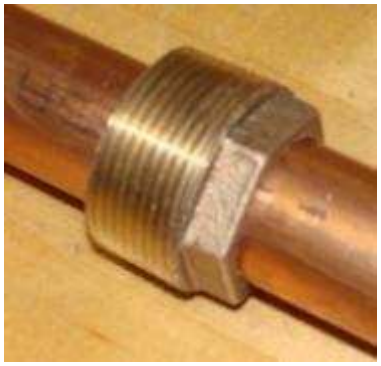

*Figure 2.7 – Brass fitting used to achieve seal between heat pipe and water tank*

*Figure 2.8 – Sealed heat pipe and water tank joint*

The supporting frame of the unit was constructed with structural grade 6061-T6 extruded aluminum channels. The necessary thicknesses and lengths of the structural components were calculated using standard mechanical design tools including basic mechanics of materials in conjunction with ANSYS, a finite element analysis software package. The frame of the unit was designed to support the total unit at 487 kg (1033 pounds). Most of this consisted of the water acting as a thermal mass amounting to 326

kg (718 pounds). This resulted in an installation or “dry” weight of the unit at 143 kg (315 pounds).

Insulation of the unit consisted of 0.0508 m (2 inches) of mineral wool with an insulating value of R-8.0 directly behind the absorber plates. The mineral wool was used to prevent outgassing which may result from insulation overheating in the possible failure of a heat pipe during operating solar conditions. Directly behind the mineral wool were three layers of 0.0217 m (1/2 inch) Styrofoam sheathing with an insulating value of R-3.0 per panel. 0.0254 m (1 inch) thick mineral wool pipe wrap was used around the adiabatic section of the heat pipes. The area surrounding the water tanks and the adiabatic section of the heat pipes was filled with mineral wool filler with an insulating value of R-4.0 per inch. Figure 2.9 shows the mineral wool and Styrofoam layers used between the absorbers and water tank along with the insulation around the adiabatic section of the heat pipe. The area shown was filled with mineral wool filler once the sheet metal skin was in place.

*Figure 2.9 - Mineral Wool and Styrofoam Insulation used in the Unit*

The rear face of the unit was designed to be covered with a black insect screen for aesthetic purposes. This would allow for the greatest amount of air exchange resulting in heat transfer while maintaining the necessary appearance for a residential or commercial installation.

The unit was installed in a south-facing window enclosure in a classroom at the University of Louisville Shelby Campus. The window unit was removed and a steel frame was constructed and installed for the support of the experimental model. Drafts of the frame construction and unit location in the wall enclosure are available in Appendix IV.

## C. Theoretical Performance of Experimental Model

Due to the experimental model being tested in true weather conditions instead of a controlled laboratory environment, a great number of conditions arose which affected the performance of the unit. These include ambient temperature, wind, and insolation variations from weather. As previously mentioned, this design work focused on thermal efficiency of the unit during heating conditions (that is, adequate solar insolation values) and during insulating conditions (that is, when ambient temperature is below room temperature and inadequate insolation is available for heating). The latter case will be very important since one of the great advantages of the heat pipe augmented solar wall design is increased insulation during nighttime and cloudy conditions.

When insolation values are large enough for heat gains to the residence, heat gains do not occur until the components upstream of the water wall have reached high enough temperatures to cause heat gain into the thermal mass. That is, heat cannot be added to the water tank until the absorbers and heat pipe are elevated above the temperature of the thermal mass. Under this limitation, if the amount of heat that is necessary in preheating the heat transfer components is significant, this will reduce the efficiency of the unit substantially, since this heat will never be able to make it into the thermal mass due to the Second Law of Thermodynamics. It should be noted that since two out of the five heating units within the experimental model were not identical, all calculations shown below apply to the three identical heat transfer units. These calculations will be compared to the actual performance of the unit. Both sets of data will reveal valuable information regarding the "thermal bottlenecks," which have the greatest impact on the system's performance. It should be noted that the only variation between

the upper and lower heating unit is in absorber plate size. The upper and lower sections receive 151% and 83.4%, respectively, of the radiation amount that strikes the center heating units.

Two thermal masses will be compared in the system: the components in the system that need to be heated prior to heat gains occurring, and the thermal mass of the water wall itself. The pre-heated components include the glazing, absorber plate, the heat pipe and refrigerant, refrigerant charging valve assembly, and assembly clamps. It should be noted that the condenser section of the heat pipe will be approximated as isothermal with the water tank temperature during preheating conditions, due to the large area of contact and high conduction value of both materials. The thermal mass consists of the plastic water tank and the water it contains.

In the comparison of thermal masses, a worst-case scenario will be accounted for in which the ambient temperature has cooled the pre-heating elements to -5°C. The room temperature will be assumed to be constant at 20°C. The amount of heat required to bring the preheated components up to heat gain conditions is determined by

$$Q = \Delta T \sum m c_p \tag{1}$$

where Q is the energy in Joules, $\Delta T$ is the temperature change in degrees Celsius, m is the mass of each component in kilograms, and $c_p$ is the specific heat of each component in J/kg K. The energy required to bring the pre-heat components up to heating conditions under the previous assumptions is 256 kJ (232 Btu). The total energy required to raise the preheating components and the thermal mass an additional 5°C, assuming 15% of refrigerant evaporation, is 1736 kJ (1645 Btu). Thus a worst-case scenario of heating

conditions results in 16.5% energy consumption in preheating of the system components. A typical operating day of experimental data yielded a 7℃ increase in the thermal mass. At this condition, with ambient temperature at 0°C, the energy losses (inefficiencies) associated with preheating the system components accounts for 11.2% of the heat gained. Thus, for normal operating conditions, inefficiencies in preheating are less than 15% for the total system gain.

For the case of nighttime conditions or inadequate solar insolation after which the unit has already released all of its excess heat into the residence, the unit acts as an insulator. The thermal resistance of a conducting solid is defined by

$$R_{th} = \frac{L}{kA} \tag{2}$$

where $R_{th}$ is the thermal resistance in K/W, L is the length of the conduction path in meters, k is the thermal conductivity of the material in W/m K, and A is the cross-sectional area of heat conduction normal to the path of heat flow in meters squared. The thermal resistance of fluid convection is defined by

$$R_{th} = \frac{1}{hA} \tag{3}$$

where h is the convection heat transfer coefficient in Watts per meters squared degree Kelvin, and A is the exposed area of convective heat transfer in meters squared. The average convection heat transfer coefficient for a vertical plane is

$$\bar{h} = \overline{Nu} * \frac{k}{d} \tag{4}$$

where d is the characteristic length of the geometry in meters and $\overline{Nu}$ is the average dimensionless Nusselt number which is correlated [Incropera *et al.* 2007] for laminar flow on a vertical plate as

$$\overline{Nu} = 0.68 + \frac{0.670Ra^{1/4}}{\left[1+(0.492/Pr)^{\frac{9}{16}}\right]^{\frac{4}{9}}} \tag{5}$$

where Ra is the dimensionless Rayleigh number and Pr is the dimensionless Prandtl number. The average Nusselt number for turbulent flow [Incropera *et al.* 2007] is

$$\overline{Nu} = \left\{0.825 + \frac{0.387Ra^{1/6}}{\left[1+(0.492/Pr)^{\frac{9}{16}}\right]^{\frac{8}{27}}}\right\}^2 \tag{6}$$

The Rayleigh number is

$$Ra = \frac{g\beta\Delta T d^3}{\upsilon\alpha} \tag{7}$$

where g is the acceleration of gravity in meters per second squared, $\beta$ is the volumetric thermal expansion coefficient in units per degree Kelvin, $\upsilon$ is the kinematic viscosity in meters squared per second, and $\alpha$ is the thermal diffusivity in meters squared per second.

Radiation heat transfer between components within the system is governed by

$$\dot{Q} = \varepsilon_1\alpha_2\sigma(T_1^4 - T_2^4)F_{12}A_1 \tag{8}$$

where $\dot{Q}$ is the heat transfer in Watts, $\varepsilon_1$ is the dimensionless emissivity of the hotter component, $\alpha_2$ is the dimensionless absorptivity of the cooler component, $\sigma$ is the Stefan-Boltzmann constant at 5.67 x $10^{-8}$ $W/m^2K^4$ , $T_1$ and $T_2$ are the temperatures in Kelvin of

the hotter and cooler components, respectively, $F_{12}$ is the dimensionless view factor of the hotter component to cooler, and $A_1$ is the area of the hotter component in meters squared. The greatest potential for radiation heat loss within the unit is from the absorber plates to the surrounding components or environment. The largest temperature difference between components will be a clear sky during nighttime conditions, where the effective sky temperature is correlated [Duffie 2006] as

$$T_s = T_a[0.711 + 0.0056T_{dp} + 0.000073T_{dp}^2 + 0.013\cos(15t)]^{1/4} \quad (9)$$

where $T_s$ and $T_a$ are in Kelvin, $T_{dp}$ is the dew point temperature in degrees Celsius, and t is solar time. For ambient and dew point temperature of 0°C, the minimum effective sky temperature is 194 K. With the absorber plates cooled to 10°C at night, an emitting surface area of 2.3 $m^2$, a view factor of 0.5 from the face to the sky temperature, an emissivity of 0.05 for the black chrome coat, a blackbody absorption of 1.0 for the sky, and an effective sky temperature of 194 K, the heat loss according to Equation 8 is 16.3 Watts.

Equation 8 only produces significant heat transfer values for large temperature differences. The largest temperature difference between components within the unit where radiation heat exchange is possible (in view of each other) would be between the absorber plate and the aluminum frame during insolation with low ambient temperatures. For the case of the absorber plate at 34°C (hottest temperature measured during testing) and the aluminum frame at approximately ambient temperature of 0°C, a view factor at a conservative 0.15, emissivity of 0.05, absorption for rough aluminum of 0.65, and an emissive surface area of 1 $m^2$, heat transfer occurs at 1.42 Watts. This conservative

calculation for a worst-case radiation heat exchange scenario justifies neglecting radiation heat exchange between components inside the solar unit, which are at much closer temperatures.

Figure 2.10 shows a diagram of the system components and thermal connections for the experimental heat pipe model.

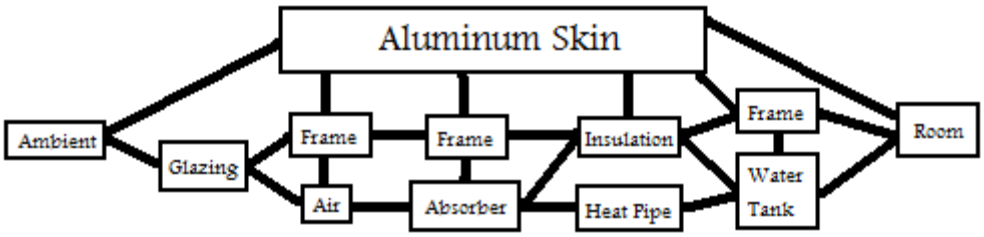


Figure 2.10 – Diagram of System Components and Thermal Connections

In Figure 2.10, every connection is a heat transfer path. Each connection drawn as well as each component itself has a thermal resistance associated with it. The full thermal resistance network is difficult to visualize and has a very large number of components. Accordingly, thermal resistance network was broken down into two main operating conditions, which correspond to two sources of heat. Under insulating conditions, the source of heat is the room. Under heating conditions, the source of heat is the absorber, where radiation is absorbed.

The thermal network used to analyze the insulation value of the unit is shown in Figure 2.11.

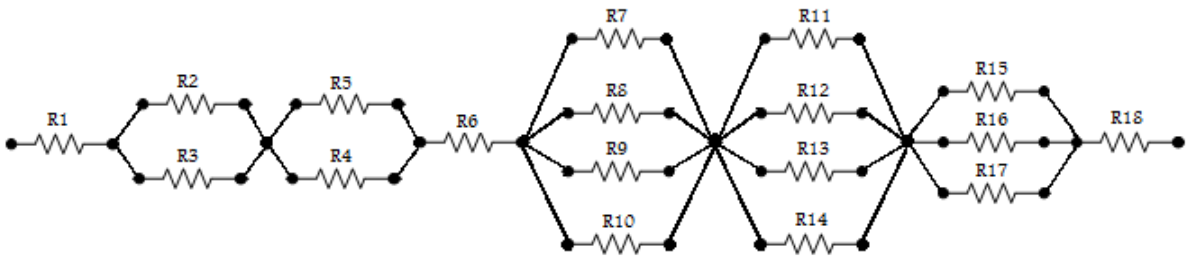


*Figure 2.11 – Thermal Resistance Network under Insulating Operating Conditions*

The system components and their corresponding calculated theoretical thermal resistances for insulating conditions are shown in Table 2.1

*Table 2.1 – System Components and Thermal Resistances under Insulating Conditions*

| Figure 2.1 Label | Thermal Resistance Component | Thermal Resistance (K/W) |
|---|---|---|
| R1 | Glazing External Convection | 0.1463 |
| R2 | Aluminum Frame Conduction | 0.0018 |
| R3 | Glazing Conduction | 0.0009 |
| R4 | Aluminum Frame Conduction | 0.0145 |
| R5 | Glazing and Absorber Convection | 4.8476 |
| R6 | Aluminum Frame Conduction | 0.0000072 |
| R7 | Aluminum Frame Conduction | 0.0290 |
| R8 | Mineral Wool Conduction | 0.5735 |
| R9 | Adiabatic Refrigerant Conduction | 283.3533 |
| R10 | Adiabatic Heat Pipe Conduction | 0.1751 |
| R11 | Aluminum Frame Conduction | 0.0217 |
| R12 | Styrofoam Conduction | 0.6194 |
| R13 | Adiabatic Refrigerant Conduction | 212.5150 |
| R14 | Adiabatic Heat Pipe Conduction | 0.1313 |
| R15 | Aluminum Frame Conduction | 0.2304 |
| R16 | Mineral Wool Conduction | 4.0485 |
| R17 | Internal Water Tank Convection | 0.1784 |
| R18 | Rear Cover Convection | 0.1767 |

The values in Table 2.1 can be somewhat deceiving since they are area intensive. That is, a very high thermal resistance may not be a relatively high thermal insulator when the cross-section across which it occurs is large. An example is that the thermal resistance of the mineral wool (R16), which is a thermal insulation building material, is less than that of the stationary refrigerant within the adiabatic section of the heat pipes (R9 and R13). Thermal resistance of the heat pipe is difficult to calculate theoretically due to possible convection heat transfer. However, this would incur small error since the thermosyphon within the heat pipe during insulating conditions would keep fluid relatively stationary. The thermal resistance of the heat pipe during heating conditions will be neglected due to its relative insignificance when compared to other system components. This is in agreement with industry standard for modeling heat pipes as isothermal.

The thermal resistances of system components in series are added. However, thermal resistances in parallel are determined by

$$R_{th} = \frac{1}{\frac{1}{\mathrm{R_1}} + \frac{1}{\mathrm{R_2}} + \cdots \frac{1}{\mathrm{R_n}}} \tag{10}$$

where $R_{th}$ is the equivalent thermal resistance in K/W, and $\mathrm{R_n}$ represents the thermal resistance of the nth component in the parallel heat flow path.

A standard unit of measure of thermal insulation for building heating and cooling load calculations is the R-value. The equivalent R-value of the experimental unit is

$$R_{eq} = R_{tot} A_{tot} \frac{10.764}{3.4121} * \frac{9}{5} \tag{11}$$

where $R_{eq}$ is the industry standard R-value in $\frac{hrs\, ft^2 F}{Btu}$, $R_{tot}$ is the total thermal resistance of the model in degrees Kelvin per Watt, $A_{tot}$ is the total cross-sectional area of the unit

normal to heat flow in meters squared, 10.8 is the number of square feet per square meter, 3.41 is the number of Btu's per hour per Watt, and $\frac{9}{5}$ is the ratio of change in degrees Fahrenheit to change in degrees Kelvin. The equivalent R-value of the experimental heat pipe augmented solar wall is a value of R-7.04.

This insulating value is significantly lower than a production unit because of heat loss through the aluminum frame. If a structural material such as high density polyethylene were to be used instead of the aluminum frame construction, the insulation value of the experimental model construction would be R-26.0. The tooling and equipment costs required to produce a unit with the supporting structures of high density polyethylene or other structural polymer were too great for the research budget. The start-up costs of a mass production facility of these units would readily include the equipment costs associated with producing units with a much higher insulation value.

Performance during the daytime when heat is being gained is essentially the same for the prototype as for the production unit with a higher R-value. During heat gain, the heat transfer inward through the insulation is small with either R-value compared to the heat transfer through the heat pipe. Performance is only different when energy is being lost from inside the house to ambient conditions. Operating performance prediction for an equivalent unit with higher insulation value is not underestimated by these insulation values for heat gain insolation values. During heating conditions, heat is added to the absorber plate by solar radiation. This heat is either transferred into the thermal mass of the unit and is heat gain to the building or lost to external surroundings. Any heat transfer back to ambient conditions reflects inefficiencies in the unit. Thus the thermal efficiency

of the unit is defined by the heat gained versus the heat available. The thermal resistance network from the absorber plate during heating conditions is shown in Figure 2.12.

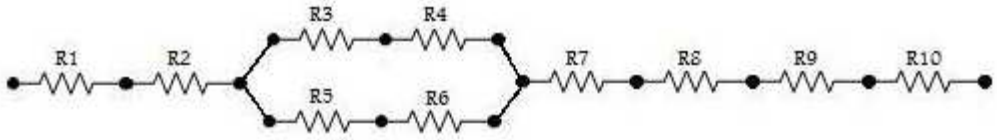


*Figure 2.12 - Thermal Resistance Network under Heating Conditions*

The system components and their corresponding calculated theoretical thermal resistances for heating conditions are shown in Table 2.2.

*Table 2.2 – System Components and Thermal Resistances under Heating Conditions*

| Figure 2.15 Label | Thermal Resistance Component | Thermal Resistance (K/W) |
|---|---|---|
| R1 | Glazing External Convection | 0.1463 |
| R2 | Aluminum Frame Conduction | 0.0145 |
| R3 | Interfacial Conduction | 0.1500 |
| R4 | Aluminum Frame Conduction | 223.6547 |
| R5 | Aluminum Frame Convection | 2.1546 |
| R6 | Absorber Plate Convection | 0.0834 |
| R7 | Interfacial Conduction | 0.0200 |
| R8 | Heat Pipe Conduction | 0.0025 |
| R9 | Heat Pipe  Convection | 0.0000 |
| R10 | Rear Cover Convection | 0.1767 |

The Nusselt number [Incropera *et al.* 2007] for free convection from the heat pipe condenser to the water tank is governed by

$$\overline{Nu} = \left\{ 0.60 + \frac{0.387 Ra^{\frac{1}{6}}}{\left[1+(0.559/\mathrm{Pr})^{\frac{9}{16}}\right]^{\frac{8}{27}}} \right\}^2 \qquad (12)$$

Design of the experimental model focused on thermal efficiency of heat transfer from the absorber plates into the thermal mass. These design aspects included plastic spacers used in the aluminum absorber plate mounts to reduce the conduction heat transfer path from the absorber plates to the mounting frame. Through the use of these spacers, the only conduction heat flow from the absorber plates is through the aluminum mounting screws, and the heat flow area was reduced from 0.0387 $m^2$ (60 $inches^2$) to 1.36 x $10^{-5}$ $m^2$ (0.0211 $inches^2$). The value for thermal resistance R4 in Table 2.2 reflects the impact of reducing the heat transfer conduction cross-section by this amount. As is evident from the total insulation value of the unit, this 99.97% reduction in heat loss path due to conduction through aluminum is very effective in isolating the heat flow path into the thermal mass. The insulation value of the components that lead to heat gain into the building is R-3.30. These consist of the absorber plate, heat pipe, and water tank. The insulation value of the components that lead to inefficiencies in heat gain is R-35.3, which consists of mostly interfacial heat transfer from the absorber plate mounting hardware to the frame of the unit. This thermal resistance is quite high because of the plastic spacers used to isolate the absorbers, thus only allowing the cross-section of three aluminum screws per absorber plate to allow conduction heat flow.

The thermal resistance of the heat pipe in Table 2.2 (R9) was averaged from data for experimental heat pipes [Dunn 1976, Corliss 1979, Albanese 2008] to predict performance. A thermal resistance model of a heat pipe is shown in Figure 2.13. The value in Table 2.2 reflects a single equivalent thermal resistance from the network shown below.

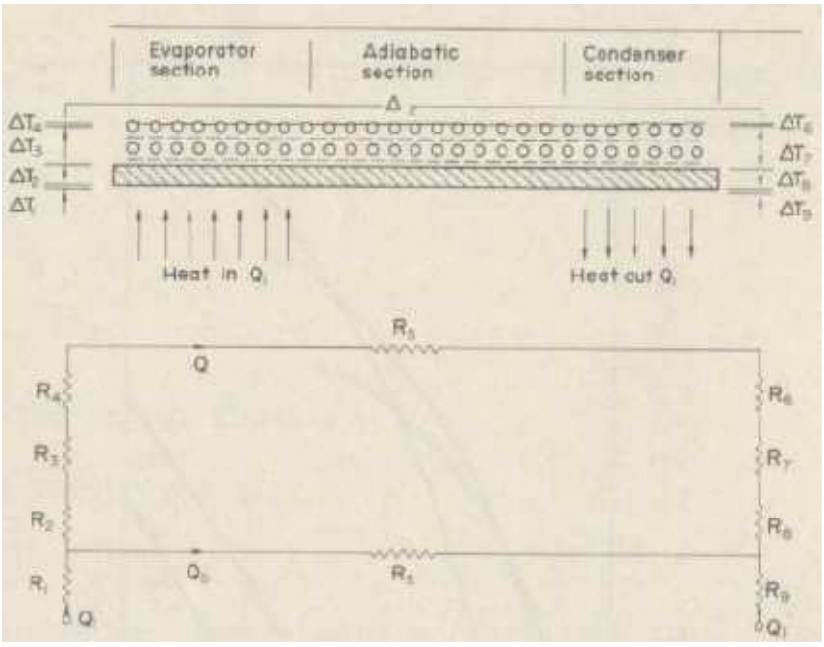


*Figure 2.13 – Thermal Resistance Model of a Heat Pipe [Dunn 1976]*

## D. Instrumentation

A total of 32 data lines were connected to the experimental heat pipe augmented solar wall to analyze the thermal efficiency of the unit under heating and insulating conditions. 31 T-type thermocouples with a selective limit of error were placed in key locations in the unit. All thermocouple lines consisted of 2.44 m (8 feet) of thermocouple lead wire soldered to 36.6 m (120 feet) of heavier gauge thermocouple extension wire. The central unit of the five heating units was singled out to be analyzed to a much higher degree than the others. This was chosen because of its equivalence to two of the other

heating units, and because the center heating element is expected to provide more predictable results because of reduced edge effects. That is, the center heating unit most closely represents the average heating properties of the total five units.

Eight thermocouples were placed on the absorber plate of the central heating unit, with four above the heat pipe groove and four below, along the heat flow paths of the unit to analyze its conductivity and heat gain. Thermocouple placement on the absorber plate is shown in Figure 2.14.

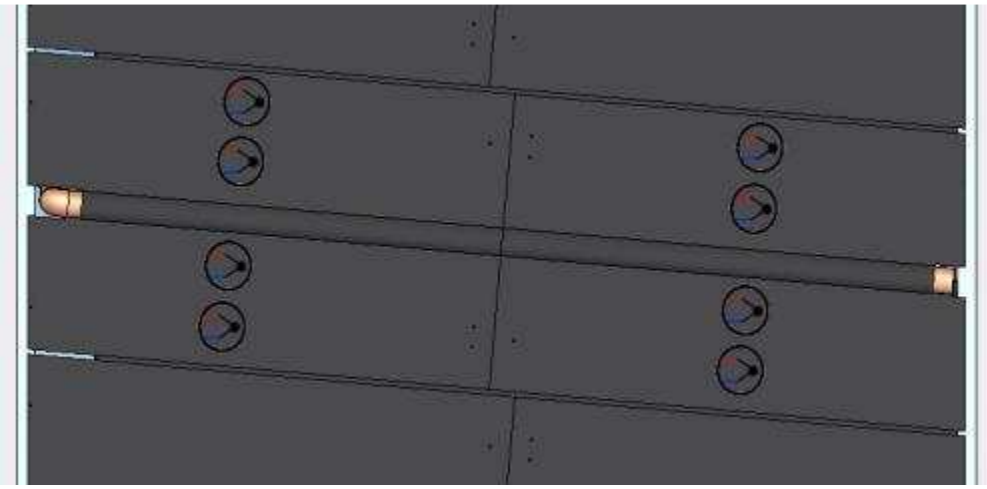

*Figure 2.14 – Absorber Plate Thermocouple Placement*

Eight thermocouples were soldered to the copper heat pipe: three along the evaporator, two along the adiabatic section, and three along the condenser. Thermocouple placement along the heat pipe is shown in Figure 2.15.

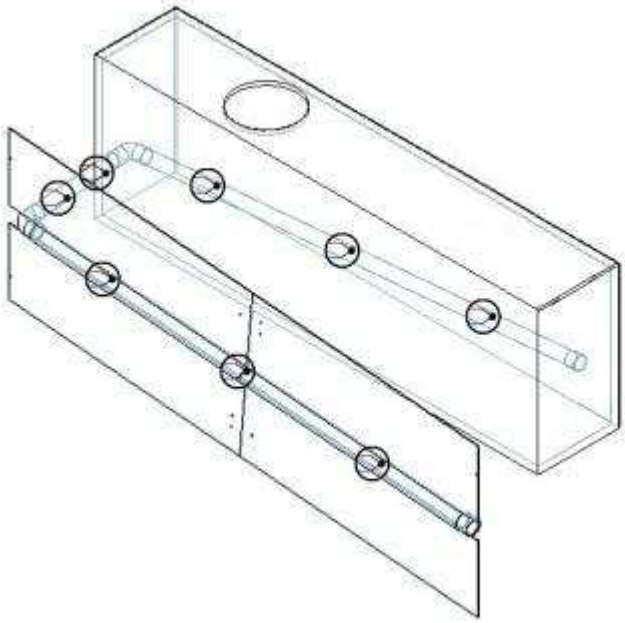

*Figure 2.15 – Thermocouple Placement on Heat Pipe*

Eight thermocouples were placed in the water tanks at various depths and locations to account for temperature variations in the horizontal direction as well as stratification in the depth of the tank from slight density changes. The depth of each thermocouple was either four inches or eight inches from the bottom surface of the tank. The thermocouples were placed ten inches from each end of the tank, and three inches apart centered on the cross-section of the tank. The thermocouple placement in the water tank is shown in Figure 2.16.

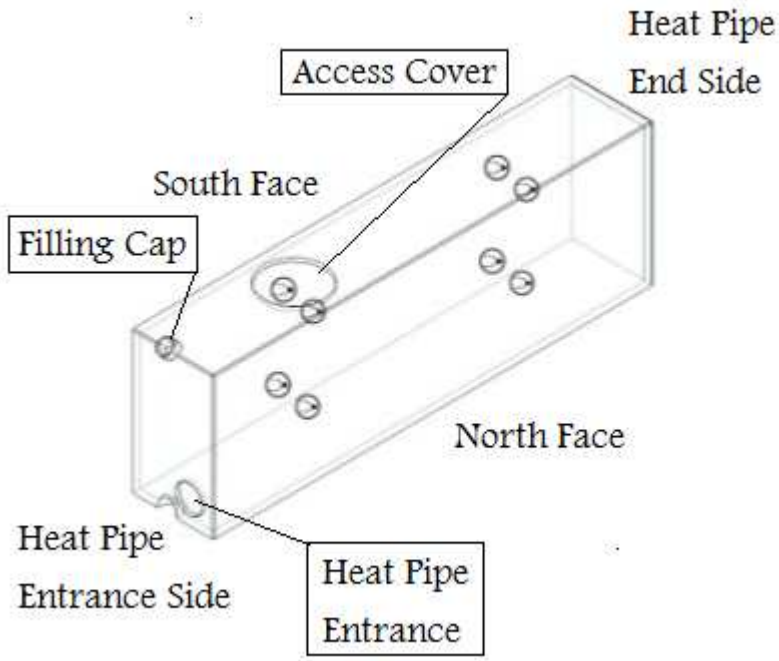


*Figure 2.16 – Water Tank Thermocouple Placement*

Two thermocouples were used to measure ambient and room temperature. Five thermocouples were placed in the water tanks of the four remaining heating units to measure the heat gain per heating unit. Four were placed at the lower rear heat pipe entrance side of the tank of each remaining tank, and the fifth thermocouple was placed at the upper rear heat pipe entrance of the water tank second from the top. Stratification with depth and horizontal location in the thermal mass was approximated using the data gathered from the center heating unit's water tank and applied to the other tanks to determine the temperature distribution.

It should be noted that all thermocouples were thermally insulated from surroundings that may have affected the validity of measurement, such as air temperature for the absorbers or water temperature for the condenser section of the heat pipe.

Insulating the thermocouples along the heat pipe consisted of several layers of electrical tape. Insulating on the absorber consisted of using plastic spacers along with an aluminum nut and bolt to clamp the thermocouple tip tightly to the absorber face for maximum conduction. This was then painted over to both protect the black chrome surface from humidity and also to further insulate the thermocouple from air temperature.

A Kipp & Zonen CM3 solar pyranometer was used to measure the insolation values during the experiment. The pyranometer and mounting is shown in Figure 2.17. The pyranometer was mounted on a vertical plane above the experimental unit to measure the amount of available radiation striking the surface of the unit. The pyranometer was 0.0508 m (2 inches) above the unit and centered horizontally. It may be noted that mounting the pyranometer on a parallel plane with the face of the unit allows variables such as ground reflectance, view factors, and horizon brightening all to be accounted for in the measurement, instead of measuring the available sky radiation and approximating these variables. These approximations would lead to much greater uncertainty in efficiency calculations.

*Figure 2.17 – Kipp & Zonen CM3 Pyranometer and Mounting*

All data was collected using a National Instruments SCXI platform in conjunction with a low-voltage thermocouple-designed SCXI-1102/B/C module. A SCXI-1600 analog to digital converter was used for the analog data inputs. LabVIEW software was used in conjunction with the data acquisition hardware to sample and log the data. The raw data collected is available in and a copy of the LabVIEW program is available on the CD in Appendix III.

## E. Procedure

### 1. Testing of Insolation Variation Across Receiver

The variation of solar insolation values across the absorber surfaces of the unit was tested to ensure accurate characterization of available radiation heat. This testing was performed with the use of three Kipp and Zonen CM3 pyranometers. The pyranometers

were placed as close as possible in front of the absorber plates of the experimental unit. Radiation data was collected at 1.0 Hz for three minutes. The data collected was used to develop a calibration so each pyranometer gives the same solar flux reading when operating under identical conditions. Next, the pyranometers were placed in several different horizontal and vertical configurations to test the insolation distribution across the absorber surfaces. Each of these orientations was tested at 1 Hz for a minimum of two minutes. The vertical and horizontal configurations tested are shown in Figure 2.18 and Figure 2.19, respectively.

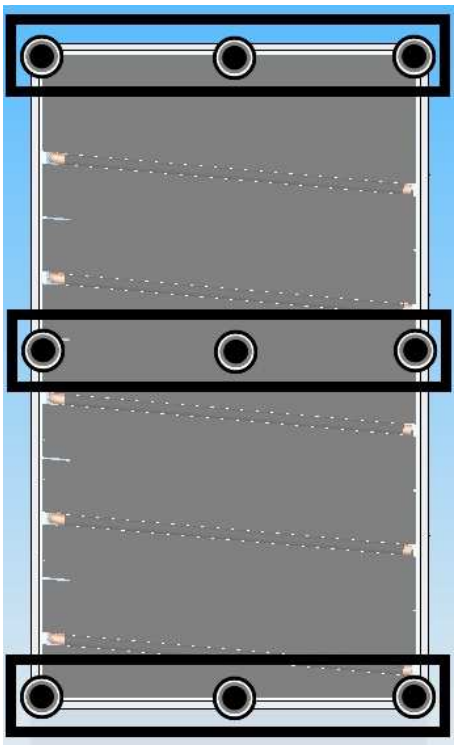

*Figure 2.18 – Insolation Distribution Horizontal Configurations Tested*

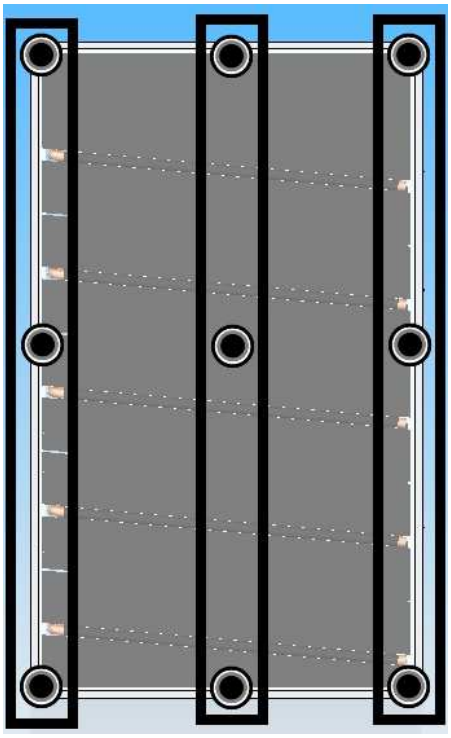

*Figure 2.19 – Insolation Distribution Vertical Configurations Tested*

The data collected from the horizontal and vertical configurations was used to determine the existence and value of radiation gradients in any direction across the absorber surfaces. These gradients would help to accurately predict the total solar radiation striking the experimental unit from the single pyranometer used during operating conditions.

2. Experimental Model Testing Conditions

The heat pipe augmented solar wall experimental model was installed on the Shelby campus at the University of Louisville at latitude of 38.18 degrees North. The installation was in a second-story window enclosure on a south-facing wall. The outer face and inner face of the installed experimental unit is shown in Figures 2.20 and 2.21, respectively.

*Figure 2.20 – External Facing of Experimental Model*

*Figure 2.21 – Internal Facing of Experimental Model*

The experimental unit was tested under actual weather conditions from April 1 – 21, 2009. The weather for these three weeks varied greatly, which is typical for Ohio Valley weather conditions. Conditions tested included temperatures as low as 4°C, and as high as 24°C. Sky conditions varied between raining, clear, and even snowing. Likewise ground conditions varied between the before mentioned range, which slightly influenced the amount of incident radiation on the absorber surfaces by the varying ground reflectance values. These highly fluctuating weather conditions represent excellent testing conditions for the heat pipe augmented unit, which has insulation advantages over other passive solar systems. Also, testing under these conditions will provide solid evidence for the viability of solar technology in "less than ideal" climates where cool and

cloudy weather is typical. Reported weather conditions for the testing period can be seen in Appendix VIII.

3. Operational Testing Procedure

The experimental model was tested and data gathered using the previously described data acquisition system. After the unit was installed, the integrity and validity of all data measurement transducers was tested. This was accomplished for the thermocouples by the use of ambient temperature measurement with a thermometer, and the pyranometer was calibrated through the use of zero insolation conditions at night.

Operational performance data was taken at 0.01667 Hz (one sample per minute) for three weeks in March and April. Data acquisition was stopped intermittently to retrieve data from the program for analysis. However, down time in which data was not being collected was kept to as little time as possible to ensure accurate data trending. Due to the very slow time response of the system to radiation and temperature changes, for down times less than 30 minutes in which significant events such as sunrise, sunset, or large ambient temperature variations did not occur, missing data was interpolated for the system. Interpolated data will be identified as such in the results.

# III. RESULTS

## A. Insolation Variation

Data was collected to calibrate three pyranometers used to detect the direct radiation insolation variation across the receiver surface of the experimental model. This data was collected with the pyranometers as close as possible to receive equivalent insolation values. The raw data used to develop calibration factors is shown in Figure 3.1.

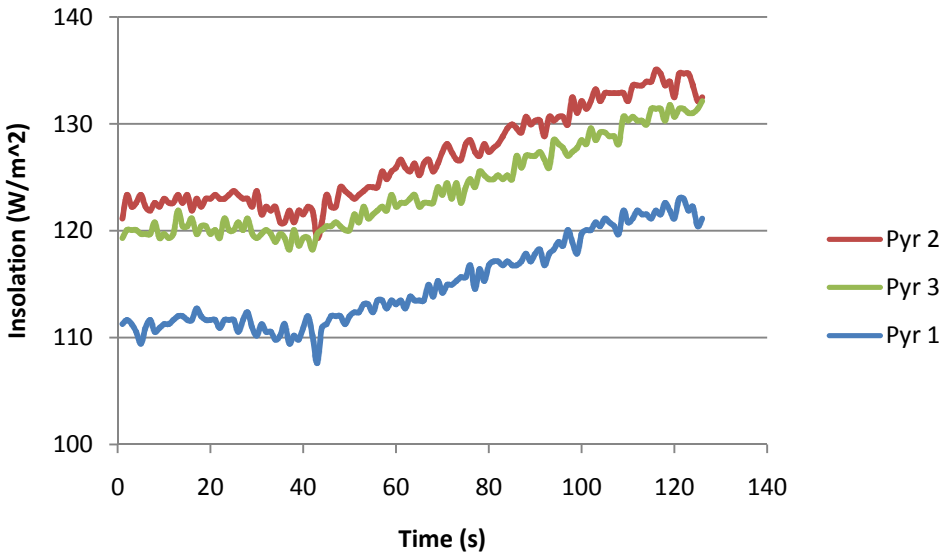


*Figure 3.1 – Raw Calibration Data for Insolation Distribution*

Pyranometer 1 was nominally chosen as the standard for determining the calibration offset. The offsets for pyranometers 2 and 3 were calculated by the average of the difference between the value indicated and the value indicated by pyranometer 1. The offsets for pyranometers 2 and 3 were determined to be 15.95 and 11.56 W/m$^2$, respectively. Offset calibration data is shown in Figure 3.2. Accordingly, any subsequent data for insolation variation reflects these offsets.

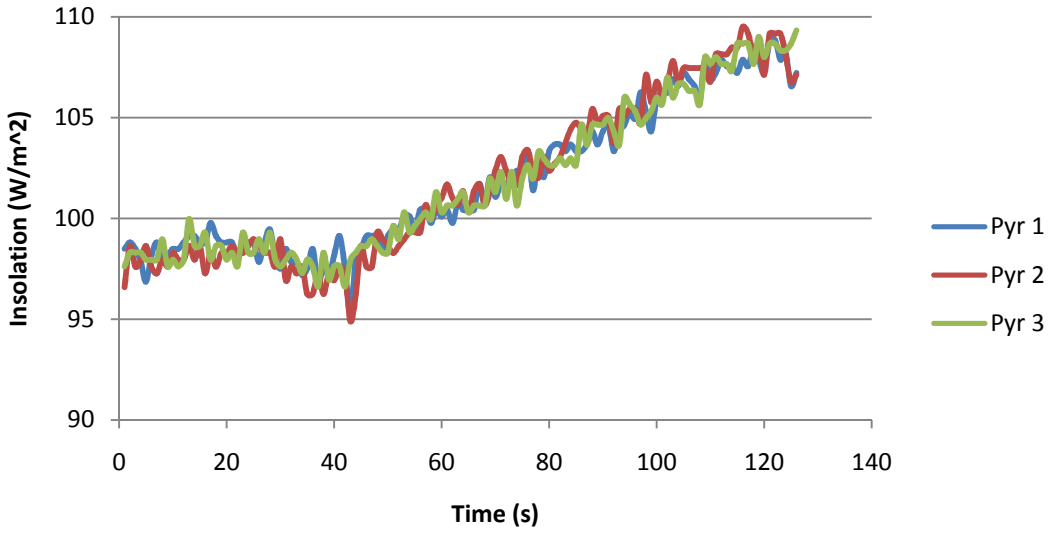


*Figure 3.2 – Calibration Data with for Insolation Distribution with Offsets*

The layouts of the pyranometers 1-3 for each directional gradient are shown in Figures 2.18 and 2.19. The radiation distribution for the center horizontal section of the unit is shown in Figure 3.3.

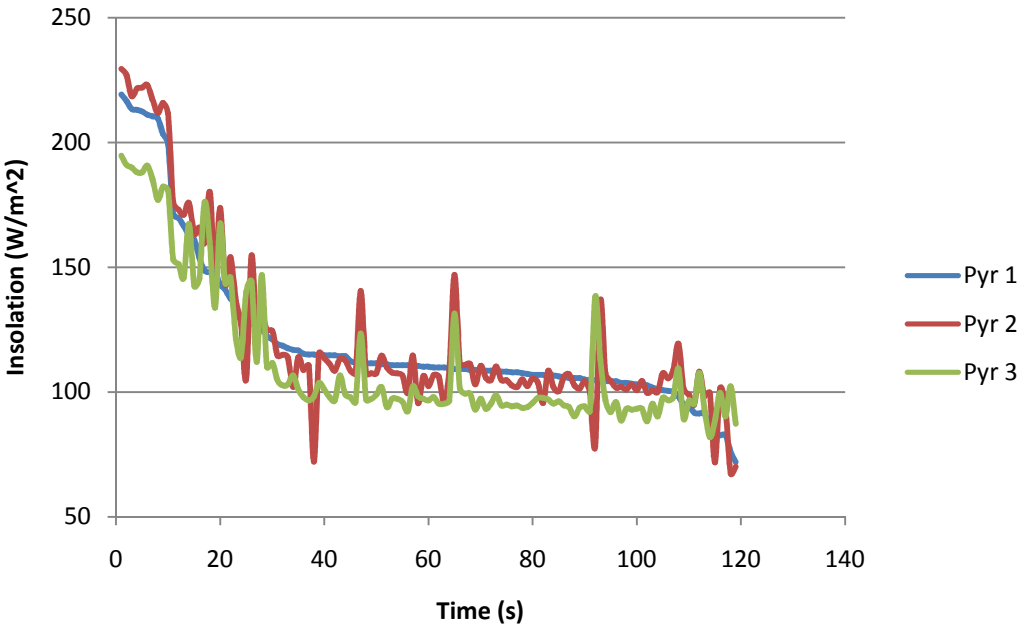


*Figure 3.3 – Offset Radiation Distribution for the Center Horizontal Section.*

The offset radiation distribution for the center vertical section of the unit is shown in Figure 3.4.

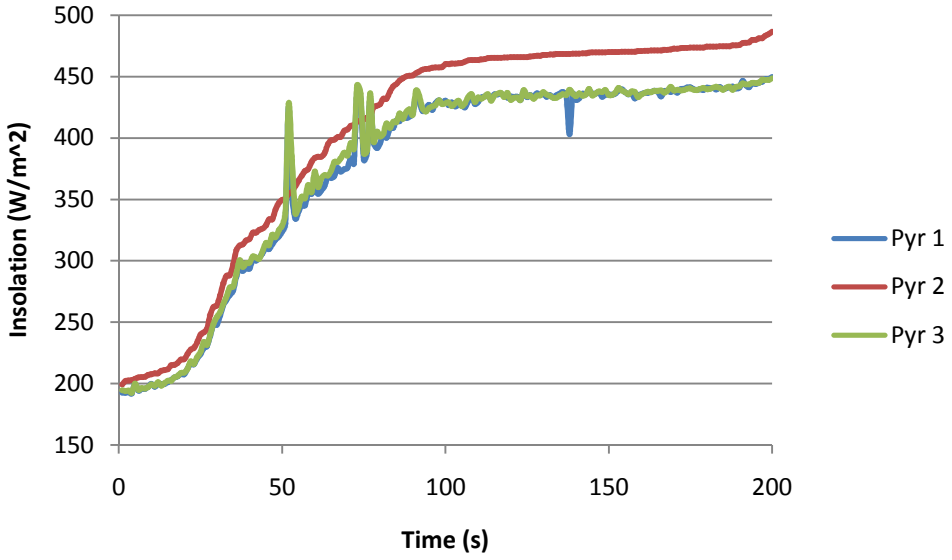


*Figure 3.4 – Offset Radiation Distribution Data for the Center Vertical Section*

Relative radiation factors were generated for the relative radiation distribution across the absorber plate and normalized to the top center location where pyranometer measurements were taken. The relative radiation factor for each area is the ratio of radiation received on the area versus the amount of radiation received on the top center section, where radiation is being measured. The results are shown in Table 3.1.

*Table 3.1 – Relative Radiation Factors for Pyranometer Readings*

| | Left | Center | Right |
|---|---|---|---|
| Top | 0.993 | 1.000 | 0.929 |
| Center | 1.062 | 1.069 | 0.994 |
| Bottom | 0.999 | 1.006 | 0.935 |

These relative radiation factors were averaged to obtain a multiplication factor of 1.02 for the total available radiation available on the receiver surface with an uncertainty of 2.83%. This multiplication factor represents the ratio of the average radiation across the absorber surface versus the radiation read by the pyranometer.

It should be noted that these values are only valid when the pyranometer (which is placed directly above the experimental model) is exposed to the direct component of radiation. The placement of the pyranometer above the experimental model is practical for winter heating conditions in which the sun is low in the sky. However, during testing periods in April, the sun was high enough in the sky for an overhang on the roof of the building to cause a portion of the upper absorber plate to be shaded, including the pyranometer, which led to incorrect insolation value readings during certain solar conditions.

Complete measurements for solar insolation were available during times in which the pyranometer was not shaded. Transition from the pyranometer being shaded to unshaded corresponded to when the zenith angle was equal to the angle from the overhang to the pyranometer. The overhang was 0.635 m (25 inches) vertically above the pyranometer, and projected 0.705 m (27-3/4 inches) horizontally from the wall. By trigonometric relations, the minimum zenith angle for direct radiation to strike the pyranometer is 47.98°. For the testing period of April 1 – 21, the earliest time at which accurate insolation measurement is available is

$$\cos\omega = \frac{\cos\theta_z - \sin\phi sin\delta}{cos\phi cos\delta} \tag{1}$$

where $\omega$ is the hour angle in degrees at 15° per hour from solar noon, $\theta_z$ is the zenith angle equal to 48.0°, $\phi$ is the latitude of Louisville equal to 38.3°, and $\delta$ is the declination in degrees. The declination is

$$\delta = 23.45 \sin\left(360 \frac{284+n}{365}\right) \tag{2}$$

where n is the day of the year equal to 111 for April 21st, which is the constraining case for these criteria, since the zenith angle of the sun at a given time is rising daily during this time of year. The declination for April 17th is 10.1°. Equations 1 and 2 yield accurate pyranometer measurement after 2:54 PM solar time for any day preceding or including April 21st. Standard time in relation to solar time is

$$Standard\ Time = Solar\ Time - 4\ (L_{st} - L_{loc}) - E \tag{3}$$

where $L_{st}$ is the standard meridian for local time equal to 75 degrees west for Eastern Standard Time, $L_{loc}$ is the local longitude of Louisville equal to 85.759 degrees west, and

E is the variation from the earth's elliptical orbit equivalent to -2.5 minutes. This yields a local time of 3:46 PM or later for accurate measurement through April 21st.

By the same argument, these calculations imply no shading before 9:46 AM for the same dates. However, a brick extension immediately east of the experimental model shaded a portion of the unit until solar noon. For this reason, calculations for the conductivity of the unit during heating conditions which require insolation values will only be made for periods which fall into this category. This does not include overnight conditions where the conductivity values of the heat pipe may still be calculated for heat losses, but only calculations that refer to heat gain from the absorber plates.

## B. Water Tank Stratification

Temperatures measured in the middle tank of the five heating units under a single heating and cooling cycle are shown in Figures 3.5 – 3.8. Identification of the water tank descriptions are as follows: The upper and lower portions differentiate between the depth of the thermocouples in the water. The upper portion of the tank was measured at a depth of eight inches in the tank, and the lower portion was measured at a depth of four inches. The north and south faces of the unit describe locations in the tank where south represents the side closest to the absorbers within the unit, and north represents the side of the tank which is visible inside the room. This corresponds to the receiving surface of the unit facing south, since testing location was in the northern hemisphere. The heat pipe enters the water tank closest to the north face (that is, closest to the room). The heat pipe entrance and end sides describe which location along the length of the tank the

thermocouple is reading. Inside the tank, the heat pipe enters at a depth of 3 inches and terminates inside the water tank at a depth of about 7 inches at the other side. See Figures 2.15 and 2.16 for more detail. The location of the heat pipe entrance on the lower north face should be noted in Figure 2.16.

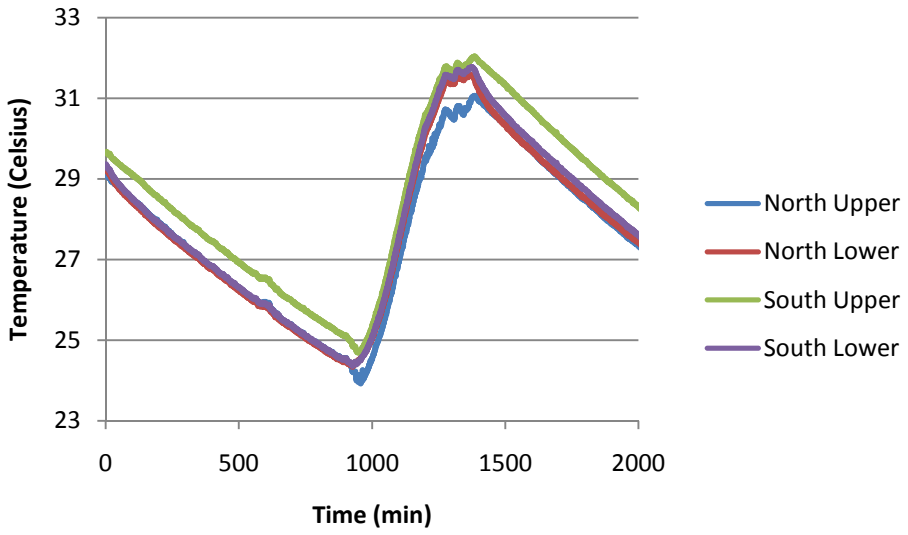


*Figure 3.5 – Temperature Distribution across the Heat Pipe Entrance Side of the Water Tank*

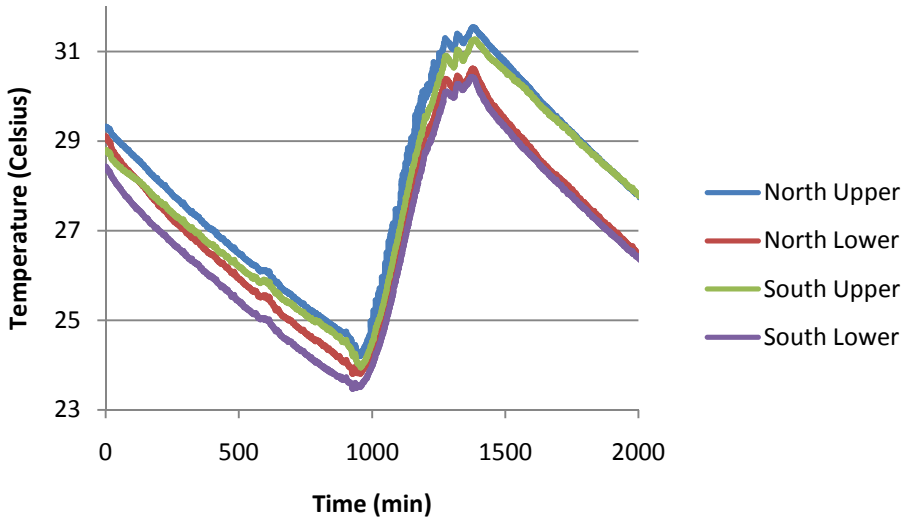


*Figure 3.6 – Temperature Distribution across the Heat Pipe End Side of the Water Tank*

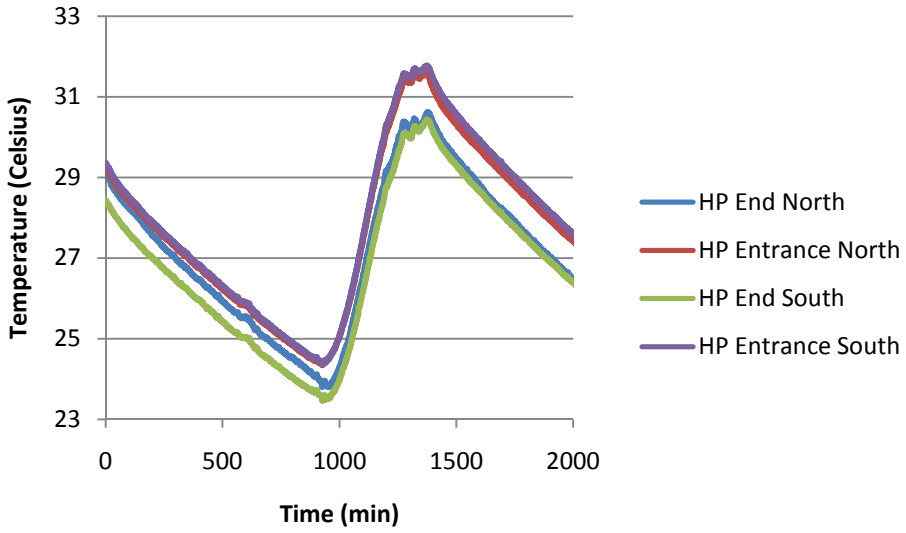


*Figure 3.7 – Temperature Distribution across the Lower Portion of the Water Tank*

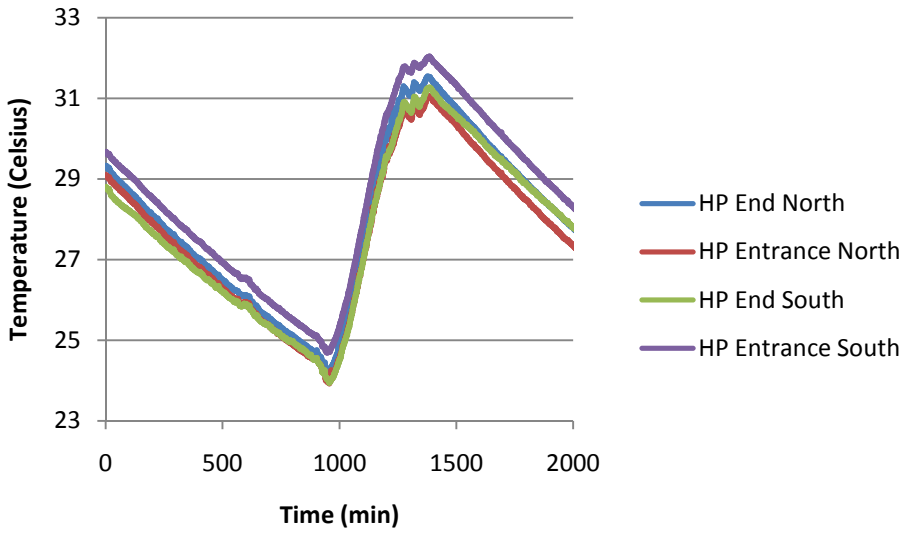


*Figure 3.8 – Temperature Distribution across the Upper Portion of the Water Tank*

In conjunction with the even spacing of the placement of the thermocouples within the tested water tank, the tank temperature which will be used in calculations that use tank temperature will be equal to the average of the tank temperature. Because the thermocouples were spaced evenly in the tank, the mean tank temperature was taken as the average of the thermocouple temperature readings. Since the remaining water tanks had only a single thermocouple each (in the heat pipe entrance rear lower portion of the tank), the mean temperatures of these were estimated by adding the difference between the mean temperature and the rear lower heat pipe entrance temperature found for the middle tank. The mean tank temperature was an average of 1.16 °C colder than the rear lower heat pipe entrance thermocouple with an uncertainty of 18.7%. It should be noted that all data sets which were used to calculate experimental performance were chosen according to the least variability in factors which would minimize the uncertainty of the

calculation, and chosen over sufficiently long periods for determined values to be reliable.

## C. Absorber Plate Thermal Trends

Temperature distribution for the absorber plates under heating and cooling conditions is shown in Figures 3.9 and 3.10. The thermocouple locations are shown in Figure 2.14 and are described as follows: upper and lower describes the location in relation to the heat pipe groove, top and bottom refer to the top or bottom thermocouple on the upper or lower portion on that side of the groove, and the left and right absorber plate describe the left or right side as shown in Figure 2.14.

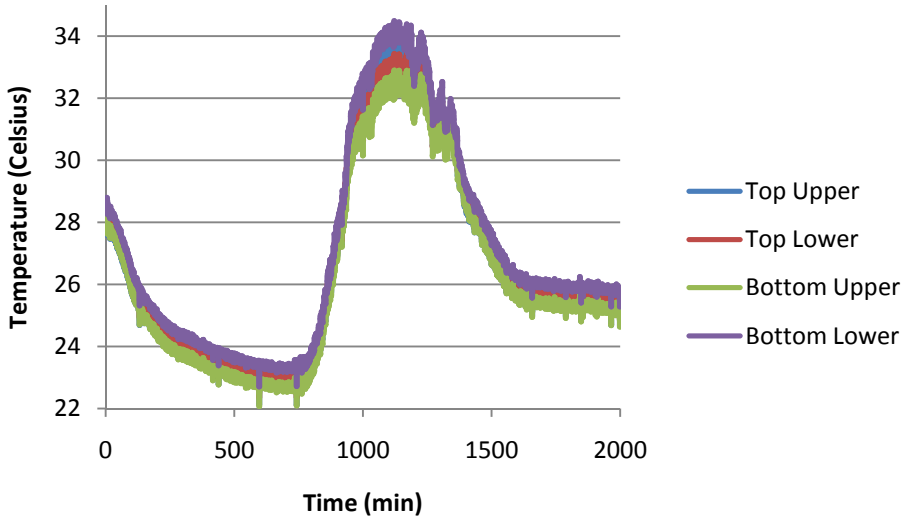


*Figure 3.9 – Temperature Distribution across the Left Absorber Plate*

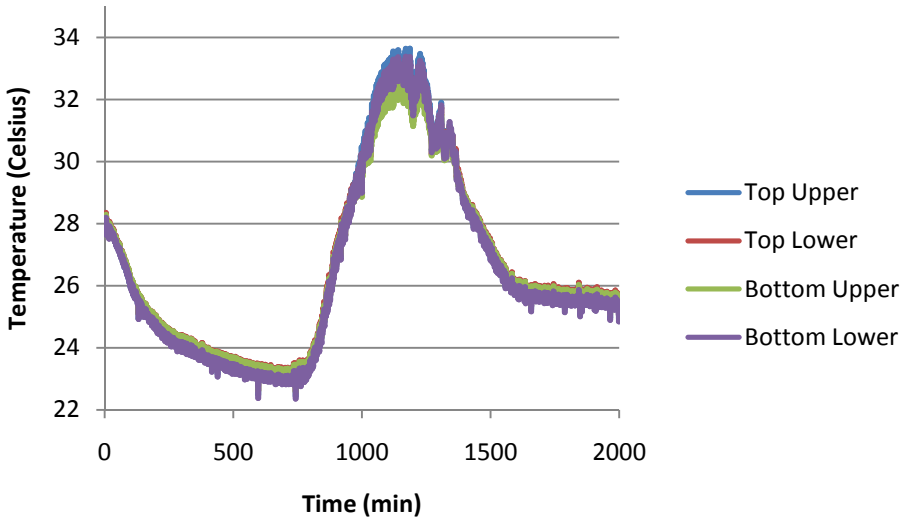


*Figure 3.10 – Temperature Distribution across the Right Absorber Plate*

Figure 3.11 shows all thermocouples along with the average on the absorber plate for a shorter heating period to show temperature variance in more detail. Far and near labels in Figure 3.11 refer to the thermocouple's relative distance to the heat pipe, and exact placement of the thermocouples can be seen in Appendix IX.

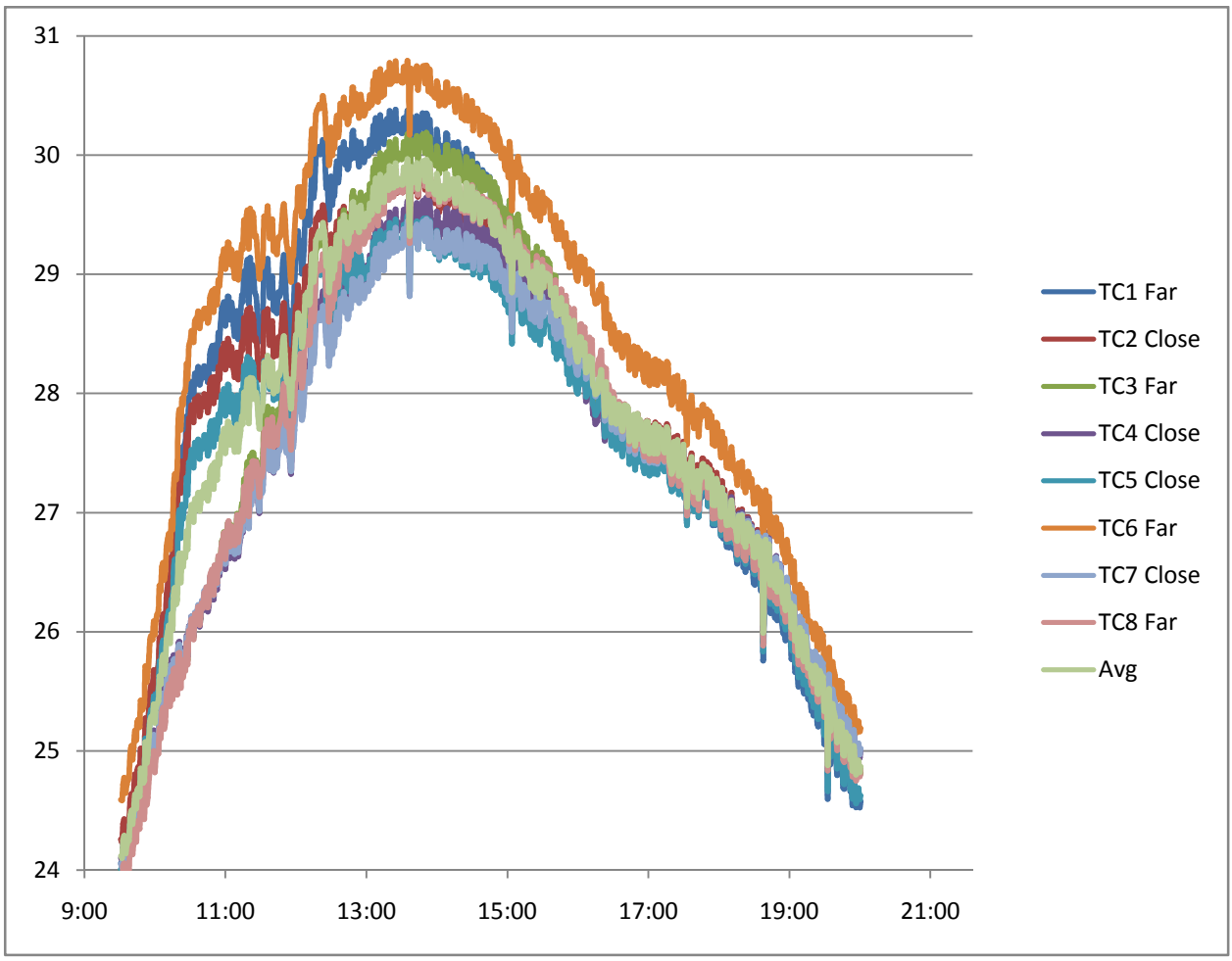


*Figure 3.11 – Absorber Plate Temperature Distribution*

## D. Insulating Performance

Insulation values for the model can be experimentally derived most easily during nighttime when there is no solar radiation and when lower outdoor temperature gives a larger driving temperature difference across the insulation. Figures 3.12 – 3.17 show overnight water tank, room, and ambient temperatures. These six runs were used to determine three insulation values. These runs vary in that they represent independent

values of heat transfer and temperature difference that can be used to solve simultaneously for more than one unknown value.

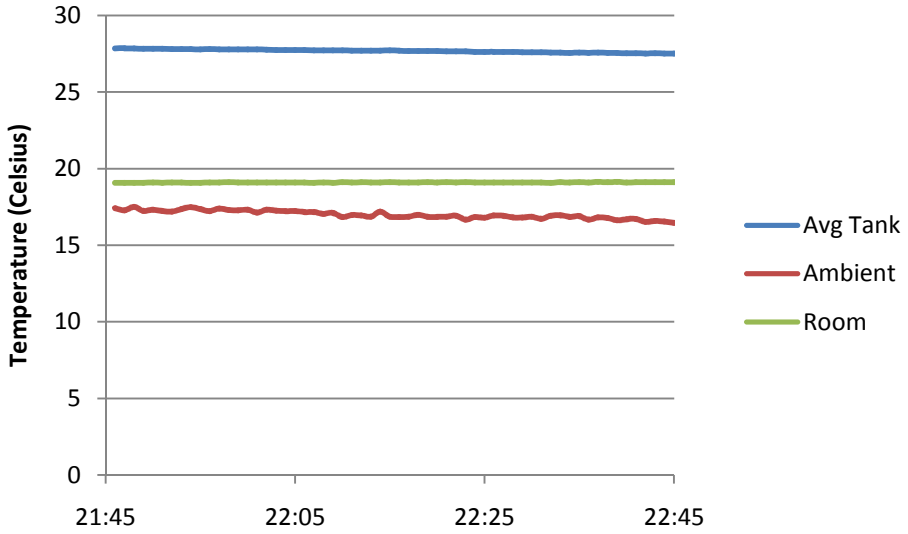


*Figure 3.12 – Run 1a for overnight Water Tank, Room, and Ambient Temperatures*

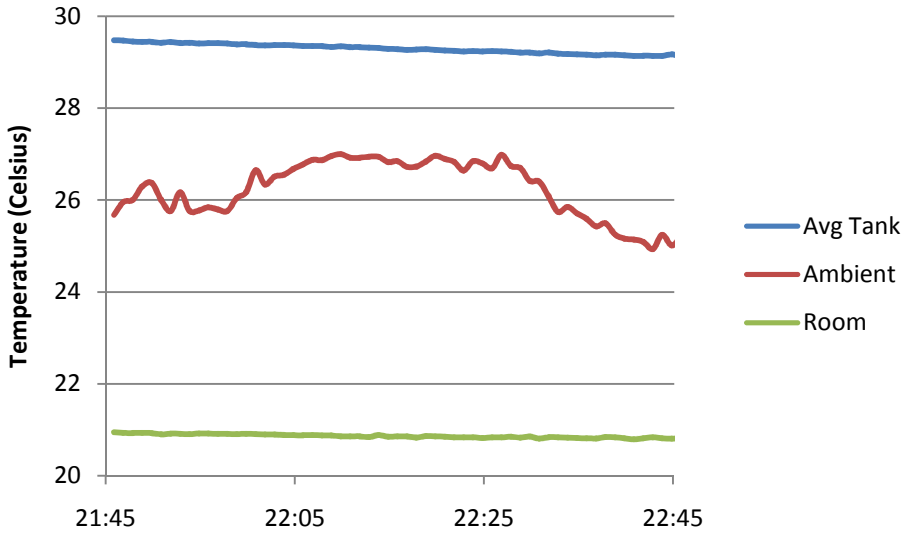


*Figure 3.13 – Run 1b for overnight Water Tank, Room, and Ambient Temperatures*

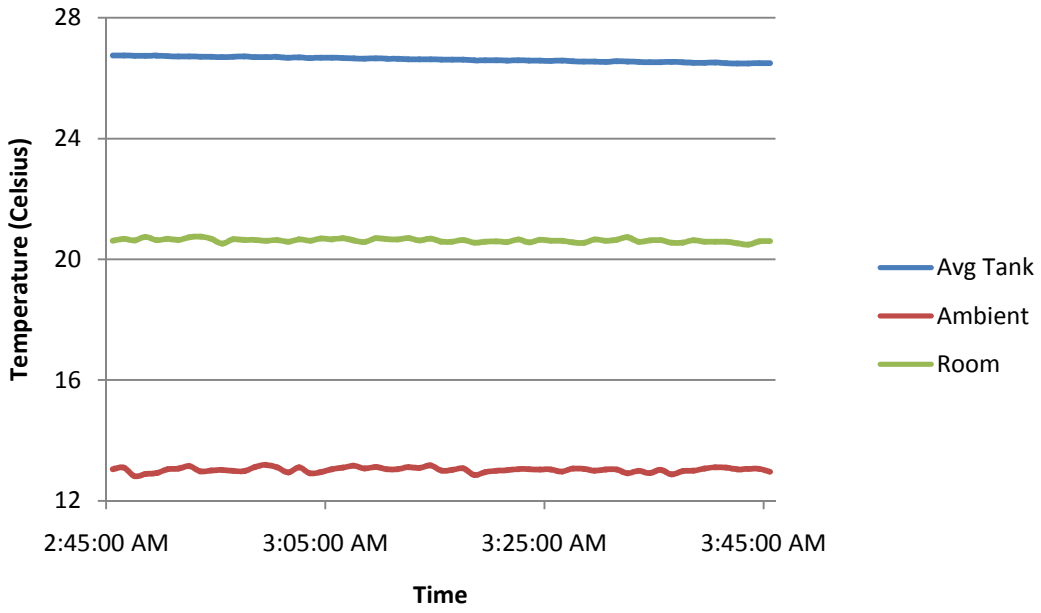


*Figure 3.14 – Run 2a for overnight Water Tank, Room, and Ambient Temperatures*

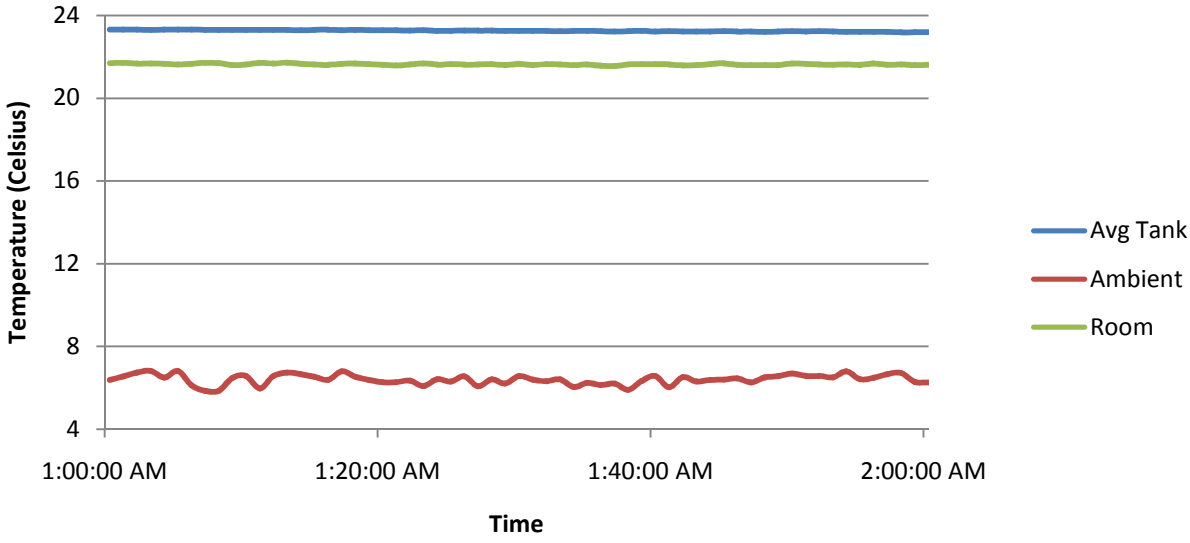


*Figure 3.15 – Run 2b for overnight Water Tank, Room, and Ambient Temperatures*

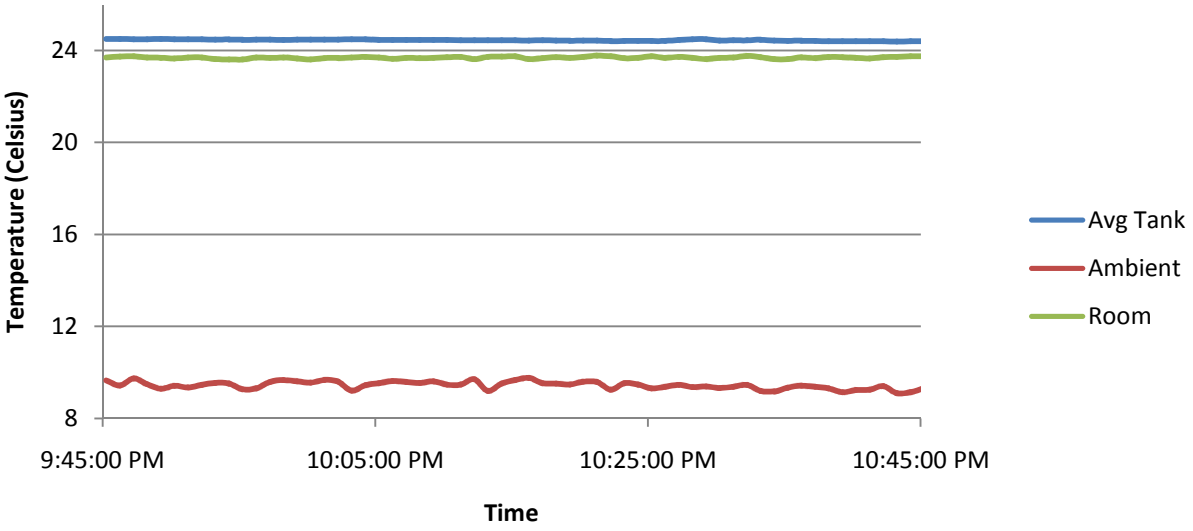


*Figure 3.16 – Run 3a for overnight Water Tank, Room, and Ambient Temperatures*

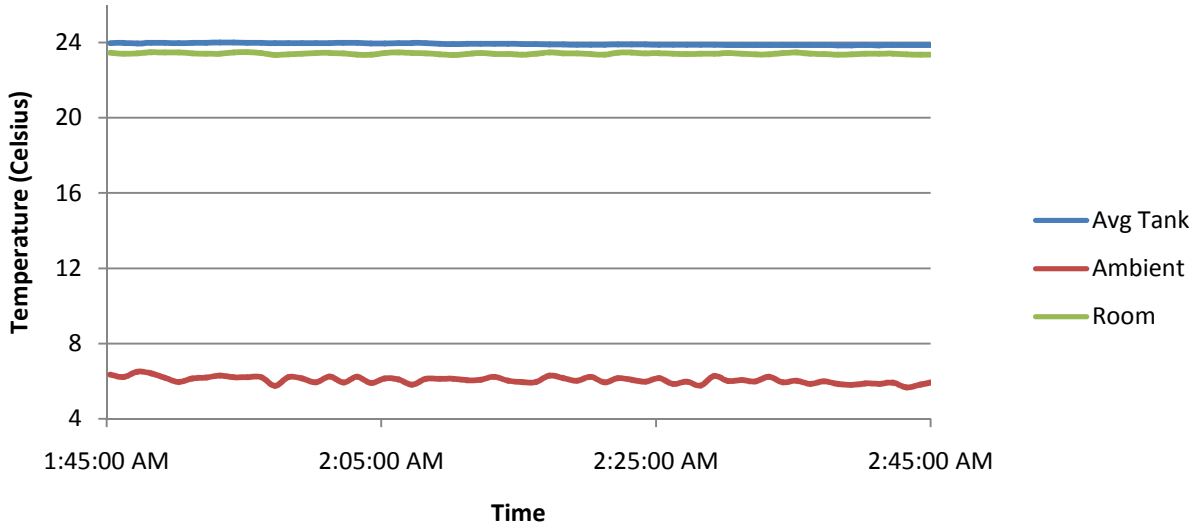


*Figure 3.17 – Run 3b for overnight Water Tank, Room, and Ambient Temperatures*

During insulating conditions, heat is lost from the tank to the room and to ambient conditions. These heat flows are determined by

$$Q_{tank} = \frac{mc_p\Delta \mathrm{T}}{\mathrm{t}} = U_o A_{tot}\Delta T_o + U_i A_{tot}\Delta T_i \quad (4)$$

where $Q_{tank}$ is the heat loss of the thermal mass in Watts, m is the mass of the water in the tank equal to 64.045 kilograms, $c_p$ is the specific heat of water equal to 4180 J/kg K, ΔT is the temperature change in degrees Kelvin, t is the time elapsed in seconds, U is the overall heat transfer coefficient for the heat path in or out in W/m$^2$ K, A is the total cross-sectional area of the unit in m$^2$, and $\Delta T$ is the temperature difference in degrees Kelvin from the ambient temperature to the water tank temperature. Applying Equation 4 to Figures 3.12 – 3.17, the overall heat transfer coefficients for heat out of the system were calculated by using two separate operating points with the two unknown overall heat transfer coefficients to the ambient and the room conditions, $U_{out}$ and $U_{in}$. With two unknowns in Equation 4, two independent sets of a minimum of an hour of data were used for determination of the overall heat transfer coefficient to room and ambient conditions, which are

$$U_{in} = \frac{\frac{Q_{Tank2}}{A} - \frac{Q_{Tank1}\Delta T_{02}}{A\Delta T_{02}}}{\Delta T_{i2} - \frac{\Delta T_{i1}\Delta T_{02}}{\Delta T_{01}}} \quad (5)$$

Data from Figures 3.12 – 3.17 yielded the results shown in Table 3.2.

*Table 3.2 – Insulation Results from Experimental Runs*

| Run | Q (Watts) | Uin (W/m^2 K) | Rin (K/W) | Uout (W/m^2 K) | Rout (K/W) |
|---|---|---|---|---|---|
| 1a | 17.8621 | 7.1230 | 0.3294 | 0.0719 | 32.6112 |
| 1b | 19.6171 | | | | |
| 2a | 19.8699 | 5.9266 | 0.3959 | 0.8171 | 2.8713 |
| 2b | 9.9647 | | | | |
| 3a | 7.7635 | 6.2017 | 0.3783 | 0.8994 | 2.6086 |
| 3b | 8.1948 | | | | |

The first run yielded data for the inside heat transfer coefficient that is close to that of the other data. However, the outside overall heat transfer coefficient for the first run is significantly smaller than the other values. This is most likely due to stagnant ambient conditions which resulted in a smaller convection heat transfer coefficient. This high resistance will be conservatively neglected for system performance prediction, since a higher thermal resistance for heat flow out of the tank results in higher efficiency. The most reliable method for determining the overall heat transfer coefficients is through data correlation. The average of the second and third run yields heat transfer coefficients of 6.42 $W/m^2$ K to the room with an uncertainty of 5.04%, and 0.858 $W/m^2$ K to ambient conditions with an uncertainty of 2.40%. This corresponds to an R-value of 2.09 to the room and 15.6 to ambient conditions.

## E. Heating Performance

Heating period data for the heat pipe system is shown in Figures 3.18 – 3.22. As discussed earlier, valid pyranometer readings are not obtained until past 3:46 PM. Although the radiation at these times may not be large enough for thermal mass temperature increase, using the previously derived heat transfer coefficients for heat out of the tank, we are able to determine the efficiency of conversion of insolation to heat gain.

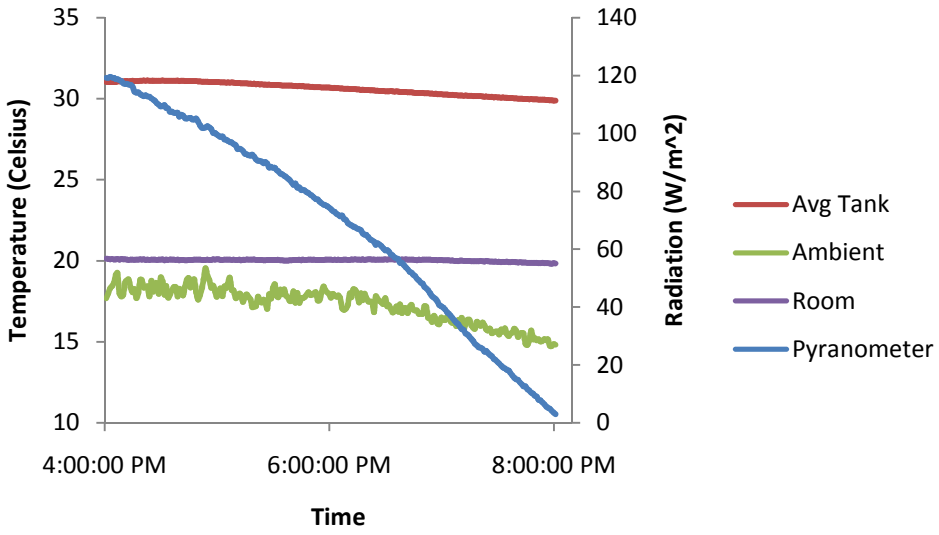


*Figure 3.18 – Run 1 for Experimental Model Efficiency*

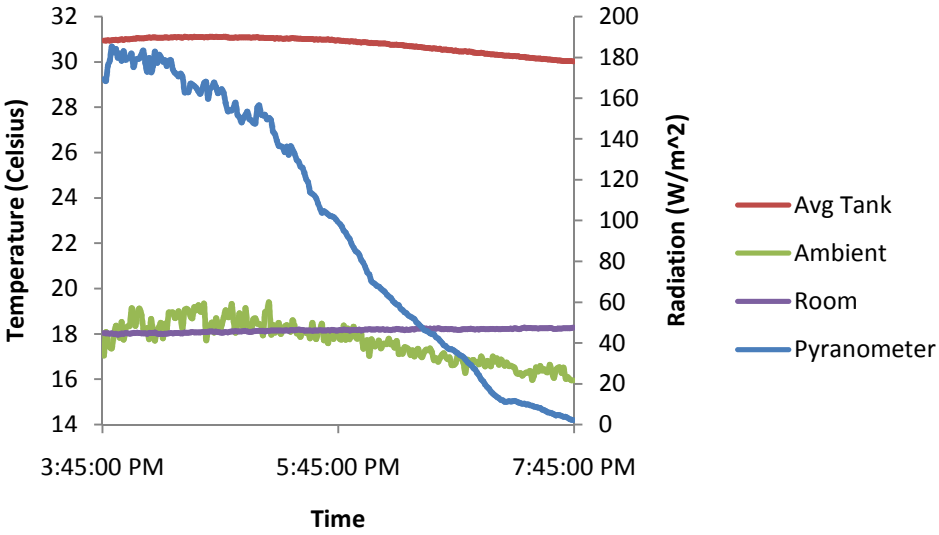


*Figure 3.19 – Run 2 for Experimental Model Efficiency*

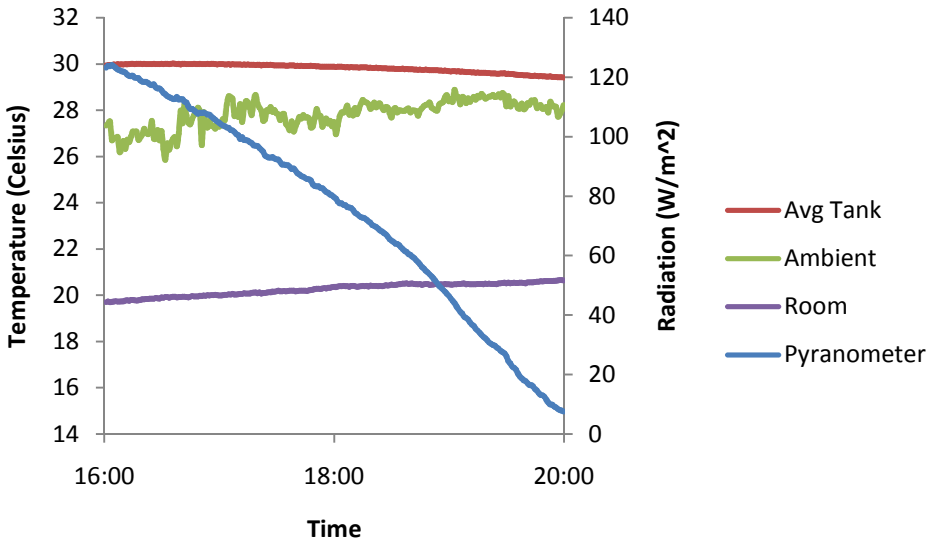


*Figure 3.20 – Run 3 for Experimental Model Efficiency*

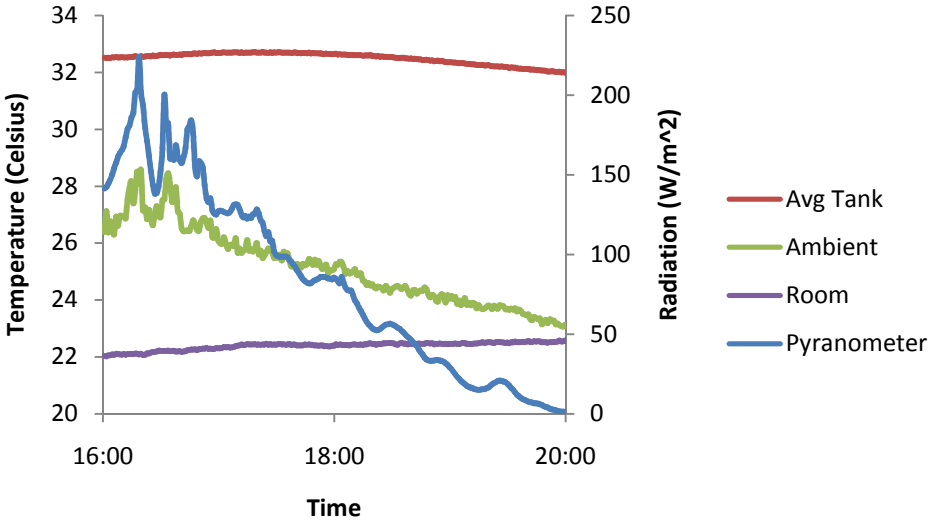


*Figure 3.21 – Run 4 for Experimental Model Efficiency*

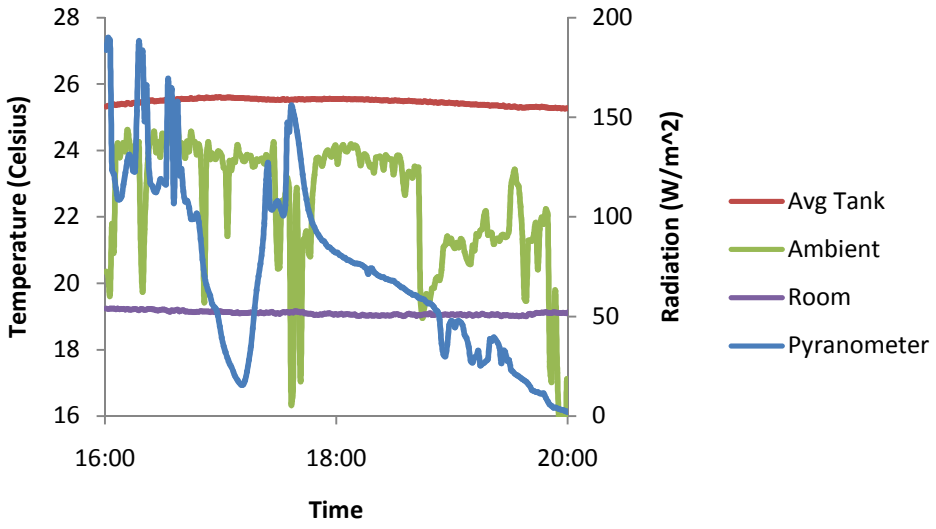


*Figure 3.22 – Run 5 for Experimental Model Efficiency*

The heat rate equation for the net heat flow through the thermal mass is equal to

$$Q_{rad,g} = Q_{tank} + U_i A \Delta T_i \tag{6}$$

where $Q_{rad,g}$ is the radiation heat gained in Watts and $Q_{tank}$ is the heat gained to the tank. The radiation heat gained is readily solved from Equation 7 using valid data sets since it is the only unknown. The total radiation heat available is

$$Q_{rad,a} = G_T A \tag{7}$$

where $Q_{rad,a}$ is the available radiation in Watts, and $G_T$ is the incident radiation on the receiver surface in W/m$^2$. The conversion efficiency of the unit for solar energy to the thermal mass is then

$$\frac{Q_{rad,g}}{Q_{rad,a}} \tag{8}$$

Table 3.3 shows the results over a minimum of two hours of the data from Figures 3.18 – 3.22.

*Table 3.3 – Experimental Efficiency for the Unit*

| | Run 1 | Run 2 | Run 3 | Run4 | Run 5 |
|---|---|---|---|---|---|
| Tank - Ambient (K) | 12.72 | 12.54 | 2.91 | 5.57 | 1.92 |
| Q loss to Ambient (W) | 4.65 | 4.59 | 1.06 | 2.04 | 0.70 |
| Tank - Room (K) | 11.01 | 13.01 | 10.12 | 10.42 | 6.31 |
| Q gain to Room (W) | 28.46 | 33.63 | 26.14 | 26.92 | 16.31 |
| Tank Gain (K) | 0.00 | -0.12 | -0.04 | -0.17 | -0.26 |
| Qtank (W) | 0.19 | -8.57 | -3.12 | -12.88 | -19.71 |
| Qrad (W) | 32.92 | 46.79 | 30.33 | 41.84 | 36.71 |
| Qavail (W) | 46.82 | 73.21 | 48.93 | 68.93 | 49.55 |
| Efficiency (%) | 70.30 | 63.90 | 62.00 | 60.69 | 74.10 |

The average thermal efficiency of the unit is 66.2% with an uncertainty of 5.93%.

## F. Heat Pipe Performance

The thermocouples at the middle of the evaporator section and the upper condenser sections were determined to be not functioning properly. This explanation with corresponding data is shown in Appendix IX. High and low location temperatures measured across the evaporator section of the heat pipe for a four-day cyclic period that were used for calculations are shown in Figure 3.23.

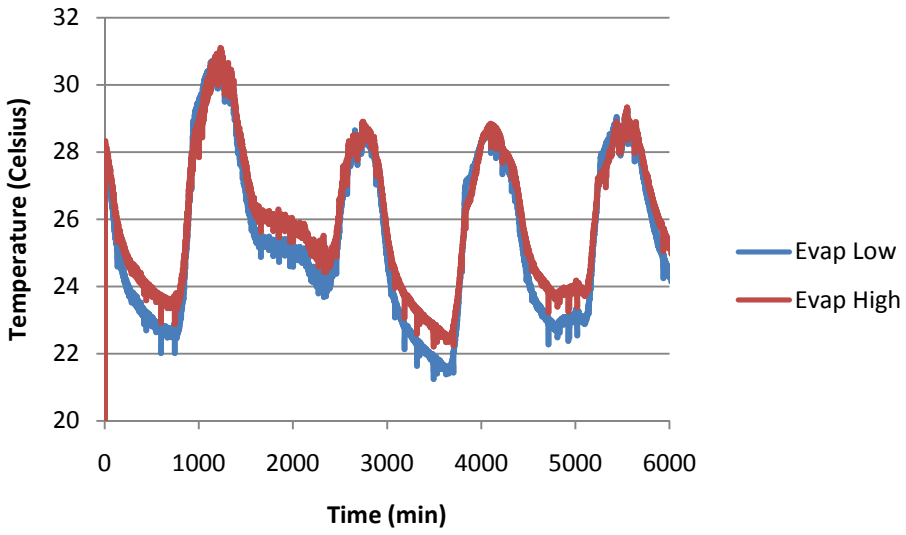


*Figure 3.23 – Upper and Lower Evaporator section Temperatures for Four Days*

Temperatures measured across the adiabatic section of the heat pipe for a four-day cyclic period are shown in Figure 3.24.

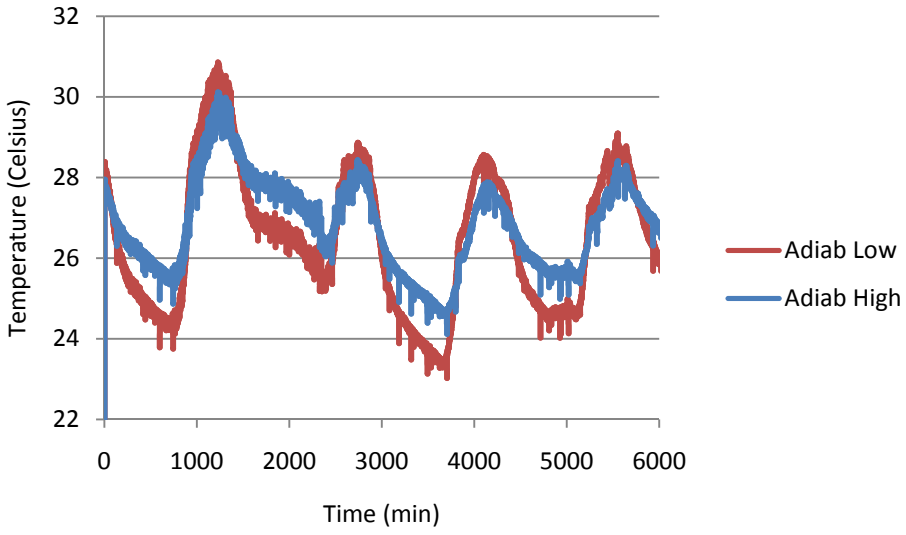


*Figure 3.24 – Adiabatic section Temperatures for Four Days*

Temperatures measured across the condenser section of the heat pipe for a four-day cyclic period are shown in Figure 3.25.

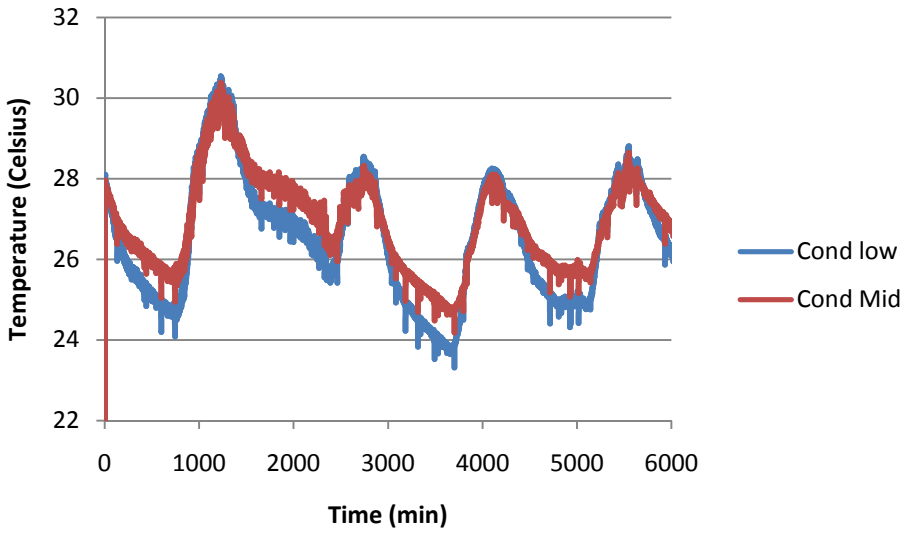


*Figure 3.25 – Condenser section Temperatures for a Four Day Cyclical Test*

Average temperatures measured across the heat pipe for a four-day heating cyclic period are shown in Figure 3.26.

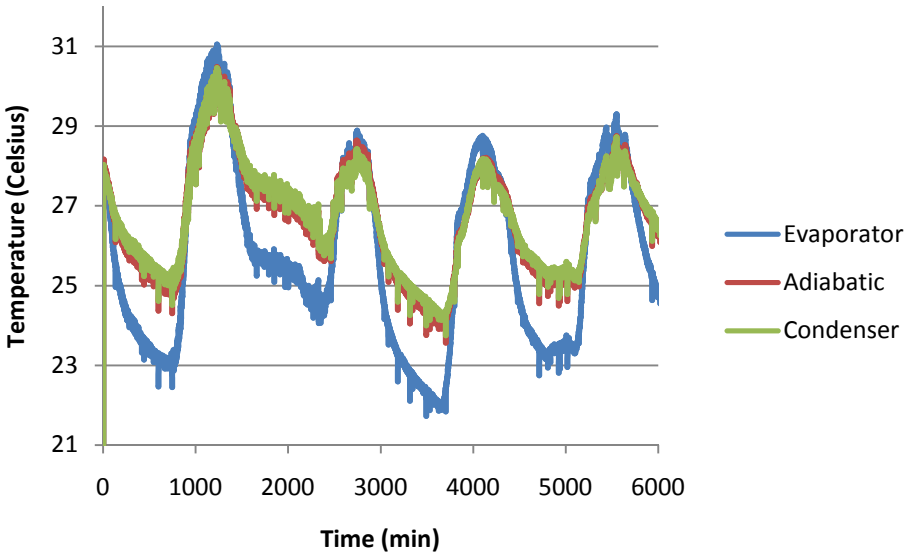


*Figure 3.26 – Average Heat Pipe Temperatures for a Four Day Cyclical Test*

The heat pipe temperature distribution for heating in runs 1 - 3 are shown in Figures 3.27 – 3.29.

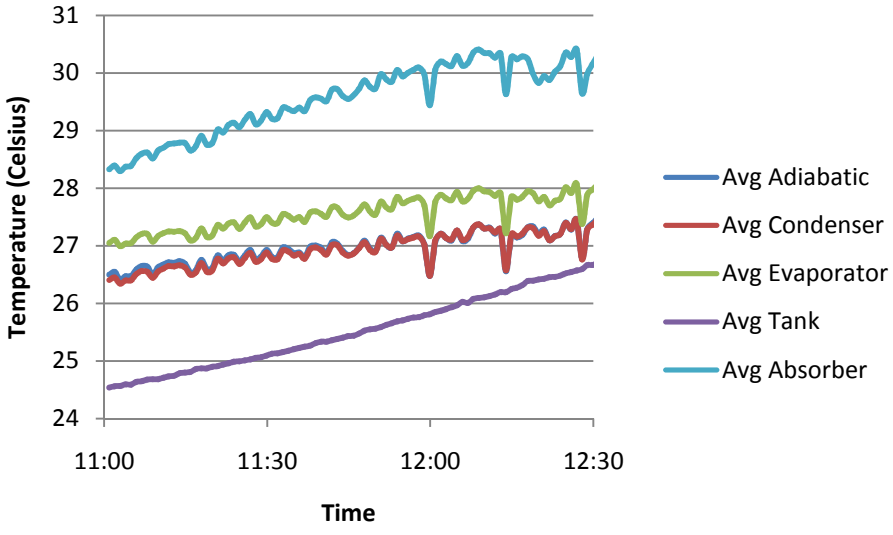


*Figure 3.27 – Heat Pipe Temperature Distribution for Heating Period Run 1*

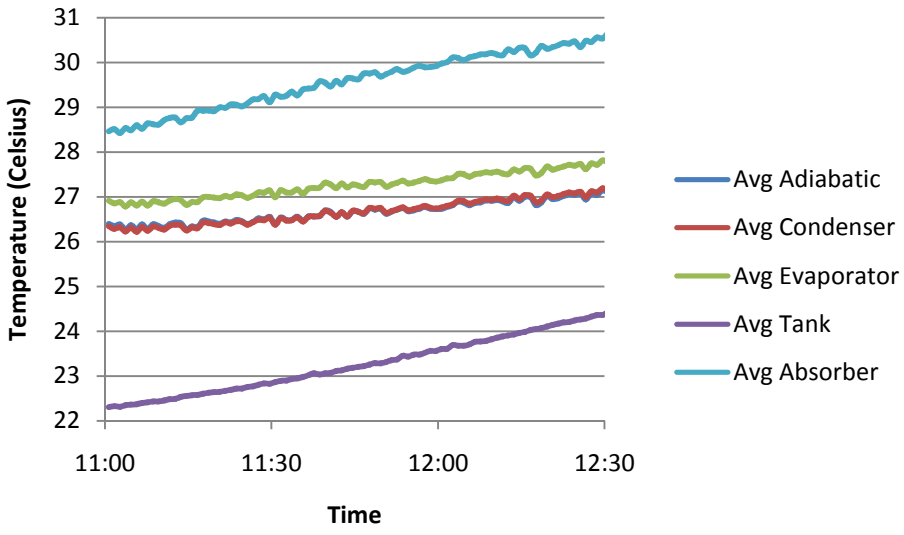


*Figure 3.28 – Heat Pipe Temperature Distribution for Heating Period Run 2*

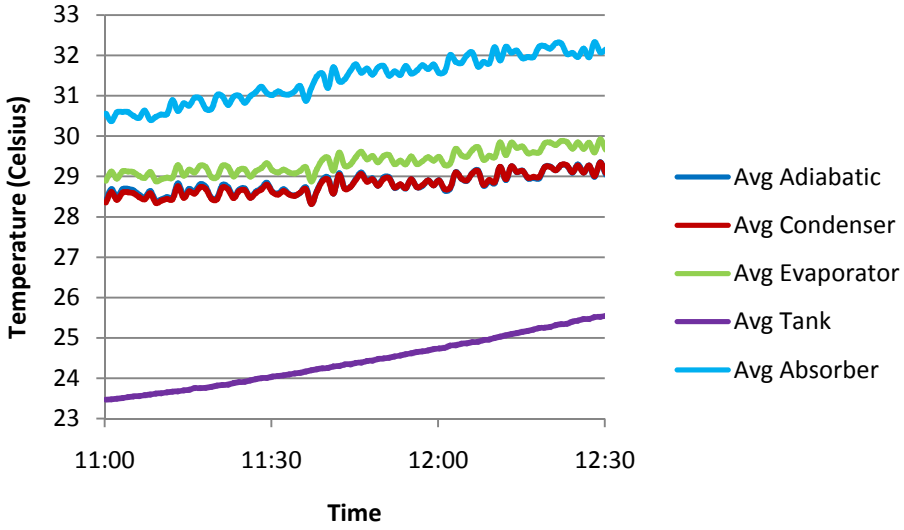


*Figure 3.29 – Heat Pipe Temperature Distribution for Heating Period Run 3*

The equivalent thermal conductivity of the heat pipe can be calculated by

$$k = \frac{QL}{A\Delta T} \tag{9}$$

where k is the equivalent thermal conductivity in W/m K, Q is the heat transfer through the heat pipe in Watts, L is effective heat transfer length in meters, A is the cross-sectional area in square meters, and $\Delta T$ is the temperature difference between the

evaporator and condenser. The conductivity of the heat pipe, as calculated from the data in Figures 3.27 – 3.29 is shown in Table 3.4.

*Table 3.4 - Operational Performance for Heat Pipe during Heating*

| | Run 1 | Run 2 | Run 3 |
|---|---|---|---|
| Tank Temperature Change (K) | 4.57 | 3.84 | 4.73 |
| Heat into Tank (W) | 113.40 | 95.07 | 117.25 |
| Tank - Room (K) | 6.27 | 9.41 | 2.64 |
| Heat into Room (W) | 16.20 | 24.33 | 6.82 |
| Heat Gain through Heat Pipe (W) | 129.60 | 119.39 | 124.07 |
| Evaporator - Condenser (K) | 0.82 | 0.87 | 0.63 |
| Thermal Conductivity (W/m K) | 62546.87 | 54610.41 | 78334.67 |

The average conductivity of the heat pipe during heating conditions is 65,164 W/m K with an uncertainty of 9.27%.

The heat pipe temperature distribution for overnight insulation in runs 1 - 3 are shown in Figures 3.30 – 3.32.

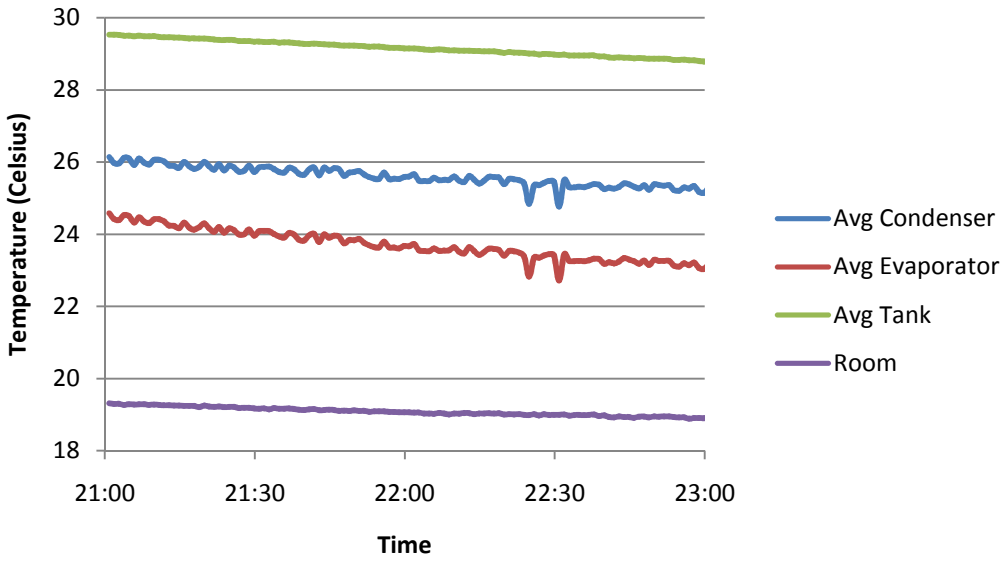


*Figure 3.30 – Heat Pipe Temperature Distribution for Insulating Period Run 1*

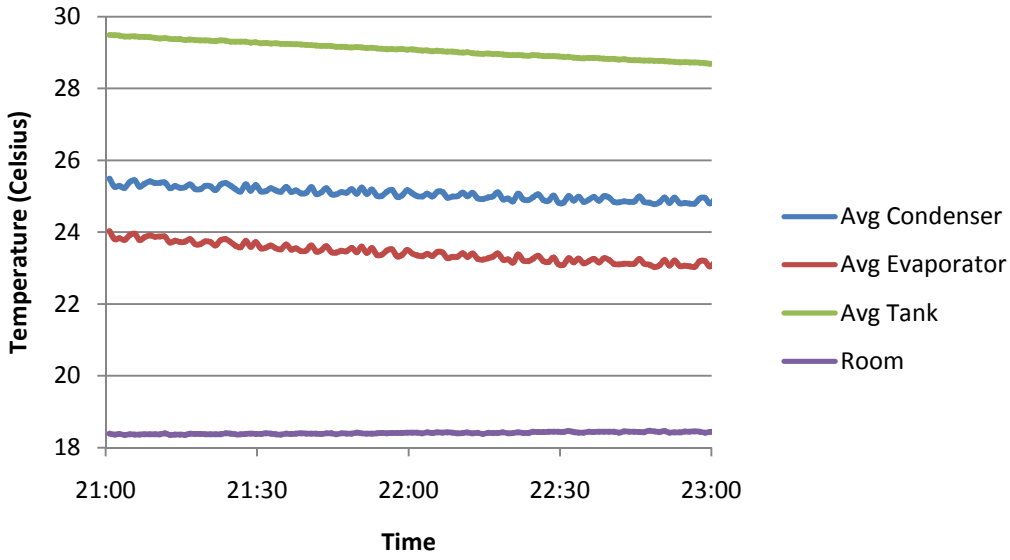


*Figure 3.31 – Heat Pipe Temperature Distribution for Insulating Period Run 2*

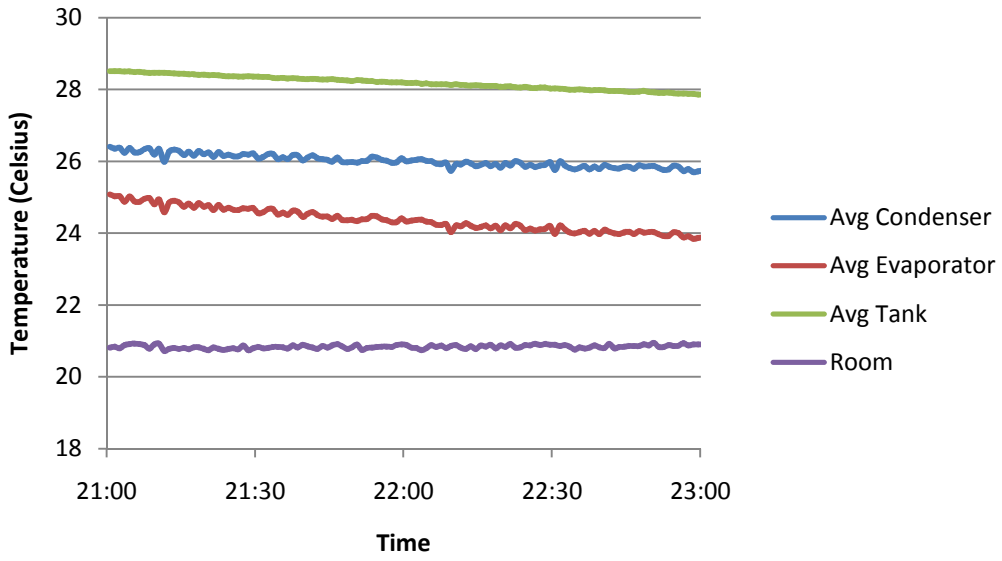


*Figure 3.32 – Heat Pipe Temperature Distribution for Insulating Period Run 3*

The data in Figures 3.30 – 3.32 were used with the results in Table 3.5 to do a net heat flow analysis on the water tank. Since the only path out of the tank that is not into the room is back through the heat pipe and to ambient conditions, the heat flow through the heat pipe can be calculated. Equation 9 was then used to calculate the equivalent thermal conductivity of the heat pipe during insulating conditions. These results are shown in Table 3.5.

*Table 3.5 – Insulating Operating Performance for the Heat Pipe*

| | Run 1 | Run 2 | Run 3 |
|---|---|---|---|
| Tank Temperature Drop (K) | 0.743 | 0.790 | 0.654 |
| Heat out of Tank (W) | 27.619 | 29.388 | 24.309 |
| Tank - Room (K) | 10.070 | 10.664 | 7.346 |
| Heat into Room (W) | 26.027 | 27.563 | 18.987 |
| Heat Loss through Heat Pipe (W) | 1.591 | 1.825 | 5.323 |
| Condenser - Evaporator (K) | 2.695 | 2.361 | 2.366 |
| Thermal Conductivity (W/m K) | 116.942 | 153.085 | 445.576 |

The average thermal conductivity for the heat pipe under insulating conditions for the three runs is 239 W/m K with an uncertainty of 37.8%.

## G. Component Thermal Resistances

Experimental thermal resistances between the condenser and the tank for insulating and heat conditions are shown in Tables 3.6 and 3.7. All thermal resistances were calculated by dividing the degree temperature difference between the two temperature nodes in question in degrees Kelvin by the heat transfer corresponding to that temperature difference in Watts.

*Table 3.6 – Thermal Resistance values from the Condenser to the Water Tank during Heating*

| | Run 1 | Run 2 | Run 3 |
|---|---|---|---|
| $Q_{pipe}$ (W) | 129.6036 | 119.3936 | 118.6941 |
| $T_{cond} - T_{Tank}$ (K) | 1.2739 | 0.1555 | 3.1102 |
| Thermal Resistance (K/W) | 0.0098 | 0.0013 | 0.0262 |

The average thermal resistance from the condenser to the water tank during heating conditions is equal to 0.0124 K/W with an uncertainty of 50.2%.

*Table 3.7 – Thermal Resistance values from the Water Tank to the Condenser during Insulation*

| | Run 1 | Run 2 | Run 3 |
|---|---|---|---|
| $Q_{pipe}$ (W) | 1.5912 | 1.8253 | 5.3227 |
| $T_{cond} - T_{Tank}$ (K) | 1.8462 | 2.1804 | 0.5711 |
| Thermal Resistance (K/W) | 1.1603 | 1.1945 | 0.1073 |

The average thermal resistance from the water tank to the condenser during insulating conditions is equal to 0.8207 K/W with an uncertainty of 30.5%.

In practice the heating thermal resistance of the heat pipe is set to zero during design, which corresponds to isothermal conditions. The experimental thermal resistance of the heat pipe during heating and insulating conditions was calculated from results shown in Tables 3.4 and 3.5, respectively. The thermal resistance during heating and insulating is 0.00608 and 1.66 degrees Kelvin per Watt, respectively.

Thermal resistances for the interface between the evaporator section of the heat pipe and the absorber plate are shown below. These values do not depend on direction of heat flow, as they are for solid conduction. The values in Table 3.8 are calculated from data shown in Figures 3.27 – 3.29.

*Table 3.8 – Thermal Resistances from the Absorber Plate to the Evaporator Section*

| | Run 1 | Run 2 | Run 3 |
|---|---|---|---|
| $Q_{heat}$ (W) | 129.6036 | 119.3936 | 124.0727 |
| Absorber - Evaporator (K) | 2.1273 | 1.9990 | 2.5310 |
| Thermal Resistance (K/W) | 0.0164 | 0.0167 | 0.0204 |

The average thermal resistance between the absorber plate and the evaporator section is equal to 0.0179 K/W with an uncertainty of 11.2%. Table 3.9 shows the thermal resistances from the water tank to the room.

*Table 3.9 – Thermal Resistances from the Water Tank to the Room*

| | Run 1 | Run 2 | Run 3 |
|---|---|---|---|
| $Q_{heat}$ (W) | 16.2044 | 24.3275 | 6.8216 |
| Tank - Ambient (K) | 6.2696 | 9.4125 | 2.6393 |
| Thermal Resistance (K/W) | 0.3869 | 0.3869 | 0.3869 |

The average thermal resistance between the water tank and the room is equal to 0.387 K/W with an uncertainty less than 0.001%. The thermal resistances from the water tank to ambient are shown in Table 3.10.

*Table 3.10 – Thermal Resistances from the Water Tank to Ambient*

| | Run 1 | Run 2 | Run 3 |
|---|---|---|---|
| $Q_{heat}$ (W) | 1.5912 | 1.8253 | 5.3227 |
| Tank - Ambient (K) | 14.3763 | 14.3763 | 13.1242 |
| Thermal Resistance (K/W) | 9.0347 | 7.8760 | 2.4657 |

The average thermal resistance between the water tank and ambient is equal to 6.459 K/W with an uncertainty of 50.9%.

## H. Daily Insolation and Temperature Data

Daily data is shown in Figures 3.33 – 3.38. This data shows the long-term trends of each system component, and is useful for making operating performance observations on the system.

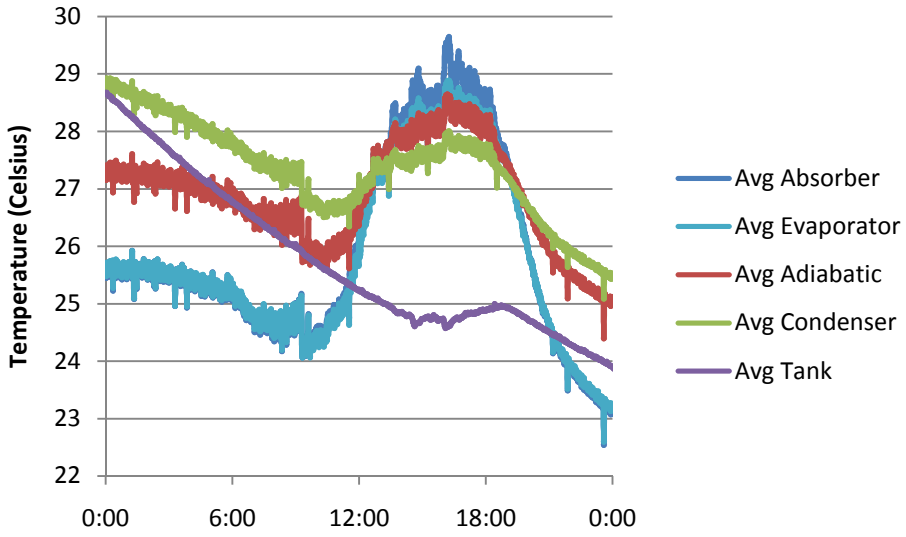


*Figure 3.33 – Unit Temperatures for Heating Cycle 1*

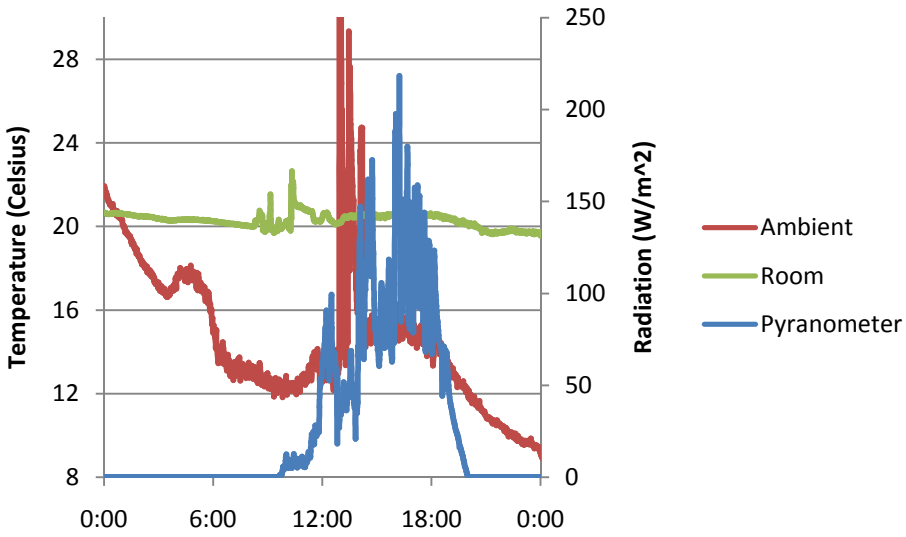


*Figure 3.34 – Ambient Temperatures and Radiation for Heating Cycle 1*

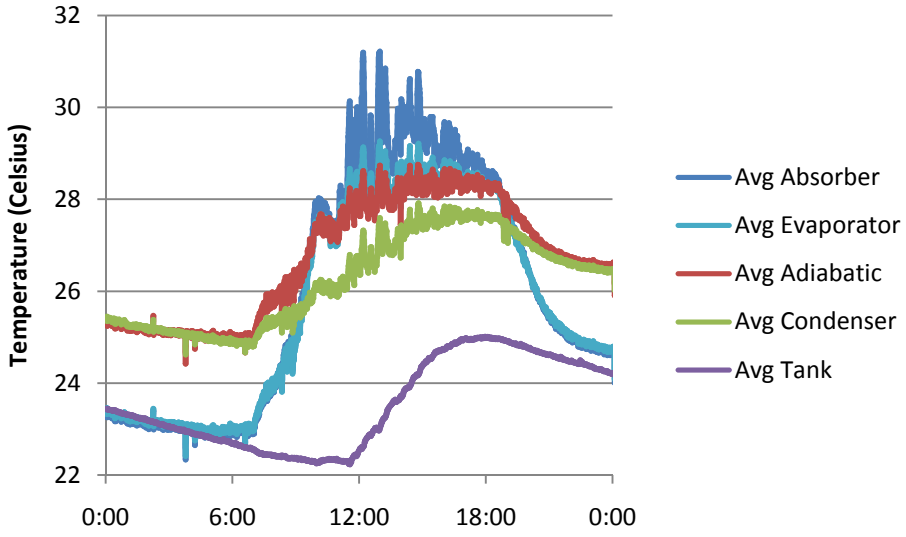


*Figure 3.35 – Unit Temperatures for Heating Cycle 2*

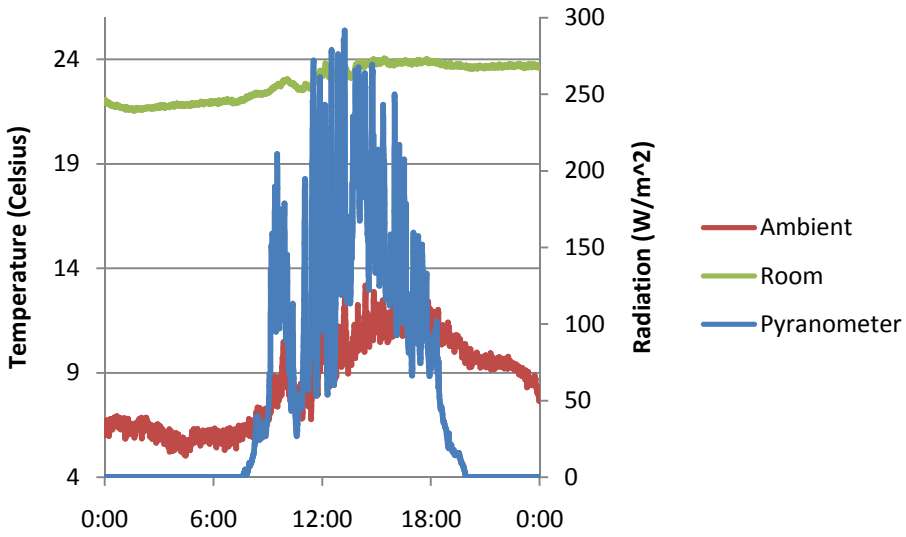


*Figure 3.36 – Ambient Temperatures and Radiation for Heating Cycle 2*

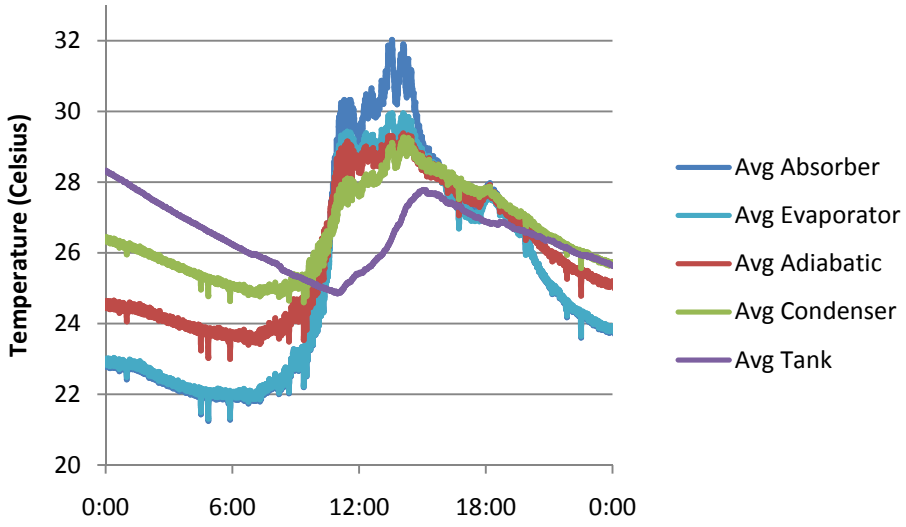


*Figure 3.37 – Unit Temperatures for Heating Cycle 3*

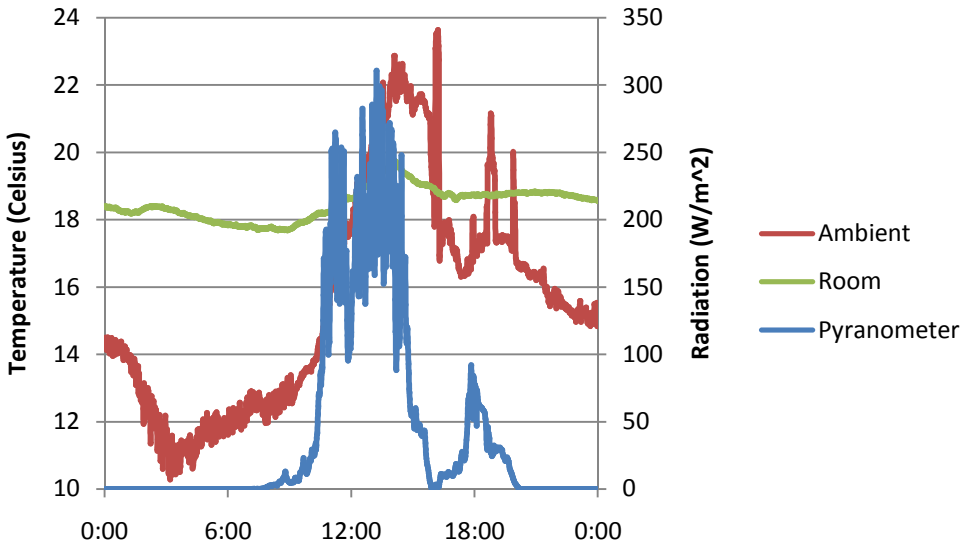


*Figure 3.38 – Ambient Temperatures and Radiation for Heating Cycle 3*

Complete ambient conditions and unit temperatures for the testing period April 1 – 21, 2009 are shown in Appendices VI and VII, respectively.

## I. Economic Analysis

Economic analysis for mass production of the unit will give insight to the feasibility of the technology under current energy and material cost conditions. A few variations from the experimental model will be used for the economic analysis. Although the experimental model was built with an aluminum frame, the unit would be more economical if produced using a polymer frame such as high density polyethylene. As mentioned before, this would also increase the thermal resistance of the unit to a much more desirable level. A polymer frame design similar to that used for the experimental model would enhance the assembly time and cost. Further modifications from the

experimental model include sheet metal screws for mounting of materials to the polymer frame, saving tapping time for aluminum screws. Also, a bulkhead could be designed which would mate to both the water tank and the copper pipe with a watertight seal. The experimental model required a machined bulkhead that greatly increased processing time for this simple component. Material cost and weight for a mass produced unit are shown in Table 3.11.

*Table 3.11 – Material Cost and Weight for Mass Production Unit*

| Description | Cost / Item | Items / Unit | Item Total Cost | Weight / Item (lb) | Item Total Weight (lb) |
|---|---|---|---|---|---|
| Absorber Plates (1/8" thick per sq foot) | $2.16 | 28 | $60.48 | 1.73 | 48.44 |
| Copper Pipe (per foot) | $2.90 | 42 1/10 | $122.09 | 0.75 | 31.58 |
| 90 degree Copper Elbows | $1.79 | 10 | $17.90 | 0.10 | 1.00 |
| Copper Pipe End Caps | $1.19 | 10 | $11.90 | 0.05 | 0.50 |
| Refrigerant Valve | $9.23 | 5 | $46.15 | 0.80 | 4.00 |
| Refrigerant Line (per foot) | $0.72 | 1/3 | $0.24 | 0.33 | 0.11 |
| Lead Free Solder | $20.87 | 1/8 | $2.61 | 0.13 | 0.02 |
| Soldering Flux | $9.94 | 1/8 | $1.24 | - | - |
| Propane (per lb) | $1.29 | 1/9 | $0.14 | - | - |
| Refrigerant (SUVA-124) | $90.00 | 1/3 | $30.00 | 3.37 | 10.10 |
| Plastic Water Tank | $50.00 | 5 | $250.00 | 14.00 | 70.00 |
| Tank Bulkhead | $0.75 | 5 | $3.75 | 0.07 | 0.35 |
| Epoxy | $5.82 | 2 | $11.64 | 0.10 | 0.20 |
| Thread Sealant | $11.40 | 1/15 | $0.76 | 0.07 | 0.00 |
| Aluminum Channel (per foot) | $2.70 | 22 | $59.40 | 0.08 | 1.65 |
| Glazing | $700.00 | 1 | $700.00 | 43.00 | 43.00 |
| Rear Screen (per foot) | $2.60 | 7 | $18.20 | 1.00 | 7.00 |
| Spline (per foot) | $0.06 | 22 | $1.21 | 0.15 | 3.30 |
| Extruded Spline Frame (per foot) | $0.25 | 22 | $5.39 | 0.08 | 1.65 |
| Selective Coat Electroplating | $50.00 | 5 | $250.00 | 0.01 | 0.05 |
| Batt Insulation (per sq foot) | $4.10 | 28 | $114.80 | 0.05 | 1.40 |
| Aluminum Sheet Metal Screws | $0.07 | 66 | $4.36 | 0.01 | 0.88 |
| Silicone Sealant | $4.00 | 3/4 | $3.00 | 0.88 | 0.66 |
| HDPE Frame | $100.00 | 1 | $100.00 | 60.00 | 60.00 |
| Shipping Materials | $75.00 | 1 | $75.00 | 60.00 | 60.00 |
| | | **Total Cost** | $1,829.78 | **Shipping Weight (lb)** | 297.44 |

Albanese did an economic analysis of a similar heat pipe unit [Albanese 2008]. The main differences between this unit and Albanese's design are the aluminum absorber plates used and the inclusion of cost of the injection molded frame [Albanese 2008]. It should be noted that the dry weight (weight of the unit with the water tanks empty) of the unit

was kept as light as possible in order to increase the ease of installation without specialized equipment.

The capital costs for startup of a company which would mass produce the units need to be considered but are not prohibitive. The tooling and components necessary to begin production are relatively inexpensive and are not specialized equipment. Table 3.12 is an approximation of the breakdown of capital investment necessary to begin production.

*Table 3.12 – Capital Equipment Investment Breakdown for a Start-up Company*

| Item | Purpose | Cost / Item | Items Needed | Item Total Cost |
|---|---|---|---|---|
| Small Hydraulic Press | Form Absorber Plates | $2,000.00 | 1 | $2,000.00 |
| Press Tooling | Form Absorber Plates | $500.00 | 1 | $500.00 |
| Small Power Band Saw | Cut Absorber Plate Notches | $1,500.00 | 1 | $1,500.00 |
| Injection Mold Machine | Form Water Tanks | $10,000.00 | 1 | $10,000.00 |
| Plastic Tank Tooling | Use with Mold Machine | $17,000.00 | 1 | $17,000.00 |
| Rotational Mold Machine | Form Frame | $10,000.00 | 1 | $10,000.00 |
| Frame Tooling | Use with Mold Machine | $23,000.00 | 1 | $23,000.00 |
| Power Drill | Install Front and Rear Cover | $50.00 | 2 | $100.00 |
| Soldering Torch | Soldering Heat Pipes | $40.00 | 2 | $80.00 |
| Cloths | Cleaning during Soldering | $0.05 | 30 | $1.50 |
| Caulk Gun | Weather Sealing | $5.00 | 2 | $10.00 |
| Pipe Cutter | Cut Heat Pipes | $115.00 | 1 | $115.00 |
| Vacuum Pump | Charge Heat Pipes | $400.00 | 1 | $400.00 |
| Charging Assembly | Charge Heat Pipes | $100.00 | 2 | $200.00 |
| Heat Pipe Fixture | Align Angles for Soldering | $100.00 | 2 | $200.00 |
| Spline Fixture | Assist in Rear Cover Assembly | $100.00 | 1 | $100.00 |
| Shipping Tooling | Prepare Unit for Shipping | $500.00 | 1 | $500.00 |
| | | | **Total Cost** | $63,206.50 |

Labor must also be included with the single unit production cost. Table 3.13 shows an analysis of the labor cost for a single unit.

*Table 3.13 – Labor Cost per Unit for Production*

| Process | Minutes / Process | Processes / Unit | Total Process Hours |
|---|---|---|---|
| Form Absorber Plate | 5 | 5 | 0.42 |
| Cut and Preassemble Heat Pipe | 15 | 5 | 1.25 |
| Solder Heat Pipe Joint | 3 | 35 | 1.75 |
| Charge Heat Pipe | 10 | 5 | 0.83 |
| Mold Plastic Tank | 20 | 5 | 1.67 |
| Mold Unit Frame | 75 | 1 | 1.25 |
| Assemble Tank to Frame | 1 | 5 | 0.08 |
| Install Insulation | 10 | 1 | 0.17 |
| Assemble Heat Pipe to Water Tank | 2 | 5 | 0.17 |
| Assemble Absorber Plate to Heat Pipe | 5 | 5 | 0.42 |
| Seal Heat Pipe to Water Tank | 15 | 5 | 1.25 |
| Install Frame Side Panel | 10 | 1 | 0.17 |
| Place Glass | 5 | 1 | 0.08 |
| Install Front Cover | 10 | 1 | 0.17 |
| Seal Front Cover with Silicone | 10 | 1 | 0.17 |
| Assemble Spline Frame and Screen | 20 | 1 | 0.33 |
| Install Rear Cover | 5 | 1 | 0.08 |
| Package for Shipping | 15 | 1 | 0.25 |
| | | **Total Hours** | 10.50 |

Labor predictions estimate close to Albanese for production of the unit. At a labor cost of 22 dollars per hour the total labor cost per unit is equal to $231. Installation labor cost will not be analyzed because the unit has been designed to be easily installed. The installation procedure has been summarized in Table 3.14.

*Table 3.14 – Installation Instructions for Consumer End-User*

| | |
|---|---|
| 1 | Find a location for installation clear of obstructions and in solar-facing orientation |
| 2 | Rough cut wall |
| 3 | Verify structural integrity of opening |
| 4 | Remove unit from packaging |
| 5 | Remove rear cover (before installation) |
| 6 | Place unit in wall with glazing facing out |
| 7 | Align glazing a minimum of 0.5 inches from outer wall |
| 8 | Shim unit in place in wall |
| 9 | Verify proper alignment in wall |
| 10 | Install anchor screws |
| 11 | Seal around unit with low-expansion sealant |
| 12 | Fill water tanks and replace cap |
| 13 | Install rear cover |
| 14 | Install molding around unit |
| 15 | Enjoy renewable heat! |

Installation of the unit by a local hardware store, renewable energy company, or even window company would amount to approximately 8 hours of labor, which would add approximately $160 to the cost of the unit.

Production economical analysis will be performed at a 20% profit margin to analyze the break-even sales numbers for the unit. A summary of the unit cost is shown in Table 3.15.

*Table 3.15 – Unit Cost Summary*

| | |
|---|---|
| Material | $1,829.78 |
| Labor | $231.00 |
| Shipping | $300.00 |
| Mark-up | $467.96 |
| Installation | $160.00 |
| Unit Cost | $2,967.74 |

The total initial capital investment for a start-up company is $1.26 Million, including $1.2 Million for real estate. The incremental cost to produce each unit is $231. The profit curve for a start-up company is shown in Figure 3.39.

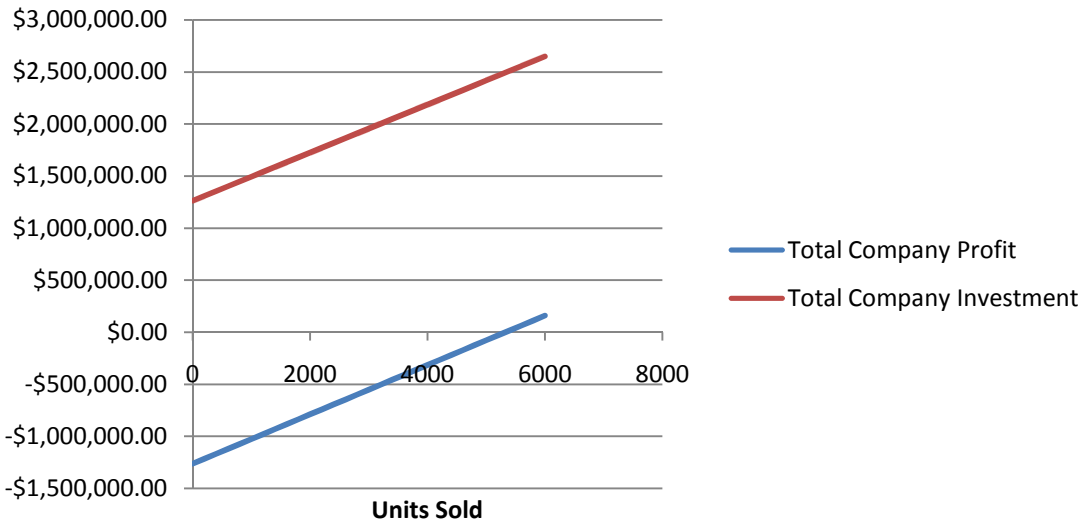


*Figure 3.39 – Start-up Company Financial Curve*

The number of units necessary for a start-up company to break even is 5331, and the corresponding capital investment required to reach the break-even point is $2.49 Million.

Positive economical performance of the unit for the consumer will highly affect the probability of the unit being implemented in homes. A Liu and Jordan method [Duffie

2006] was used to estimate the average daily radiation available on the collector surface for latitude of 45 degrees, clearness index of 0.50, surface azimuth angle of zero degrees, ground reflectance of 0.20, and an orientation angle β of 90°. These conditions represent a somewhat cloudy climate in a region a little further north where there is slightly less radiation available. The monthly mean solar radiation on the collector is correlated [Duffie 2006] by

$$\overline{H_T} = \overline{H_b R_b} + \overline{H_d}\left(\frac{1+cos\beta}{2}\right) + \overline{H}\rho_g\left(\frac{1-cos\beta}{2}\right) \quad (10)$$

Equation 10 yields the data shown in Table 3.16.

*Table 3.16 – Radiation and Energy Conversion Estimates for Economic Analysis*

| | $MJ/m^2$ | N | MJ | kW h |
|---|---|---|---|---|
| Jan | 12.5 | 31 | 561.53 | 155.55 |
| Feb | 12.8 | 28 | 519.36 | 143.87 |
| Mar | 12.2 | 31 | 548.06 | 151.82 |
| Apr | 11.0 | 30 | 478.21 | 132.47 |
| Sep | 12.0 | 30 | 521.68 | 144.51 |
| Oct | 12.8 | 31 | 575.01 | 159.28 |
| Nov | 13.0 | 30 | 565.16 | 156.55 |
| Dec | 12.8 | 31 | 575.01 | 159.28 |
| | | | **Total** | 1203.33 |

For a thermal efficiency of 66.2% and heating period of September through April, the total energy gained by the system is 1203 kW h. At a cost of $0.09 per kW h for the East Central region of the United States [EIA 2009], inflation rate of 4%, and a discount rate of 3%, the payback period for the unit including installation cost is equal to 25 years. For an overall life cycle of 30 years, this yields a return on investment of 26.6%. For available radiation at this level and energy cost per kW h at $0.18 (average in New

England [EIA 2009]), the payback period for the unit including installation is 13 years, with a 30 year return on investment of 153%.

Federal and state tax credits are significant for the consumer purchase of these units. Current federal tax credits are at 30% of total cost and Kentucky state tax credits meet 30% up to $500. With these tax credits and current energy costs in the East Central, the system cost is reduced to $1577.42, payback period is reduced to 14 years, and the return on investment for a 30 year period is equal to 130%. Life cycle analysis values are shown in Tables 3.17 and 3.18.

*Table 3.17 – Life Cycle Analysis for current East Central Rates*

| year | Fuel Cost Savings | PW Fuel Cost Savings | Total PW Savings |
|---|---|---|---|
| 0 | $108.30 | $104.13 | $104.13 |
| 1 | $112.63 | $105.15 | $209.28 |
| 2 | $117.14 | $106.17 | $315.45 |
| 3 | $121.82 | $107.20 | $422.64 |
| 4 | $126.70 | $108.24 | $530.88 |
| 5 | $131.76 | $109.29 | $640.17 |
| 6 | $137.03 | $110.35 | $750.52 |
| 7 | $142.51 | $111.42 | $861.94 |
| 8 | $148.22 | $112.50 | $974.44 |
| 9 | $154.14 | $113.59 | $1,088.04 |
| 10 | $160.31 | $114.70 | $1,202.73 |
| 11 | $166.72 | $115.81 | $1,318.54 |
| 12 | $173.39 | $116.94 | $1,435.48 |
| 13 | $180.33 | $118.07 | $1,553.55 |
| 14 | $187.54 | $119.22 | $1,672.77 |
| 15 | $195.04 | $120.37 | $1,793.14 |
| 16 | $202.84 | $121.54 | $1,914.69 |
| 17 | $210.96 | $122.72 | $2,037.41 |
| 18 | $219.39 | $123.91 | $2,161.32 |
| 19 | $228.17 | $125.12 | $2,286.44 |
| 20 | $237.30 | $126.33 | $2,412.77 |
| 21 | $246.79 | $127.56 | $2,540.33 |
| 22 | $256.66 | $128.80 | $2,669.13 |
| 23 | $266.93 | $130.05 | $2,799.18 |
| 24 | $277.60 | $131.31 | $2,930.49 |
| 25 | $288.71 | $132.59 | $3,063.08 |
| 26 | $300.26 | $133.87 | $3,196.95 |
| 27 | $312.27 | $135.17 | $3,332.12 |
| 28 | $324.76 | $136.48 | $3,468.61 |
| 29 | $337.75 | $137.81 | $3,606.42 |
| 30 | $351.26 | $139.15 | $3,745.56 |

*Table 3.18 – Life Cycle Analysis at current New England Rates*

| year | Fuel Cost Savings | PW Fuel Cost Savings | Total PW Savings |
|---|---|---|---|
| 0 | $216.60 | $208.27 | $208.27 |
| 1 | $225.26 | $210.29 | $418.56 |
| 2 | $234.27 | $212.33 | $630.89 |
| 3 | $243.64 | $214.39 | $845.28 |
| 4 | $253.39 | $216.47 | $1,061.76 |
| 5 | $263.53 | $218.58 | $1,280.34 |
| 6 | $274.07 | $220.70 | $1,501.03 |
| 7 | $285.03 | $222.84 | $1,723.88 |
| 8 | $296.43 | $225.00 | $1,948.88 |
| 9 | $308.29 | $227.19 | $2,176.07 |
| 10 | $320.62 | $229.40 | $2,405.47 |
| 11 | $333.44 | $231.62 | $2,637.09 |
| 12 | $346.78 | $233.87 | $2,870.96 |
| 13 | $360.65 | $236.14 | $3,107.10 |
| 14 | $375.08 | $238.43 | $3,345.54 |
| 15 | $390.08 | $240.75 | $3,586.28 |
| 16 | $405.69 | $243.09 | $3,829.37 |
| 17 | $421.91 | $245.45 | $4,074.82 |
| 18 | $438.79 | $247.83 | $4,322.65 |
| 19 | $456.34 | $250.24 | $4,572.88 |
| 20 | $474.60 | $252.67 | $4,825.55 |
| 21 | $493.58 | $255.12 | $5,080.67 |
| 22 | $513.32 | $257.60 | $5,338.26 |
| 23 | $533.86 | $260.10 | $5,598.36 |
| 24 | $555.21 | $262.62 | $5,860.98 |
| 25 | $577.42 | $265.17 | $6,126.15 |
| 26 | $600.51 | $267.75 | $6,393.90 |
| 27 | $624.53 | $270.34 | $6,664.24 |
| 28 | $649.52 | $272.97 | $6,937.21 |
| 29 | $675.50 | $275.62 | $7,212.83 |
| 30 | $702.52 | $278.30 | $7,491.13 |

# IV. DISCUSSION

## A. Insolation Variation Results

As seen in Table 3.2, insolation on the receiver surface area is greatest in the middle of the unit. Although the direct radiation component is constant for the entire surface because of the adequately large distance from the radiation source, the diffuse radiation component varies across the absorbers. This variation differs because of view factors from the receiver to the atmosphere. The largest radiation gradient across the surface exists in the horizontal direction as the distance to the right increases. The cause of this gradient may be explained by the brick column directly next to the unit which projects 0.324 m (12-3/4 inches) past the exposed glazing surface. The radiation decrease with increase in vertical position from the middle of the unit corresponds to the overhang which was accounted for during shading conditions in Equations 3.1 – 3.3. It may be noted that although this overhang is a very beneficial design component for the efficiencies of the building due to the shading in the cooling months and exposure in the heating months, shading began to interrupt accurate data measurement after installation in

late March, and thus resulted in a larger amount of time necessary to accumulate accurate data.

For the lower part of the unit, the view factor of the unit to the atmosphere decreases due to proximity to the ground. The difference, however, is less than that caused by the overhang on the upper part of the unit. On the left part of the absorber face, the insolation values decrease slightly. This is most likely due to the change in view factor from a tree on that side of the unit. This tree, although large, is approximately 15 m (49.2 feet) from the unit, so the relative change in radiation is small.

## B. Tank Stratification Results

### 1. Heating Conditions

Tank locations described in the following section may be referenced in Figures 2.15 and 2.16. Stratification in the tank during heating and insulating conditions was beneficial to the operation of the experimental model. Stratification within the tank was taken advantage of during design, and the heat pipes were placed as low as possible in the water tanks. Due to the low heat pipe placement in the water tank, stratification within the tank due to the Rayleigh effect allowed heating of the tank to continue even if the upper portion of the tank was at the temperature of the heat pipe. This trend is reflected in Figures 3.5 – 3.8 by the upper portion of the tank heating up initially, followed by the lower portions of the tank after the stratification level lowers down towards the heat pipe during the day. Stratification also led to some difficulty in reading the data, since during some conditions the average temperature reading of the tank was very close to the

condenser section of the heat pipe while the average temperature of the tank was still increasing. This was due to the lower thermocouples in the tank being higher than the entrance height of the heat pipe in the water tank. This implies that stratification within the tank had not yet been forced down to the entrance depth of the heat pipe.

Locations in the tank which were at an equivalent depth showed local heating around the heat pipe before the level fully reached isothermal conditions. This does not occur until the stratification level is close enough to the thermocouples to maintain higher temperatures at the level of the thermocouples. Buoyancy effects within the fluid from heating were not strong enough to create convection flow currents because of the relatively high density and low viscosity of water.

2. Insulating Conditions

Stratification in the water tank also increased operational performance of the heat pipe during insulating conditions. During these conditions, a portion or even the entire heat pipe could remain below the stratification level of the water tank, and did not contact the hotter water in the stratification level. Thus the upper portions of the water tank which were at a high temperature released more heat to the room, not being in contact with the heat pipe. It is also evident from Figures 3.5 – 3.8 that local cooling at equivalent depths within the water tank occurred around the heat pipe. These local temperature variations are much less significant in the tank than during heating due to much smaller heat transfer rates under insulating conditions than heating conditions.

Heat transfer from the north face of the tank to the room is the dominating heat transfer during insulating conditions, and temperature variations from the south to north

face of the tank show this trend. Stratification during insulating conditions occurred on the bottom of the tank. Just as a small plume of heated water rises from the heat pipe to the top of the tank during heating conditions and causes stratification, a small plume of cooled water at a higher density falls to the bottom of the water tank and causes a cold stratification layer to rise from the bottom of the tank.

### C. Absorber Plate Results

Temperature trends for the absorber plates reflect expected results. As seen in Figures 3.9 and 3.10, the temperature increases with increase in distance away from the evaporator section of the heat pipes, as well as with height increase along the length of the heat pipe. Temperature variations across the absorbers are also quite small, indicating a small thermal resistance across the aluminum absorber surfaces.

### D. Insulating Performance Results

Thermal distributions in Figures 3.12 – 3.17 show the data necessary to calculate the equivalent thermal resistance of the system during insulating conditions. The system was designed to retain heat in the thermal mass as it is slowly given off to the room. Thus, a much higher thermal resistance from the tank to ambient conditions than from the tank to the room was necessary, as any transfer of heat to ambient conditions represents heat lost by the system. The final values shown in Table 3.2 for the overall heat transfer coefficients between the thermal mass and room conditions and between the thermal

mass and ambient conditions correspond to expected ratios of heat transfer in and out of the system. A certain amount of error will also be incurred from deriving steady-state values from the experimental results of a dynamic transient system. However, an error of less than 6% for these values shows that experimental results yield relatively consistent data. The results of run 1 demonstrate a slight inconsistency by predicting a lower overall outside heat transfer coefficient. However, neglecting this value gives a more conservative experimental result from Equation 3.5.

The factors affecting heat transfer that go into the derivation of Equation 3.5 include external convection heat transfer coefficients. These values, though quite stable for relatively similar wind conditions, can vary greatly between natural convection conditions and windy forced convection conditions. A possible explanation for the inconsistency is that the data which was used for run 1 of Table 3.2 was affected by stagnant ambient air conditions, which would lead to a lower value of heat transfer coefficient. A brief calculation of forced convection coefficients versus natural convection coefficients shows several orders of magnitude between these values. This assumption is also reinforced by the close values obtained from runs 2 and 3.

## E. Heating Performance Results

Heating performance data proved difficult to obtain due to the restrictive solar conditions requiring the absorber and pyranometer to be completely exposed to direct insolation. For radiation values that yielded significant heat gains, accurate radiation measurements were not obtained. However, operational performance data from the other

components of the system enabled the data during the later portion of testing days to be used for these calculations. That is, once heat transfer from the tank to room and ambient conditions are quantified, the heat transfer into the dynamic system can be calculated.

Susheela and Sharp achieved thermal efficiencies of 40-60% during peak solar insolation periods [Susheela 2001]. An average experimental efficiency of 66.2% shows good results for the passive solar system. The efficiency of the unit ranged from 60-75%, and these values were during solar insolation periods where the incidence angle on the solar glazing was significant enough to cause reflection to affect performance. Reflectance of solar insolation on the glazing at these angles is estimated to be at 5% [Duffie 2006]. Thermal efficiencies upwards of 80% are likely for the experimental model during peak insolation conditions.

## F. Heat Pipe Results

Evaporator section temperatures in Figure 3.23 are lower at the bottom of the heat pipe during insulating conditions. The heat path from the absorbers is the same for all points in insulating conditions. That is, the variation in temperature from the bottom of the evaporator section to the top are not driven by temperature gradients in the absorber plates. This temperature change instead represents the insulating conditions of the heat pipe in which the lowest density liquid refrigerant settles at the bottom of the heat pipe and does not circulate.

Temperatures across the adiabatic section of the heat pipe in Figure 3.24 reflect expected behavior for a component with no heat transfer out. That is, this section should

be between the evaporator and condenser section at all times. However, as can be seen in Appendix VII on April 11 and 12 during heating conditions, the adiabatic section is lower than both the evaporator and the absorber. This is because although the evaporator and condenser section thermocouples were wrapped with electrical tape to insulate them from outer temperature readings, the thermocouples on the adiabatic section were not taped because they were in direct contact with mineral wool insulation. The temperature of the air within the mineral wool, which at that location is most likely closest to room temperature, is slightly affecting the true measurement of the heat pipe adiabatic section.

Temperature distribution for the condenser section of the heat pipe shown in Figure 3.25 reveals standard operating characteristics of the heat pipe. During heating conditions, the temperatures along the condenser are very close, yielding high conductivity. Figure 3.26 shows the practical application of heat pipes for one way heat transfer for gain into the system by the very small temperature change across the unit for heating compared to that during insulating conditions. Thus the initial heating condition design approximation of isothermal operating conditions of a heat pipe, and infinite conductivity.

Figure 3.27 – 3.29 and the corresponding equivalent conductivity for the heat pipe shown in Table 3.4 for heating conditions show very good results for the heat pipes in the system. The high conductivity of the heat pipe, coupled with the thermal diode effect allow the heat pipe augmented solar wall to have much higher overall efficiencies when compared to indirect and isolated gain systems. During heating conditions where the heat pipe is almost isothermal, the only limiting factor for heat transfer is the absorber plate temperature.

The equivalent insulating conductivity values of the heat pipe shown in Table 3.5 show a strong contrast to the heating conductivity shown in Table 3.4. Figures 3.30 – 3.32 show much larger temperature differences across the heat pipe, and correspondingly much lower insulating conductivity. Although an insulating conductivity of 239 W/m K is larger than that of aluminum, the very small cross-section of the heat pipe across which heat transfer occurs greatly limits heat losses through the heat pipe. The ratio of heating conductivity to insulating conductivity of over 250 shows very good operating conditions of the heat pipe. This reflects the largest advantage of the heat pipe augmented passive solar wall over other systems.

## G. Thermal Resistance Results

Thermal resistance values from the condenser to the thermal mass shown in Table 3.6 are low due to the circulation of fluid and latent heat transfer during heating conditions. Insulating thermal resistances in Table 3.7 for the water tank to the condenser section of the heat pipe are 66 times greater than the thermal resistance during heating. This corresponds to the fact that during heating conditions, liquid and vapor are in constant contact with the copper pipe within the water tank. This direct convection transfer allows for a much lower thermal resistance than during insulating conditions in which the only contact to the copper pipe in the water tank is to vapor with a much lower conductivity.

The thermal resistance values from the absorber to the heat pipes shown in Table 3.8 reveal good heat transfer between the two components. This can be attributed to the

large amount of contact force placed between the heat pipes and absorbers during installation. This is also due to the high conductivity paste that was used to fill in the interface between the two components which would have otherwise been filled with small air pockets. The strong clamping of the heat pipes to the absorber plates also ensured that the interface thickness between the two components would be reduced as much as possible.

Thermal resistances in Table 3.9 from the thermal mass to the room are somewhat larger than the resistances of other components. This can be attributed to the natural convection heat transfer coefficients and the low conductivity of air. However, this larger thermal resistance allows for more gradual heat release from the unit. This is most advantageous during nighttime conditions in which other solar units with smaller insulation values will have already lost all of their heat gains. It is also important to note that although the thermal resistance from the tank to room conditions is somewhat larger than that of other components into the system, the thermal resistance from the tank to ambient conditions is much higher, as seen in Table 3.10. Thus, longer heat release times do not necessarily result in greater heat losses during non-heat gain conditions. It is important to note from Table 3.9 how stable the thermal resistance is from the water tank to the room. This suggests that negligible variation in convection heat transfer between the thermal mass and the room will occur.

## H. Daily Insolation and Temperature Results

Daily cyclical operational data shown in Figures 3.33 – 3.38 show the high fluctuation of insolation and ambient temperature conditions which affect the performance of the heat pipe system. It may be noted that the insolation data for the times in which the pyranometer may have been shaded if direct sunlight conditions occurred are quite "noisy". These values, although useful for general system performance observations, were not used for analysis calculations.

Spikes in ambient temperature as seen in Figures 3.34 and 3.38 most likely resulted from short periods of still ambient air and local heating around the solar unit under radiation. Shading during which values from the pyranometer could not be used can be clearly seen in Figure 3.36, which was most likely a very clear day in which the diffuse radiation during the shaded period was still quite high.

It may also be noted that the response of the system to radiation step inputs in morning conditions is almost immediate. This can best be seen for the morning shown in Figures 3.37 and 3.38. This short response time to insolation conditions reflects the relatively small thermal mass of the preheating components, as determined in the Methods section. Again, this shorter response time allows for greater solar gains since the larger response time of other indirect or isolated gain passive systems results in inefficiencies, which result in heat available not converted into heat gained.

## I. Economic Results

Economic analysis results for the system shed positive light on the plausibility of a start-up company producing the units at a competitive energy cost. The material costs of a production unit can be kept at a minimum by using many of the features of the experimental unit such as aluminum absorber plates, heat pipe to absorber clamps, and the nearly identical production of all five heating units requiring very little variation between each unit. Material cost of the high-density polyethylene components would greatly reduce cost of the unit. For the mass-produced unit, an injection molded frame and rotational molded thermal mass water tanks would greatly increase the rate at which parts could be produced, would reduce both the cost per unit produced over a sufficiently large production volume, and would eliminate much of the assembly time associated with multiple-section frames. HDPE is also relatively light when compared with other structural materials, has very good long-term corrosion resistance, is a very good thermal insulator, and can be impregnated with solar corrosion inhibitors for outside installations.

The capital investment for a company to begin producing the units is a relatively small value for a business venture. A total start-up cost of around $1.25 Million for full-scale production of the units becomes much more attractive when the break-even number of units is 5331. It may also be noted that production of these units does not require specialized tooling or highly technical engineering support, since all associated machinery is not expensive or complicated to use and maintain. Thus overhead and other associated specialization costs for the production of the unit would be kept to a minimum.

The consumer economic results for the system have positive implications for marketing of the units. Significant cost reduction associated with current federal and state tax credits, which reduce the payback period to 14 years and the return on investment for a 30 year period over up to 130%, should greatly enhance market interest in these units. Environmental awareness will also spur the use of the units, and marketing could focus on the many positive factors of the unit such as consumer installation, maintenance-free operation, very long life cycle, and a relatively small investment for the unit.

## J. Error Analysis

Error for the thermocouples used in the system was first tested by welding several thermocouples and reading the variation in temperature reading in an ice bath. An Omega Instruments TB5 Thermocouple/Thermistor/RTD unit was used to directly read the temperature reading of the thermocouples. The TB5 unit included temperature compensation for the cold junction temperature in the form of a thermistor in the data card at the point of measure. Temperature readings from the thermocouples were also compared to direct readings from a thermistor. The temperature variation between the thermocouples was less than the highest degree of precision of the reading device - that is, the TB5 unit only read to the hundredth of a degree, and the thermocouples which were tested read the same output temperature. Testing was then performed on the possible introduction of error in the 36.6 m (120 feet) of thermocouple extension wire necessary to reach the data acquisition system. The extension wire was soldered to the thermocouple wire and insulated from contact and electrical noise using electrical tape

and heat shrink wrap. The thermocouple with extension wire was then tested alongside of the original length of thermocouple wire, without change in the value measured. This process was then repeated for a warmer temperature insulated bath, with equivalent results. Error for the temperature measurement may then be approximated as a maximum of one half of the smallest unit output from the TB5 module, or 0.005°C. On an absolute scale this value becomes .0018% for the lowest temperature measurement of 0°C.

The published error for the CM3 pyranometers used was 2%. The uncertainty in the analog to digital conversion for the SCXI-1600 and the USB-6211 data acquisition cards is negligible as both 16 bit units yield an error of less than 0.001%. The uncertainty of any system is

$$U = \sqrt{\sum_1^n (a_n \varepsilon)^2} \tag{1}$$

where U is the uncertainty, $a_n$ is equal to the exponent of the nth term, and $\varepsilon$ is the uncertainty of the nth component. The error associated with the overall heat transfer coefficients in Table 3.2 are 5.04% for the external coefficient and 2.40% for the inside coefficient. These values used in Equation 3.6 yield an uncertainty of 5.58% for the heating power of the system. Equation 3.8 thus yields an uncertainty of 5.93% for unit thermal efficiency. Large uncertainties associated with experimental thermal resistances and conductivities are a result of the very slow response time of the thermal mass and the dynamic driving conditions of the unit. Regardless of the uncertainty in the performance of individual system components, the overall thermal efficiency of the unit has a relatively small uncertainty.

# V. CONCLUSION

The experimental model performed at an average efficiency of 66.2% with an uncertainty of 5.93%. The efficiency ranged from approximately 60% to 75%. Testing was limited due to geometrical constraints around pyranometer measurement, which led to high angles of incidence during testing. Efficiency is estimated to be 5% higher for peak solar insolation conditions.

Radiation variation across the unit was small enough to not significantly affect performance. Stratification within the tanks was beneficial to the overall performance of the tank, both during heating and insulating conditions. Absorber plate and other system components performed as expected, with only overall insulating values being slightly lower than anticipated.

Operational insulation properties for the experimental unit were significantly less than that of a well insulated wall and would prohibit marketing of the unit as a good insulator. The insulation value of the experimental unit was R-7.04, and an equivalent mass production model would be 26.0. Predictions for the mass-production insulation value of injection molded polymer materials in place of the aluminum frame used in the

experimental model yield more than adequate insulation values. The low insulation value of the experimental model did not prohibit operational performance of a mass-produced unit due to thermal isolation of the working components from the aluminum frame, which was the largest factor in heat loss. One example of this was using plastic spacers to insulate the absorber plates from the frame.

Overheating (unwanted heat gains during cooling season) of the unit could not be analyzed due to cool ambient conditions and room heating being required during the test period. Heat gains during cooling season would adversely affect overall system performance. Although this is an undesired feature, all passive solar systems have some amount of overheating. Prediction of the magnitude of the effect of elevated ambient temperatures is difficult to simulate for the heat pipe due to varying heat fluxes, and experimental values will be most beneficial for characterization.

Design drafts and solid models of the unit were created which could be directly used to begin production of the unit. These models, which are included in Appendices I, II, and IV in both paper and electronic form, could be modified for production units. Construction assembly instructions which may be used for mass-production are included in Appendix V.

Installation location in a classroom at the University of Louisville and the involvement of the Kentucky Pollution Prevention Center places the unit in a highly visible environment which will increase awareness of the technology. Display of operational performance data with the unit as well as promotion of the research by UofL

and KPPC will also help promote interest and increase market demand for the technology.

The experimental model heating performance will be very close to that of a mass-produced unit due to the emphasis during construction on avoiding custom details that would not be cost or time efficient for mass-production methods. The design of the unit also emphasized efficiency of fabrication and assembly. Installation of the unit required no specialized equipment or training, which greatly enhances the marketability of the unit to home builders and home owners. Design of the water tanks to be filled after installation also kept weight to a minimum which made the unit easier to handle during placement and shipping.

Economic assessment for material cost and production methods demonstrates the viability of mass production of the units. The purchase, shipping, and installation cost of the unit with Kentucky state and federal tax credits is $1580. The experimental performance data and economic estimates included in the thesis demonstrate the feasibility of the system as the basis of a business venture. These results also suggest that widespread adoption of the system would significantly reduce energy use in buildings and, therefore, benefit the environment. We only now require that sound decisions be made by policy makers to promote alternative energy, and for the general public to embrace these new technologies.

# VI. RECOMMENDATIONS

The experimental heat pipe augmented solar wall would differ from a mass manufactured unit in a couple ways. First, and most importantly, the aluminum frame would be with a structural polymer material which could be produced much more quickly and would result in significantly higher insulation properties. This polymer frame could be produced to be more aesthetic behind the insect screen on the inside face of the unit.

The unit could also incorporate a shading device which would help prevent overheating, as well as potential mechanical modifications. One possible mechanical solution is the inclusion of a valve on the adiabatic section of the heat pipe, which could be closed during overheating conditions to prevent fluid circulation. Investigation of the affect this would have on heat pipe heating and insulating performance would have to be investigated. A pull-down shading device could be used where shading extensions on buildings becomes difficult or undesirable. However, any overheating prevention method which involves regular maintenance or work for the end-user will greatly inhibit customer satisfaction and marketability, and should be avoided. Characterization of the overheating properties of the unit through continued research would be highly beneficial.

It would also be beneficial to do further testing of the unit during winter conditions where much colder temperatures may affect the unit more significantly. Long term testing could be performed to determine the components which may break down or reduce efficiencies during operation. These could include overheating and breakdown of the refrigerant inside the heat pipe, or the effects of the glazing getting dirty after a certain period of use. Experimental testing in more cloudy climates where solar technology is considered unusable by the general public would also have a significant impression on the market for the units. Work with architects or interior designers would also be beneficial for optimization of the unit for general use. Smaller unit design could also be considered so a homeowner could replace a window with the unit and avoid the large amount of work associated with installation in an existing wall.

The need for implementation of these and other sound renewable energy resource devices cannot be exaggerated. The implications of continuing current energy production and consumption practices places a very large responsibility on engineers, politicians, media, and the general public to make significant changes. It is strongly recommended that business and marketing strategizing is begun with the goal of mass production of the heat pipe augmented solar wall.

# REFERENCES


Agnihotri, O. P., Gupta, B. K. 1981. *Solar Selective Surfaces*. New York, New York: Wiley and Sons.

Albanese, Michael. 2008. Private Communication.

Bairamov, R., and Toiliev, K. 1981. Heat pipes in solar collectors. *Fourth International Heat Pipe Conference*. Perfamon, London. 47-54.

Bienert, W. B., Brennan, P. J. 1971. Transient Performance of Electrical Feedback Controlled
Variable – Conductance Heat Pipes. ASME Paper 71 – Av – 27, *SAE/ASME/AIAA Life Support and Environmental Control Conference*. San Francisco, California: July 12 – 14.

Brost, O., Behrmann, P. 1990. High Temperature Lithium Heat Pipe Furnace for Space Applications: Investigations of Temperature Stability and Reproducibility., *7th International Heat Pipe Conference*. Minsk, Belarus. Preprints.

Cheung, Henry. 1968. *A Critical Review of Heat Pipe Theory and Applications.* TID-4500, UC-4.

Corliss, J. M. 1979. *Evaluation of heat pipe application for passive solar systems*: *Department of Energy Report*, Department of Energy, Washington, D.C.

Cotter, T.P., Deverall, J., Erickson, G.F., Grover, G.M., Keddy, E.S., Kemme, J. E., and Salmi, E. W. 1965. *Status Report on Theory and Experiments on Heat Pipes at Los Alamos.* LA-DC-7206, 1-12.

Dahl CA & McDonald L. 1998. Forecasting energy demand in the developing world. *Energy Sources* 20:875-889.

Duffie, John A., Beckman, William A. 2006. *Solar Engineering of Thermal Processes, Third Edition*. Hoboken, New Jersey: John Wiley and Sons, Inc.

Energy Information Administration. 2008. *Renewable Energy Trends in Consumption and Electricity.*

Faunce, S. F., Sliwkowski, J., Guceri, S. 1978. Application of phase change materials in a passive solar system. *AS/ISES Second National Passive Solar Conference.* Philadelphia, 475-480.

"Federal Tax Credits for Energy Efficiency." *ENERGY STAR*. revised March 18. energystar.gov/taxcredits. accessed April 14, 2009.

Gaugler, Richard. 1944. U.S. Patent Office 2,350,348.

Grover, G. M., Cotter, T. P. and Erikson, G. F. 1990. Structures of Very High Thermal Conductivity. *Journal of Applied Physics* 35(6).

Incropera, F. P., Dewitt, D. P., Bergman, T. L., Lavine, A. S. 2007. *Introduction to Heat Transfer, Fifth Edition*. Hoboken, NJ: John Wiley and Sons.

Koltun, M. M. 1981. *Selective Optical Surfaces for Solar Energy Converters*. New York, New York: Allerton Press.

Kreider, Jan F., Curtiss, Peter S., Rabl, Ari. 1994. *Heating and Cooling of Buildings: Design for Efficiency, Second Edition*. New York, New York: McGraw Hill Higher Education.

Marcus, B. D. 1971. *Theory and Design of Variable Conductance Heat Pipes: Reports no. 1 and 2.* TRW 13111 – 6027 – RO – 00. Contract NAS 2 – 5503.

Mar, H. Y. B., Lin, J. H., Zimmer, P. B., Peterson, R. E., and Gross, J. S. 1975. *Optical Coatings for Flat Plate Solar Collectors*, Energy Research and Development Administration, Washington, D. C. Contract No. NSF-C-957 (AER-74-09104).

Muramoto, H. 1985. Studies on heat transfer system using heat pipes. *International Symposium on Applications of Solar Energy.* Hakone, Japan. 259-264.

P.D. Dunn & D.A. Reay. 1994. *Heat Pipes: Fourth Edition*. Pergamon Press.

Peterson, G. P. 1994. *An Introduction to Heat Pipes: Modeling, Testing, and Applications*. Wiley Interscience.

Riffat, S., Zhao, X., and Doherty, P. 2005. Developing a Theoretical Model to Investigate Thermal Performance of a Thin Membrane Heat-Pipe Solar Collector. *Applied Thermal Engineering* 25(1):899-915.

Saman, W. Y.,Al-Fakhri, A. A., Yaseen, N. J. 1989. Utilization of heat pipes for reducing heat load of walls. *Journal of Solar Energy Research* 7:1.

Schobert, Harold H. 2002. *Energy and Society, an Introduction*. New York, New York: Taylor and Francis.

"State Tax Credits On Energy Efficiency and Renewable Energy." *Kentucky Department for Energy Development and Independence, Kentucky Division of Corporation Tax.* revised March 18, 2009. www.energy.ky.gov. accessed April 14, 2009.

Susheela, N., Sharp, M. K. 2001. Heat Pipe Augmented Passive Solar System for Heating of Buildings. *Journal of Energy Engineering* April:18-36.

Tester, Jefferson W., Drake, Elisabeth M., Driscoll, Michael J., Golay, Michael W., Peters, William A. 2002. *Sustainable Energy: Choosing Among Options*. Cambridge, Massachussetts: MIT Press.

Trefethen, L. 1962. On the Surface Tension Pumping of Liquids or a Possible Role of the
Candlewick in Space Exploration. *General Electric Technical Information: Series Number* 615 D114.

Trefethen, L. M. 1970. Natural convection inside inclined tubes. *Proceedings of the Fourth International Heat Transfer Conference*. Versailles, France. NC2.12.

Twidell, John and Weir, Tony. 2006. *Renewable Energy Resources, Second Edition.* New York, New York: Taylor and Francis Group.

United Nations General Assembly, 96th Plenary Meeting. *Report of the World Condition on Environment and Development*. December 11, 1987. Provided by United Nations Department of Economic and Social Affairs.

Van Dijik, H. A. L., Dordrecht, D. Reidel. 1983. High performance passive solar heating system with heat pipe energy transfer and latent heat storage. Solar *Energy Applications to Dwellings Proceedings EC Contractor's Meeting.* The Netherlands, 118-130.

Vanek, Francis M., Albright, Louis D. 2008. *Energy Systems Engineering: Evaluation and Implementation*. New York, New York: McGraw Hill.

Waters, E. D. 1974. Arctic Tundra Kept Frozen by Heat Pipes. *The Oil and Gas Journal* August 26:122-125.

APPENDIX I

COMPONENT DESIGN DRAFTS

NOTE : Plastic frame drafts are too large for hard copy – see files on CD in Appendix IV

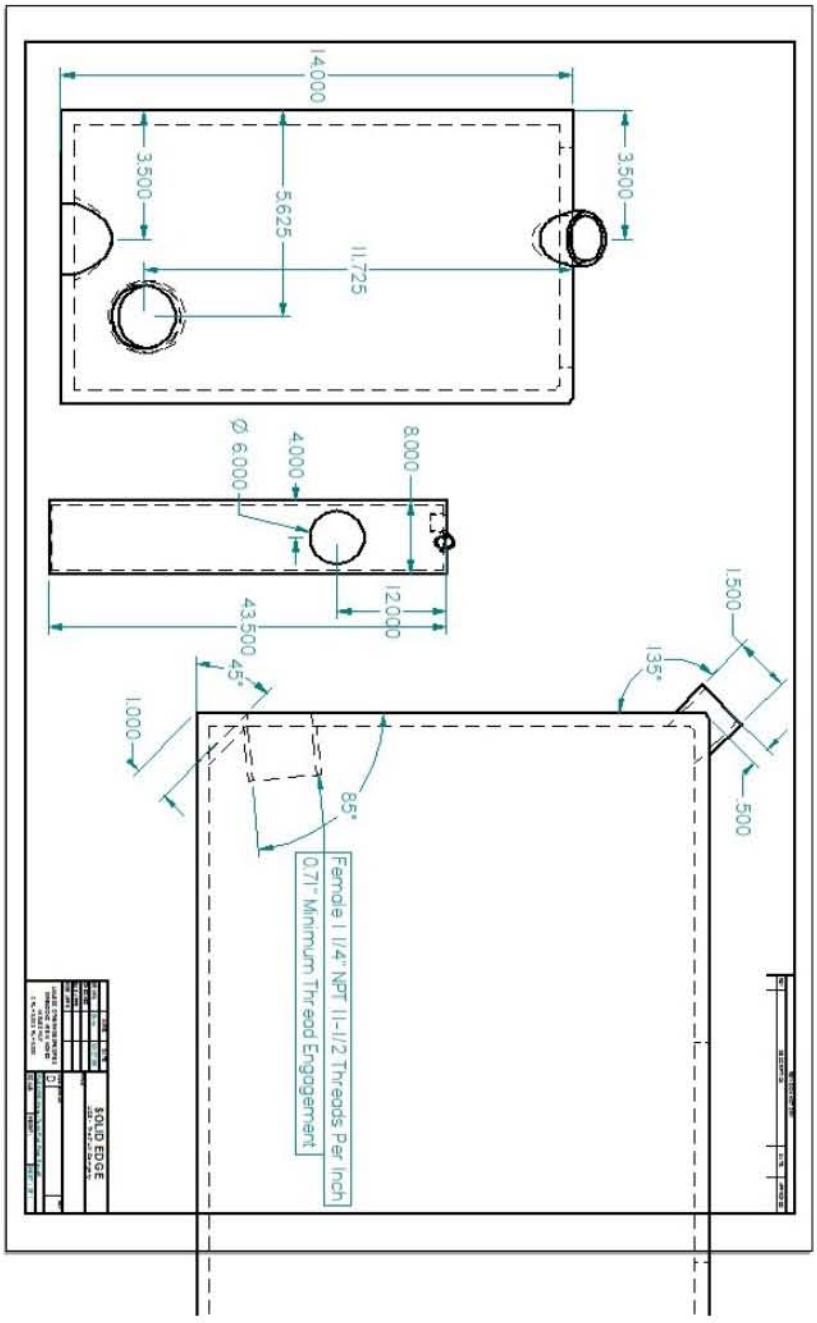


*Figure I.1 – Water Tank Draft*

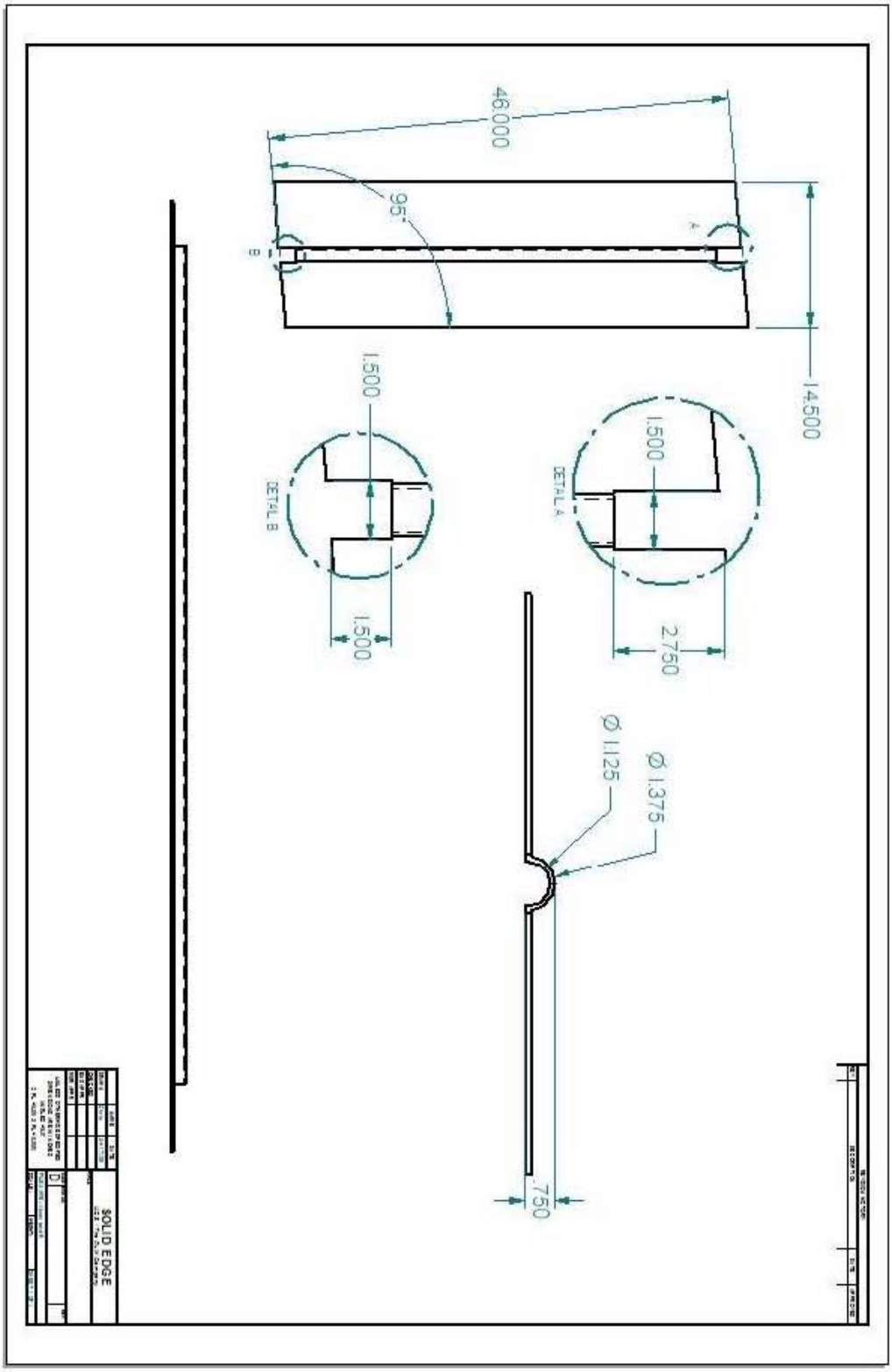


*Figure I.2 – Standard Absorber Plate Draft*

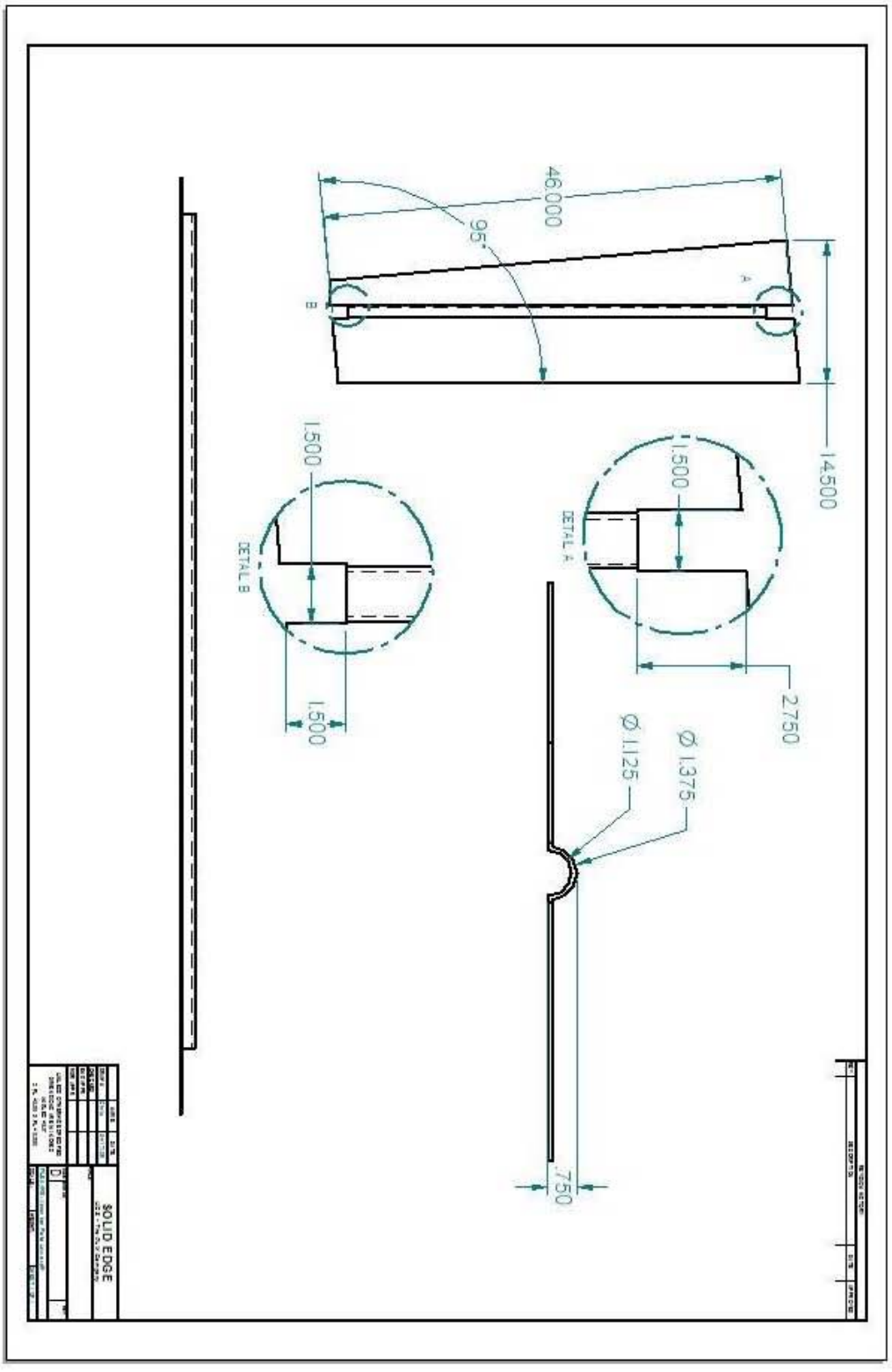


*Figure I.3 – Lower Absorber Plate Draft*

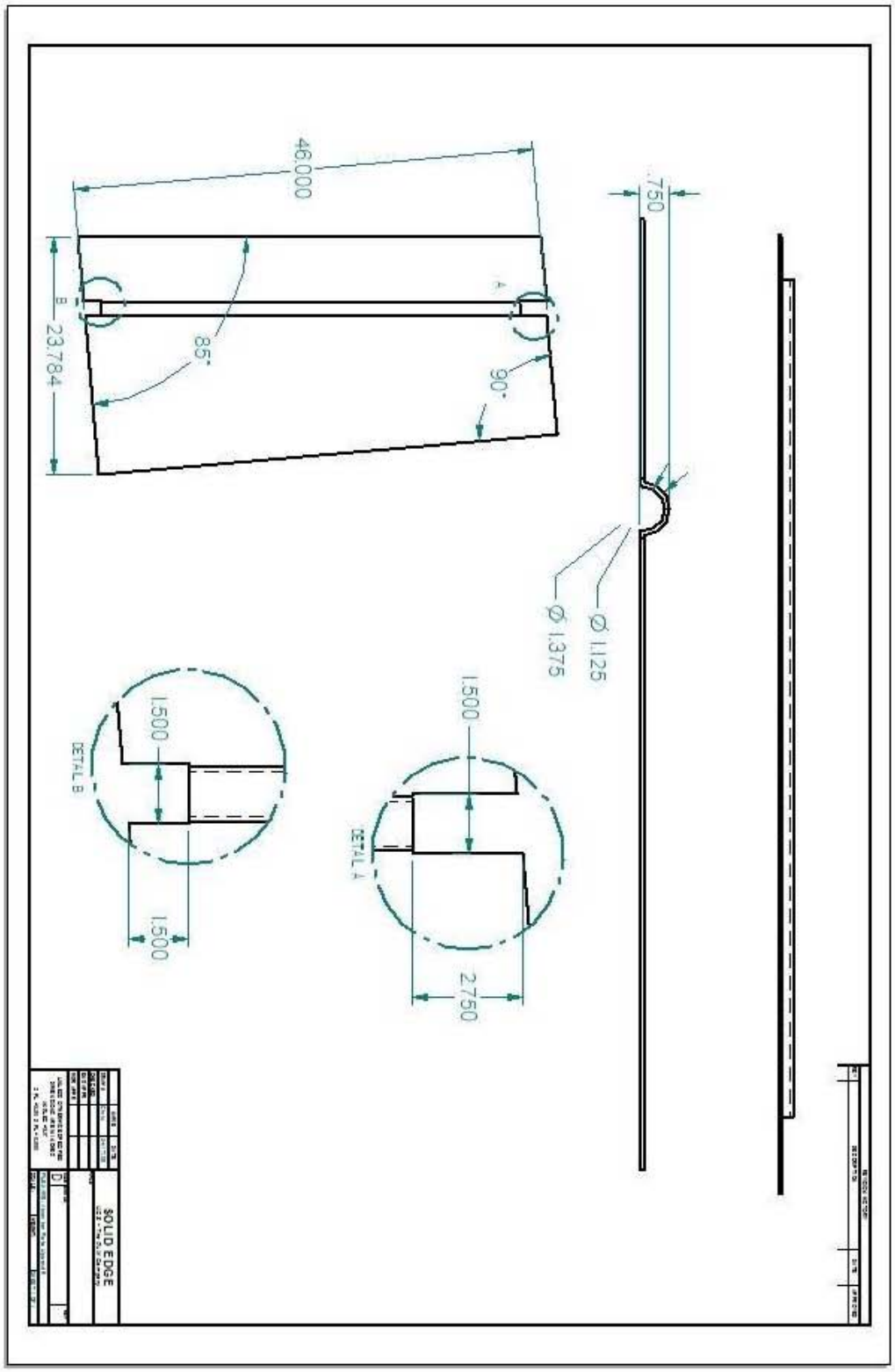


*Figure I.4 – Upper Absorber Plate Draft*

APPENDIX II

EXPERIMENTAL UNIT SOLID MODEL ASSEMBLY

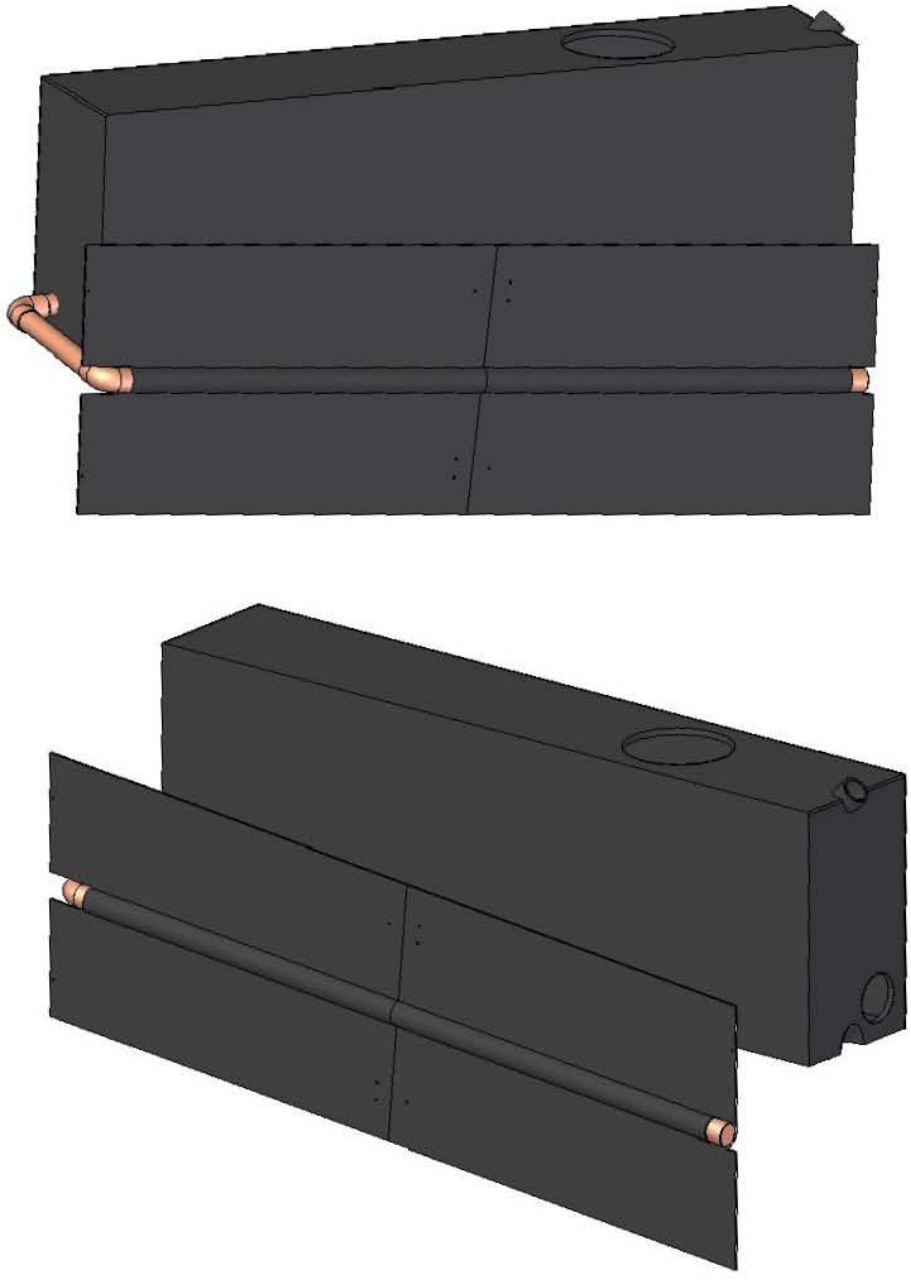

*Figure II.1 – Single Heating Unit*

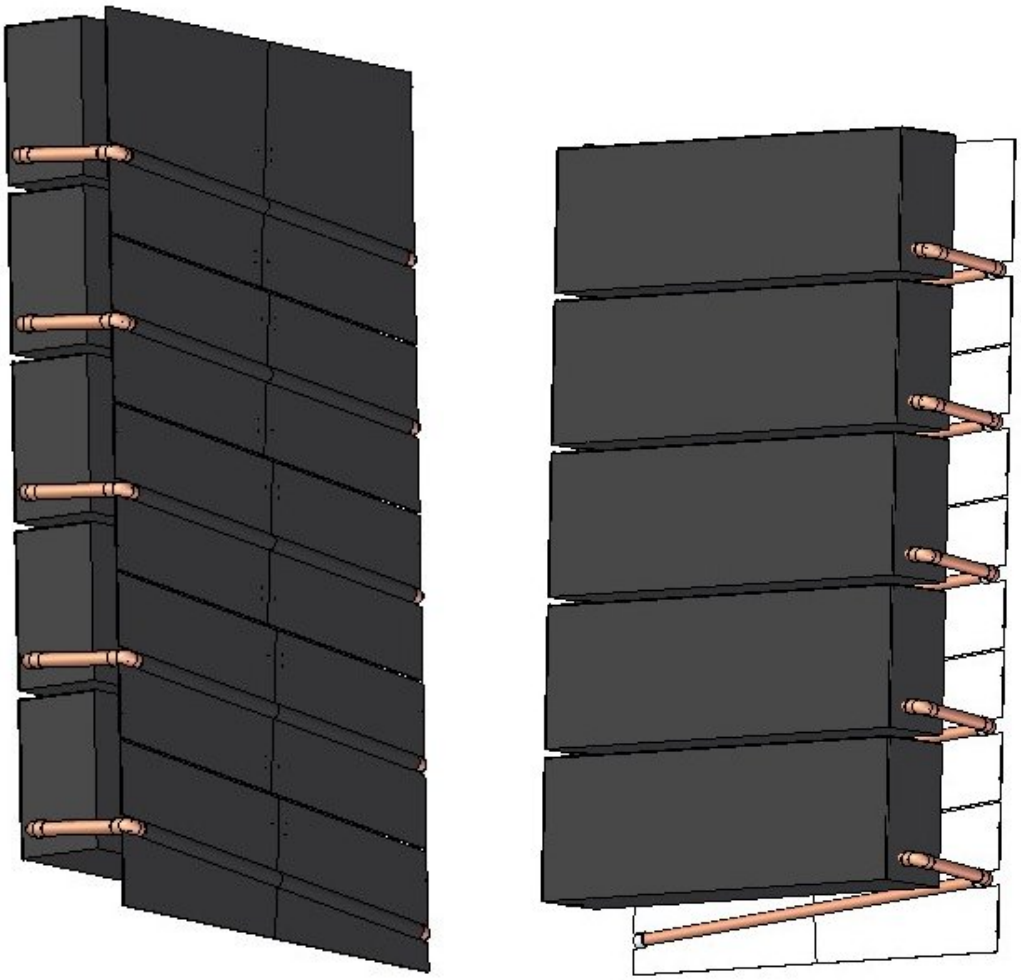

*Figure II.2 – All Heating Units*

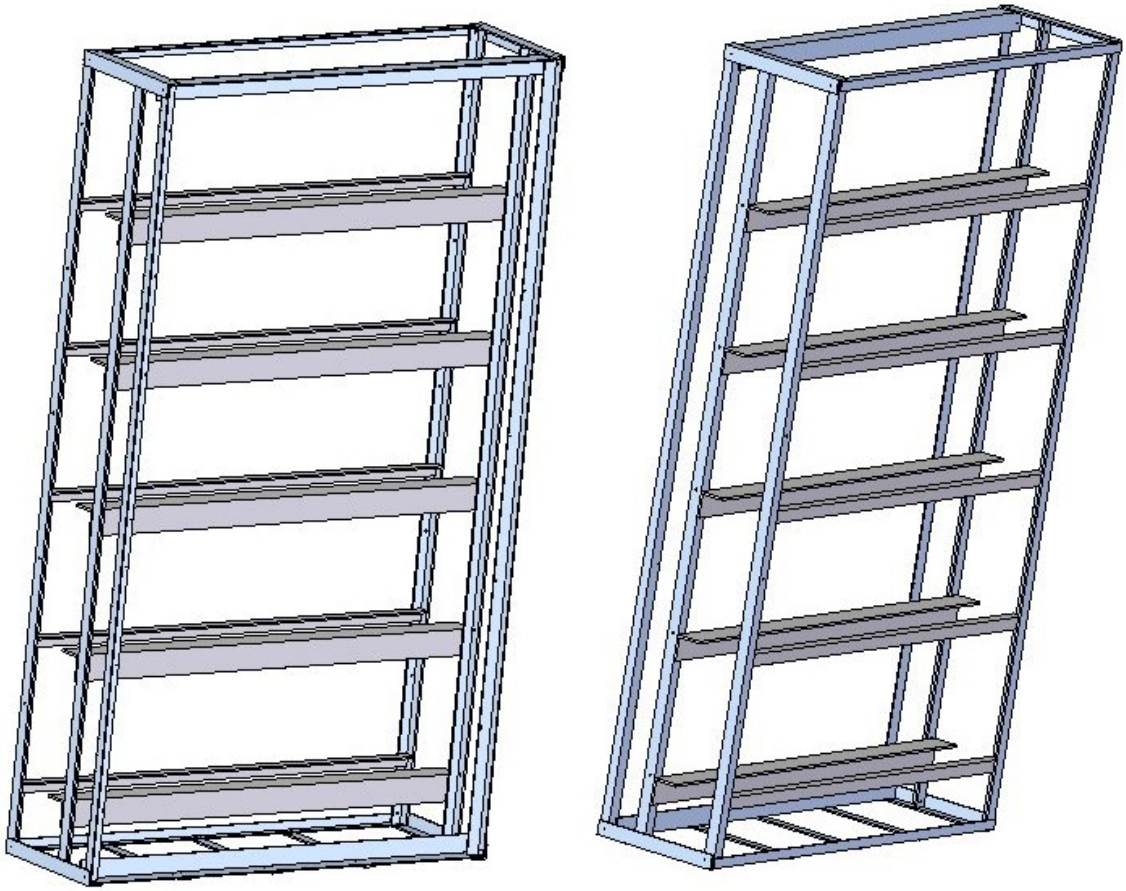

*Figure II.3 – Experimental Model Aluminum Frame*

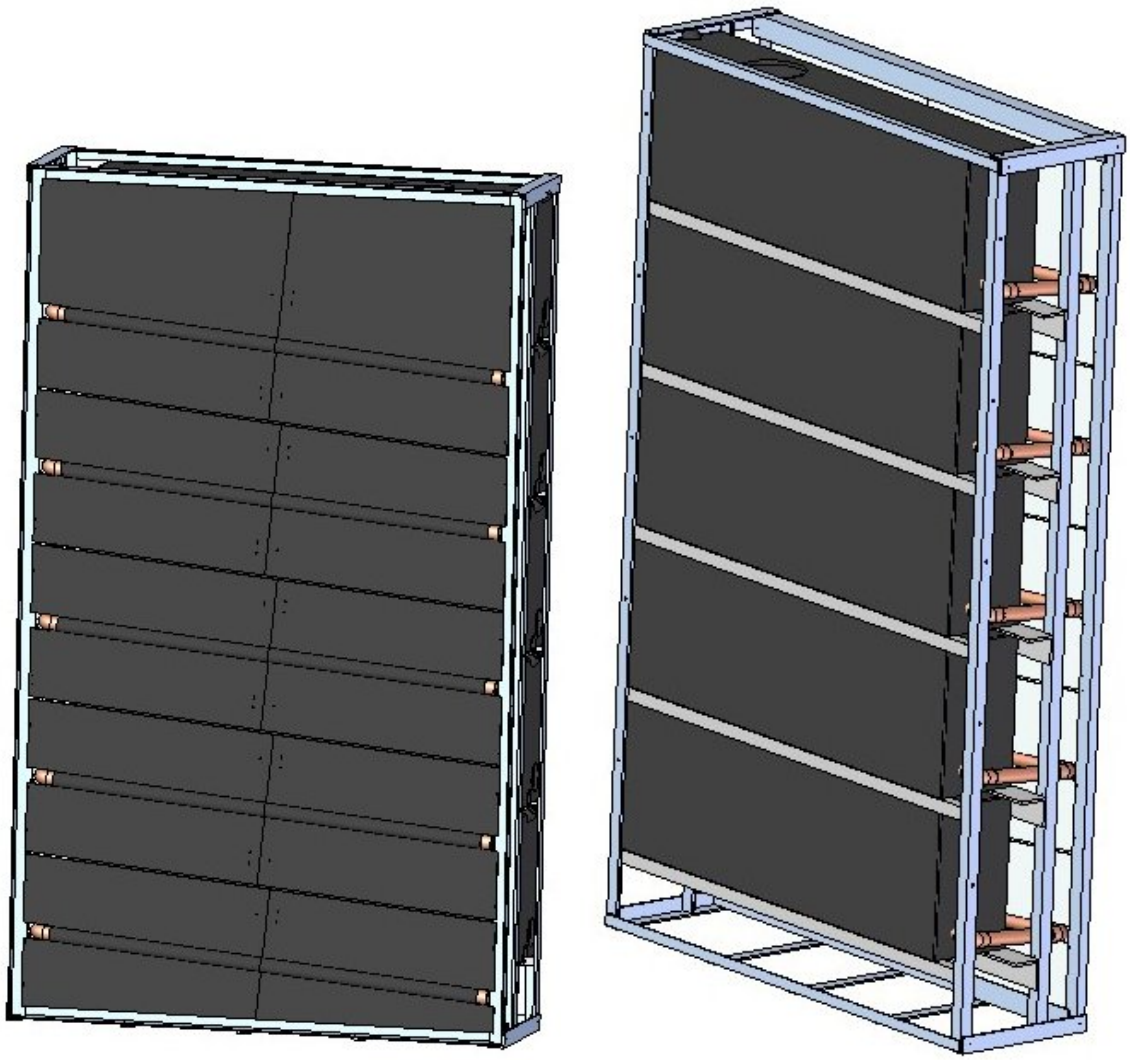

*Figure II.4 – Experimental Model Aluminum Frame with Heating Units*

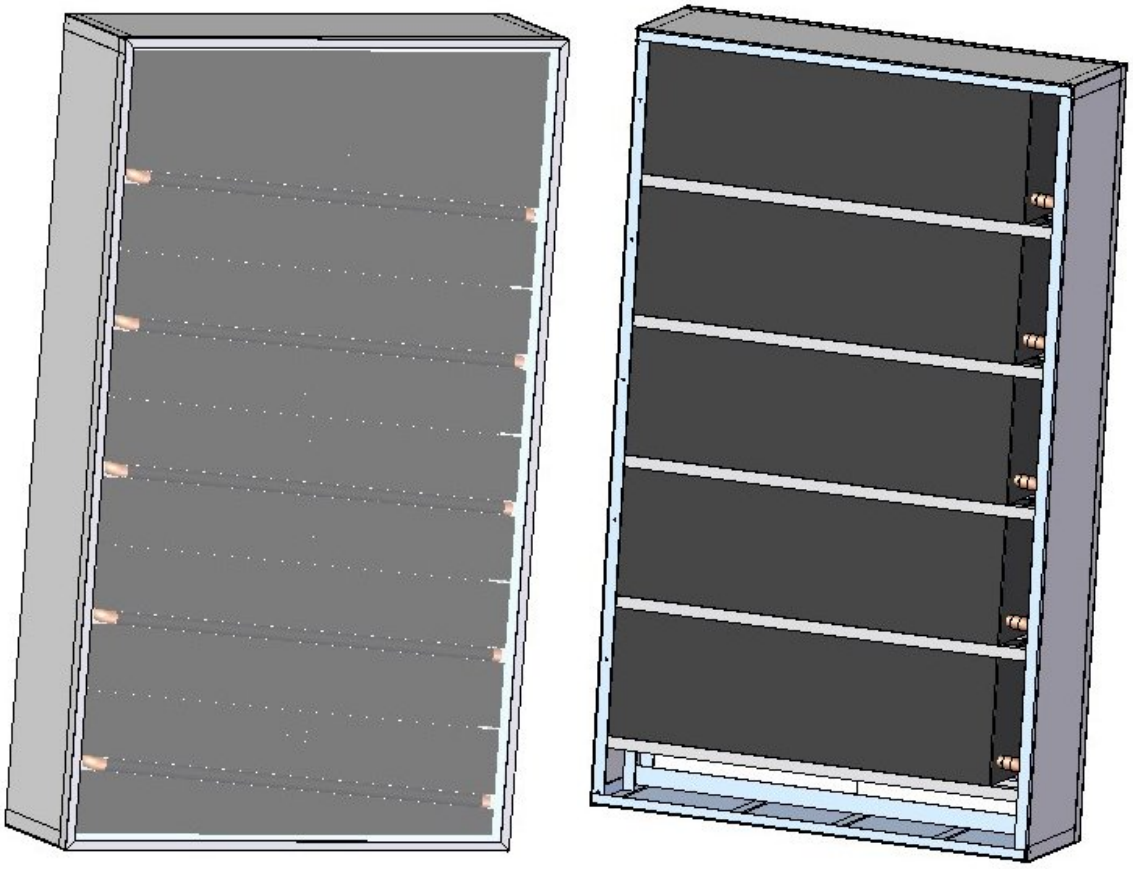

*Figure II.5 – Full Experimental Model*

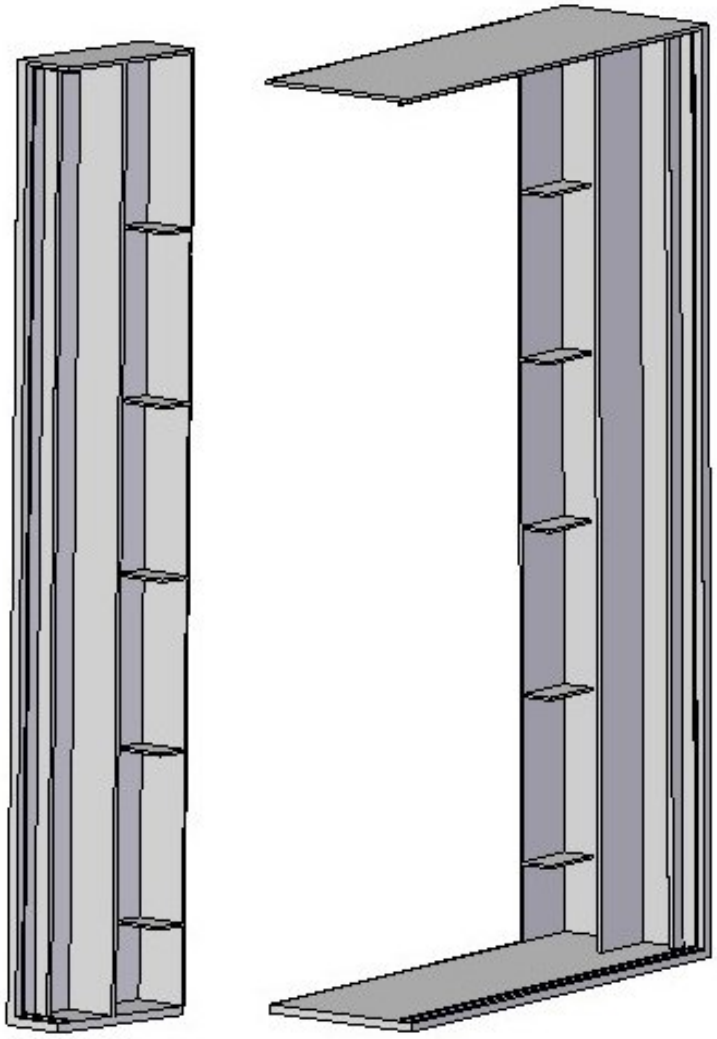

*Figure II.6 – Mass Production Design Plastic Frame*

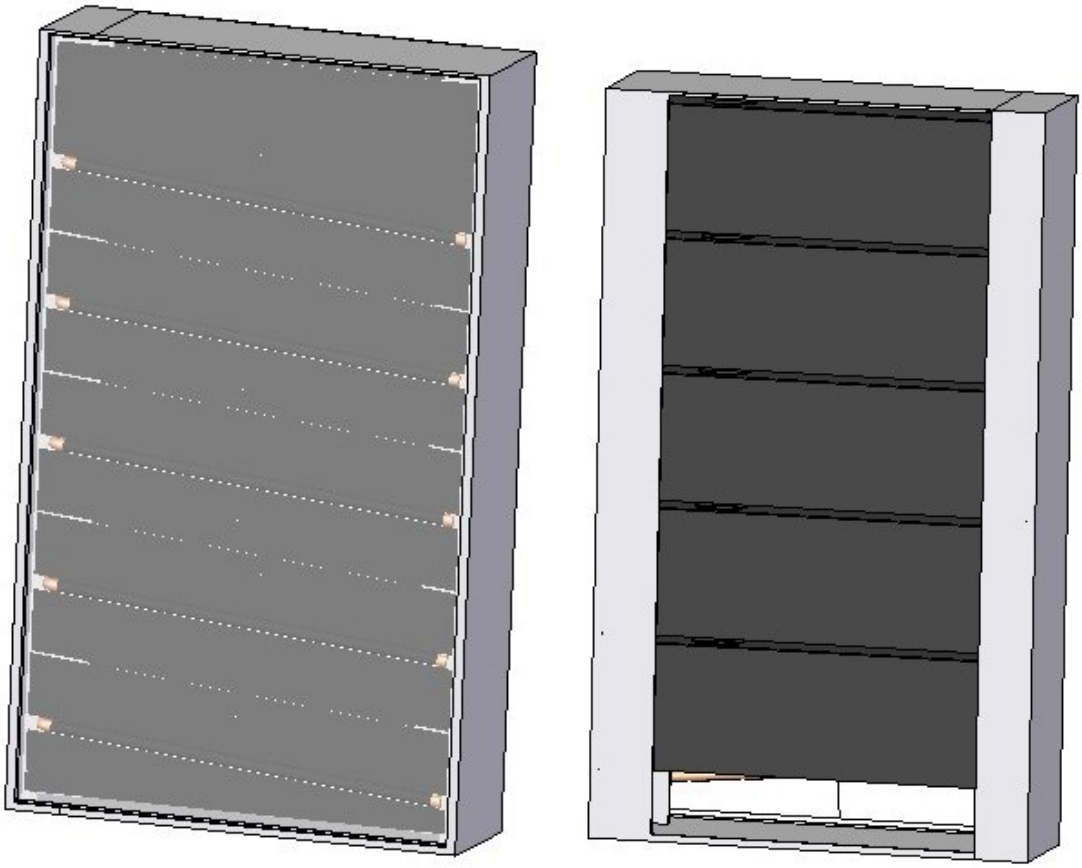

*Figure II.7 – Full Mass Production Unit*

# APPENDIX III

## CD WITH DRAFTS, SOLID MODELS, AND DATA

APPENDIX IV

SUPPORT FRAME AND INSTALLATION DETAIL

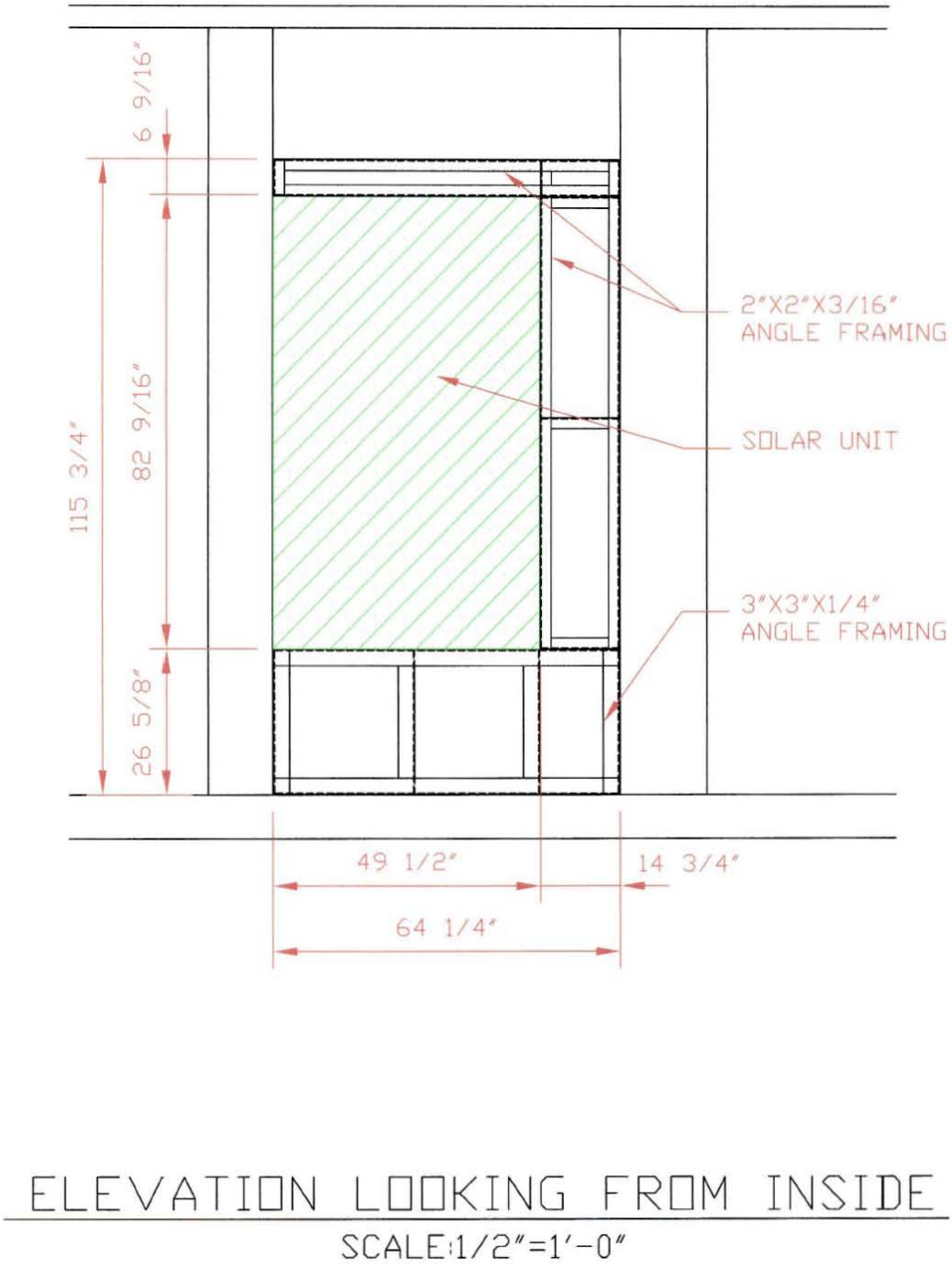


*Figure IV.1 – Support Frame and Installation Detail Front View*

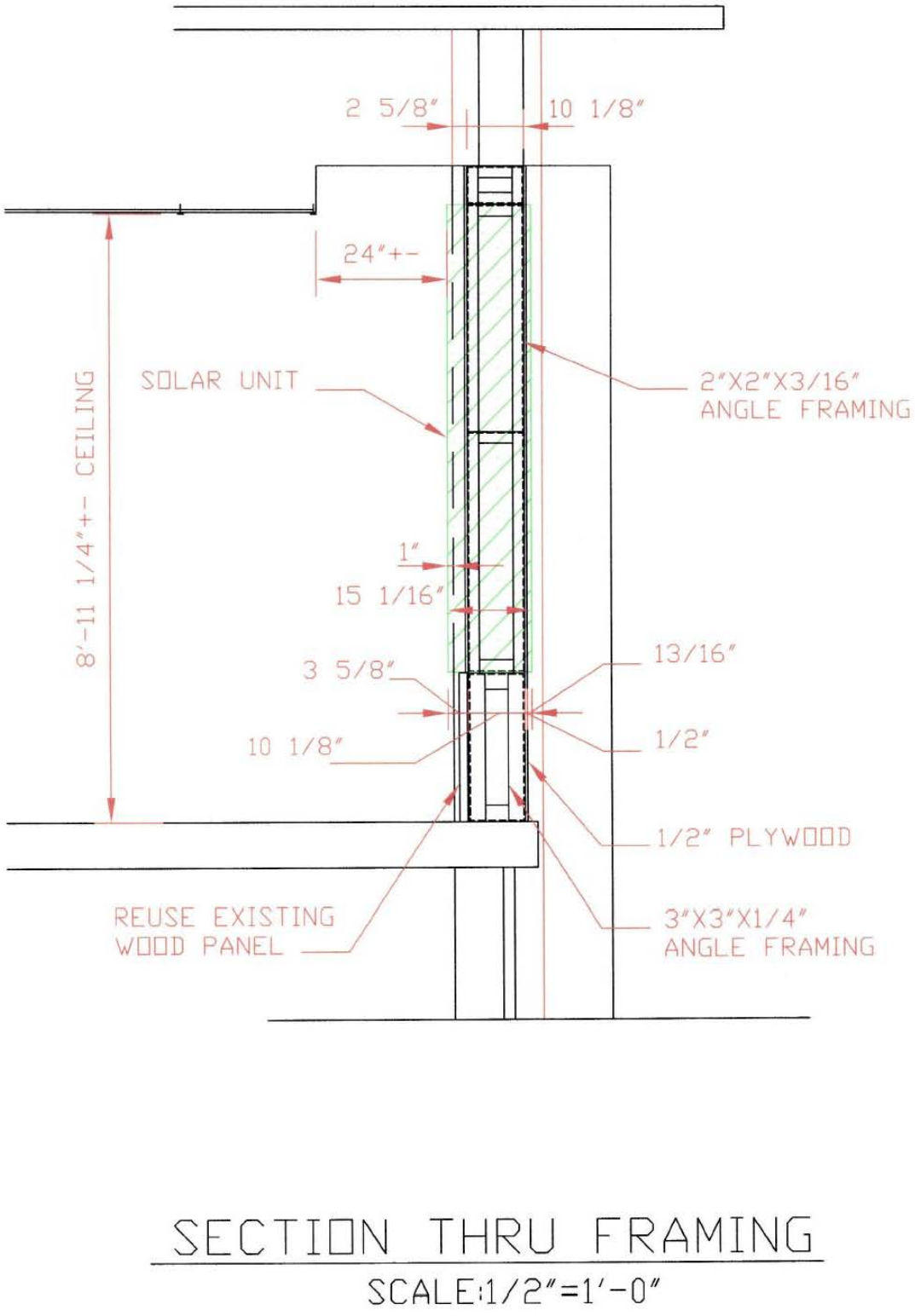


*Figure IV.2 – Support Frame and Installation Detail Side View*

# APPENDIX V

## ASSEMBLY AND PRODUCTION INSTRUCTIONS

1. Cut copper pipe to evaporator, adiabatic, and condenser section lengths.
2. Sand and flux all soldering joints on copper pipe sections, end caps, and elbows.
3. Place heat pipe components in soldering fixture (fixture necessary to achieve angle requirements).
4. Solder all heat pipe joints (4 places).
5. Drill 1/8 inch hole in adiabatic section at charging location.
6. Use punch to create indent for refrigerant line.
7. Cut refrigerant line to length.
8. Solder charging valve on refrigerant line.
9. Solder refrigerant line to heat pipe adiabatic section.
10. Charge heat pipe with refrigerant.
11. Slide plastic water tanks into main polymer frame.
12. Install batt insulation into polymer frame.
13. Place bulkhead over heat pipe condenser section.
14. Slide heat pipe into place in main polymer frame.
15. Install bulkhead with sealant where applicable.
16. Install and clamp absorber plates in front facing of main polymer frame (install 50 clamping screws).
17. Slide glazing into slot in main polymer frame.
18. Slide secondary polymer frame into place (install 10 clamping screws).
19. Seal polymer frame seams and glazing slot with silicone.
20. Cut rear cover spline materials to length.
21. Install screen into rear cover.

22. Tape bag of surplus rear cover screws into unit.
23. Install rear cover (install 4 screws).
24. Assemble shipping box and styrofoam.
25. Place unit into shipping container.
26. Assemble shipping units onto pallets.

APPENDIX VI

EXPERIMENTAL AMBIENT CONDITIONS

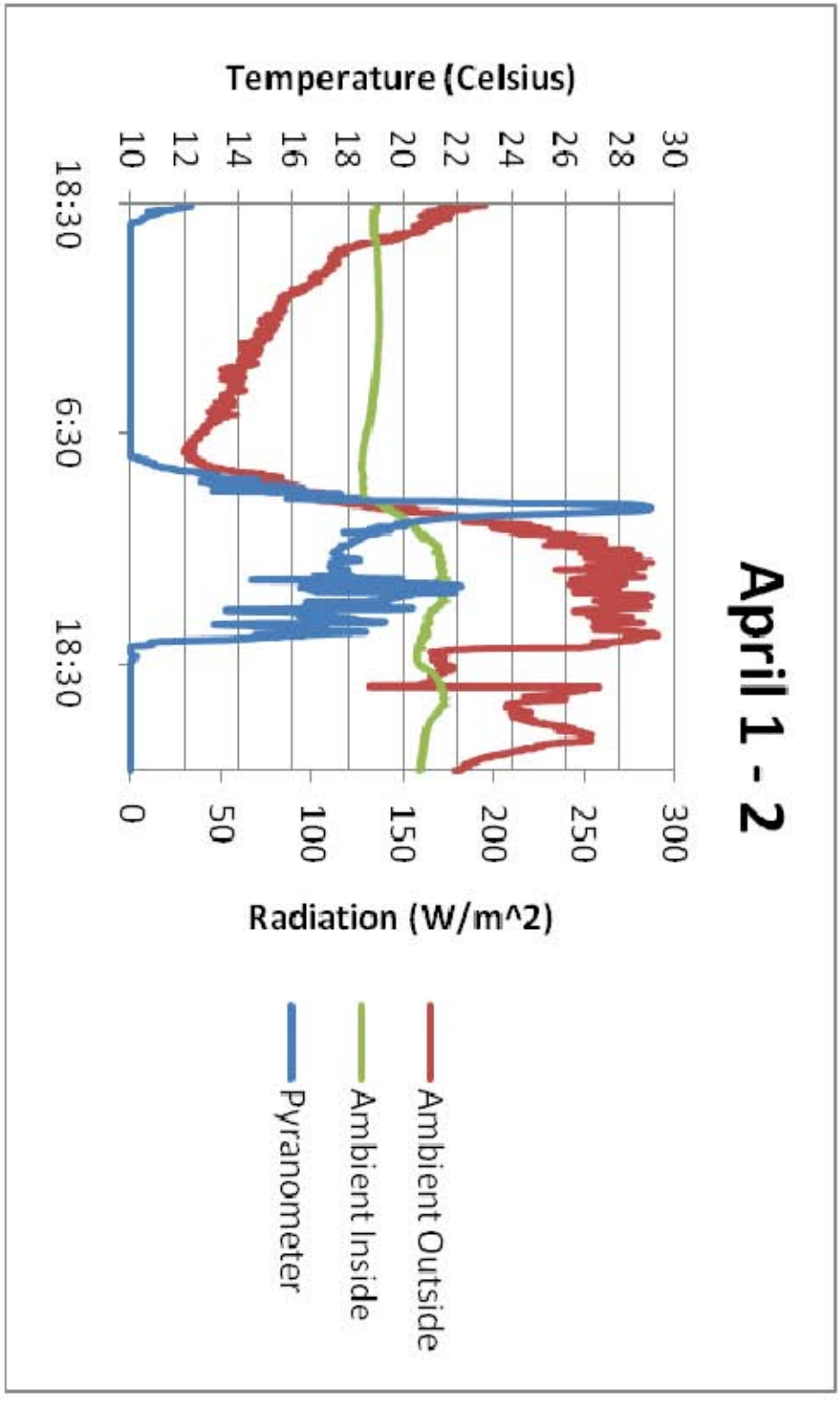

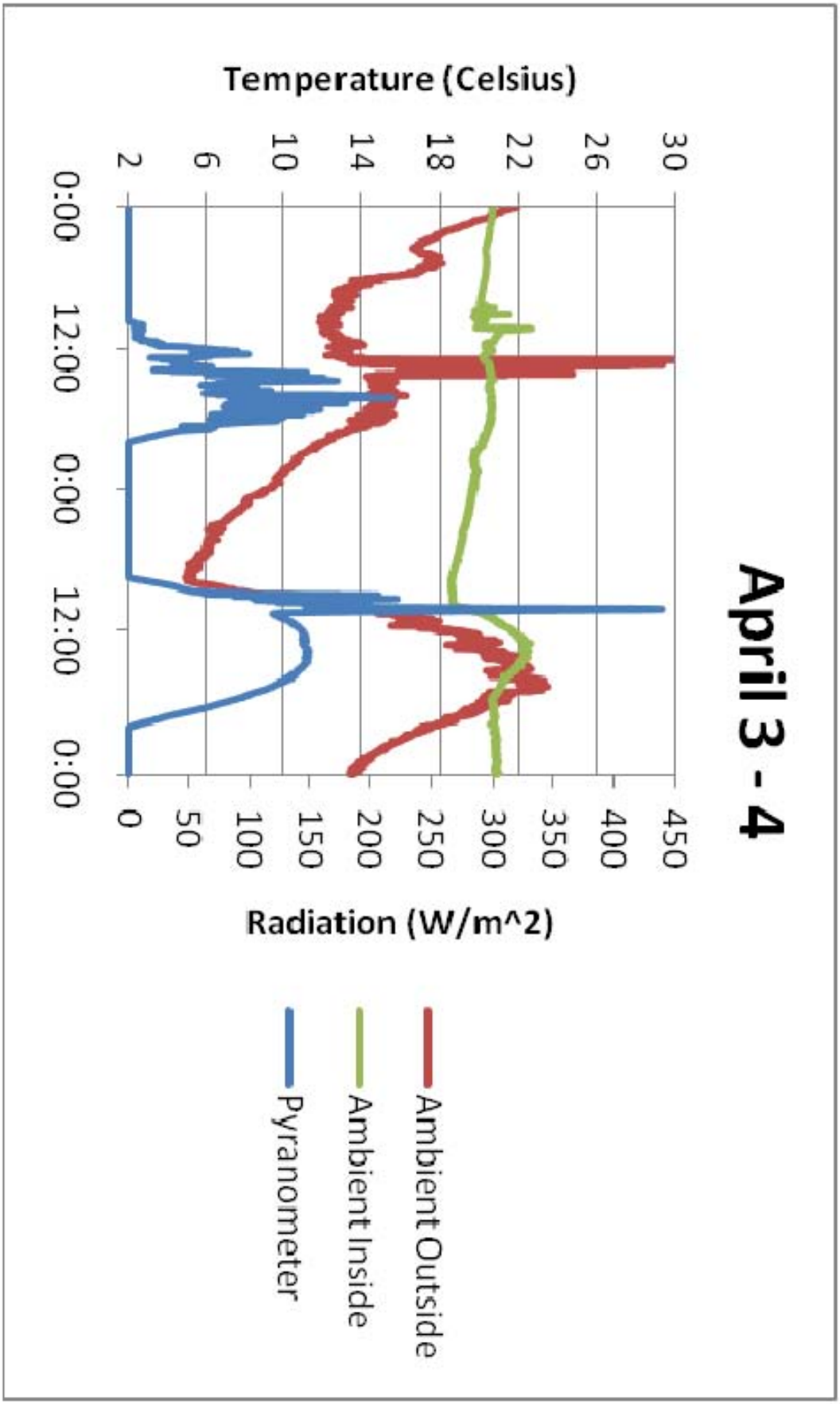
April 3 - 4
Temperature (Celsius)
30
26
22
18
14
10
6
2
0:00
12:00
0:00
12:00
0:00
0
50
100
150
200
250
300
350
400
450
Radiation (W/m^2)
Ambient Outside
Ambient Inside
Pyranometer

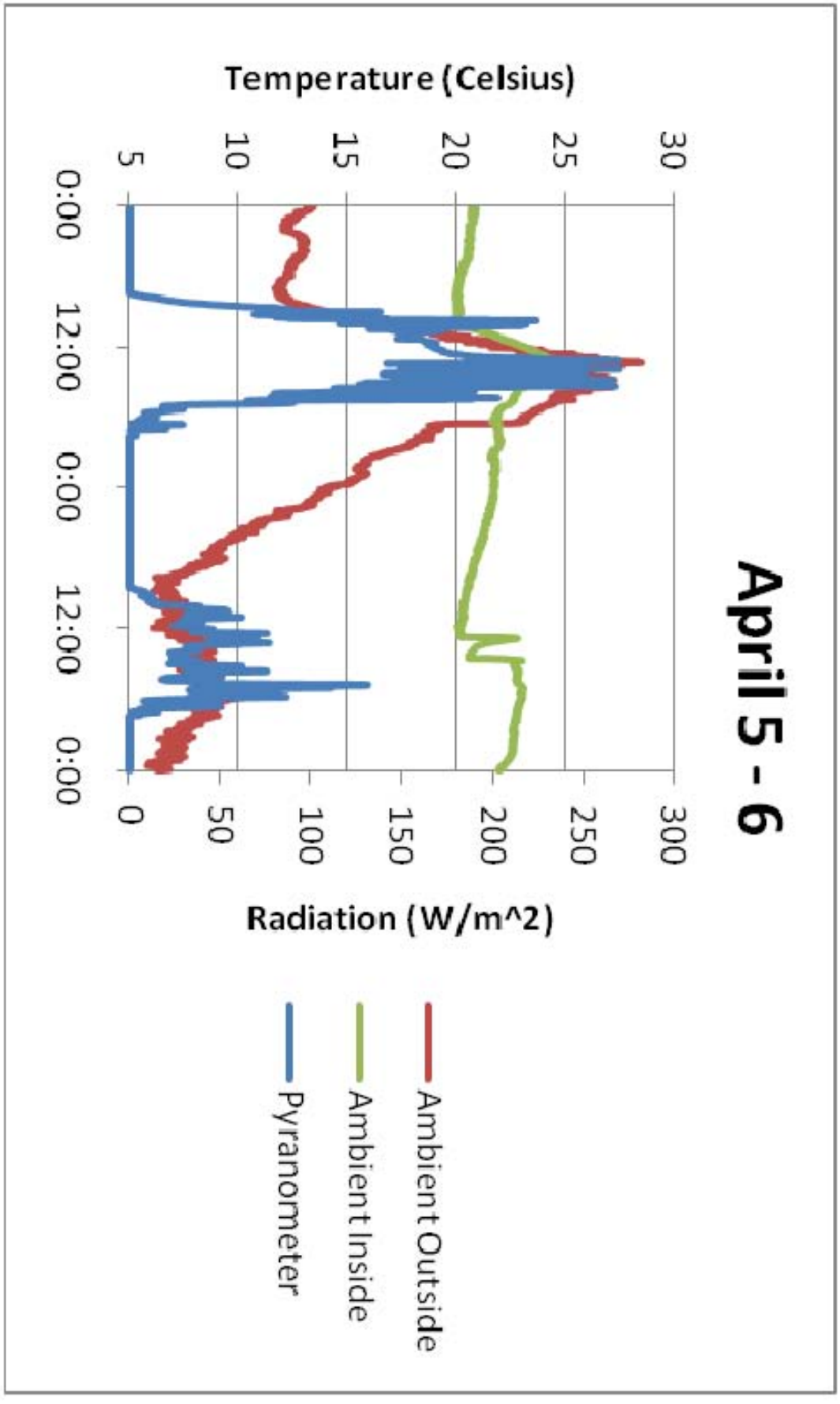
April 5 - 6
Temperature (Celsius)
5
10
15
20
25
30
0:00
12:00
0:00
12:00
0:00
0
50
100
150
200
250
300
Radiation (W/m^2)
Ambient Outside
Ambient Inside
Pyranometer

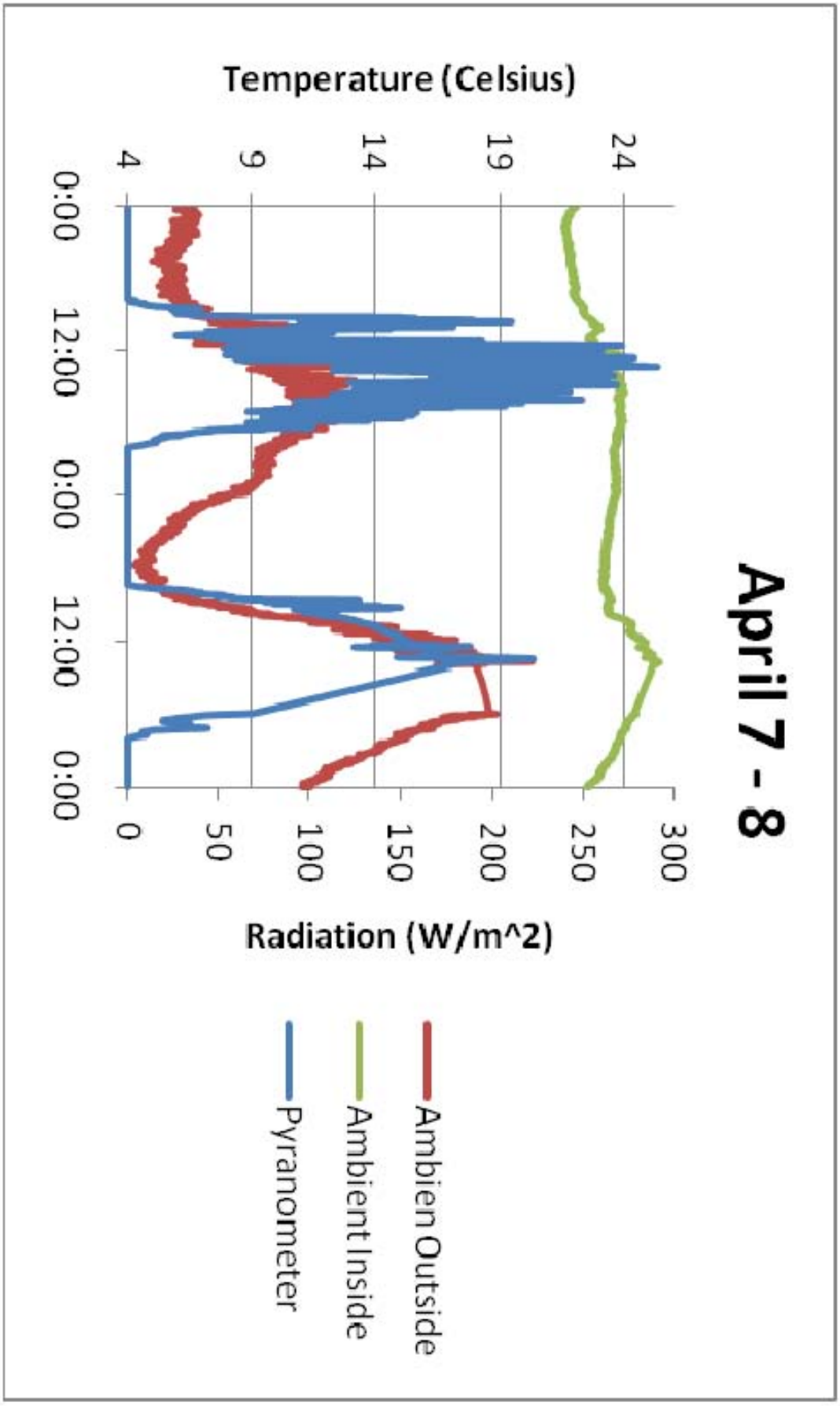
April 7 - 8
Temperature (Celsius)
4
9
14
19
24
0:00
12:00
0:00
12:00
0:00
0
50
100
150
200
250
300
Radiation (W/m^2)
Ambien Outside
Ambient Inside
Pyranometer

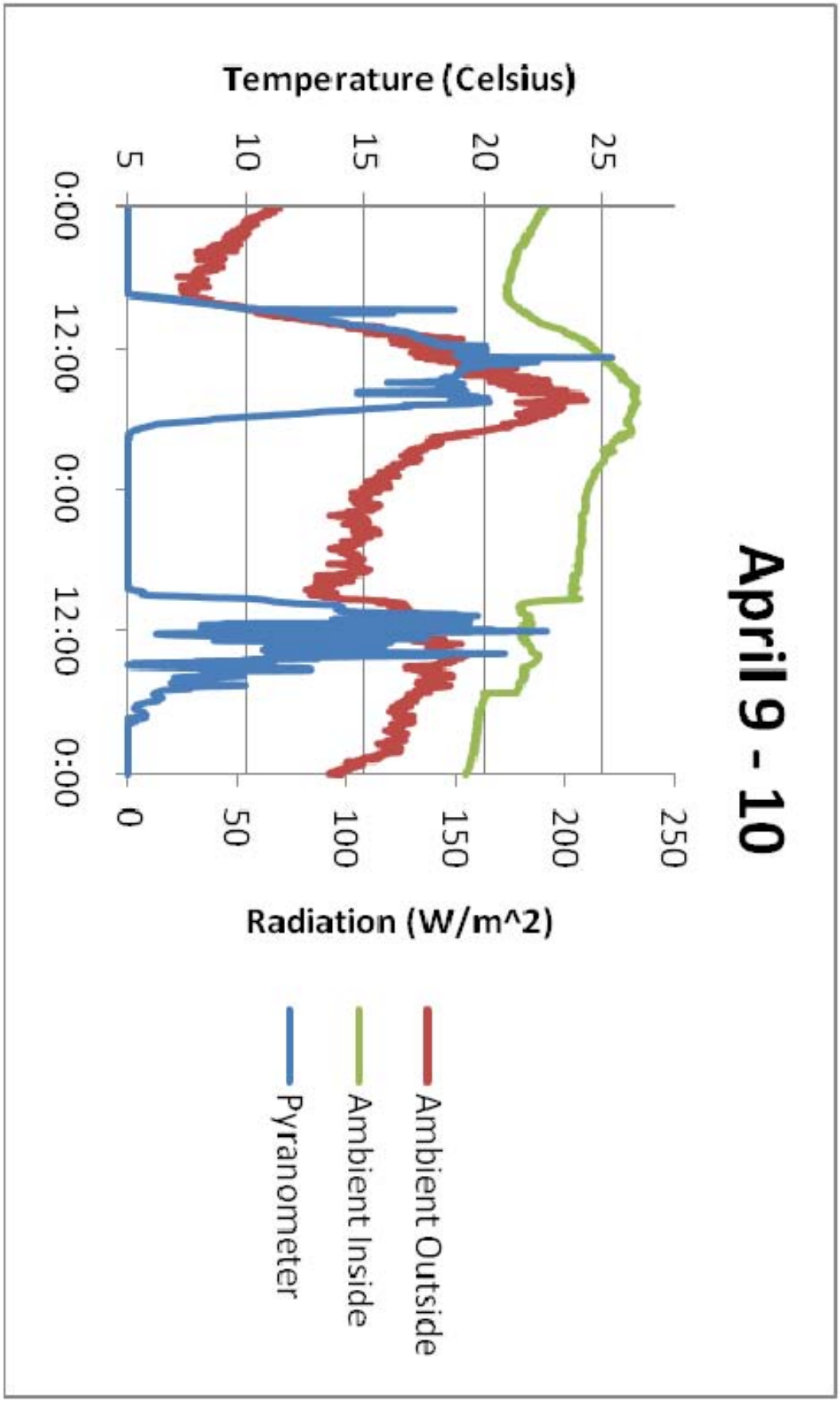
April 9 - 10
Temperature (Celsius)
5
10
15
20
25
0:00
12:00
0:00
12:00
0:00
0
50
100
150
200
250
Radiation (W/m^2)
Ambient Outside
Ambient Inside
Pyranometer

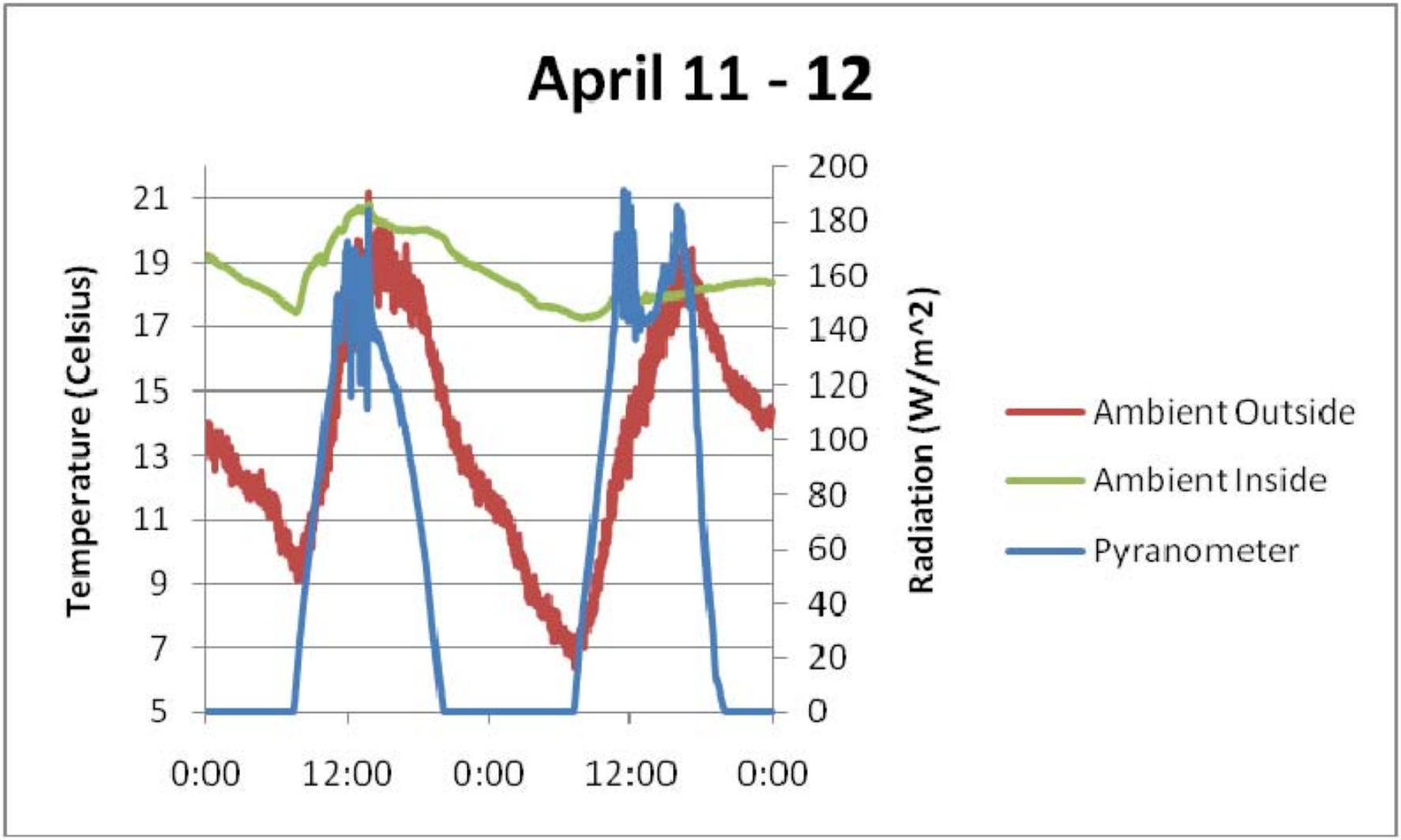
April 11 - 12
Temperature (Celsius)
21
19
17
15
13
11
9
7
5
0:00
12:00
0:00
12:00
0:00
200
180
160
140
120
100
80
60
40
20
0
Radiation (W/m^2)
Ambient Outside
Ambient Inside
Pyranometer

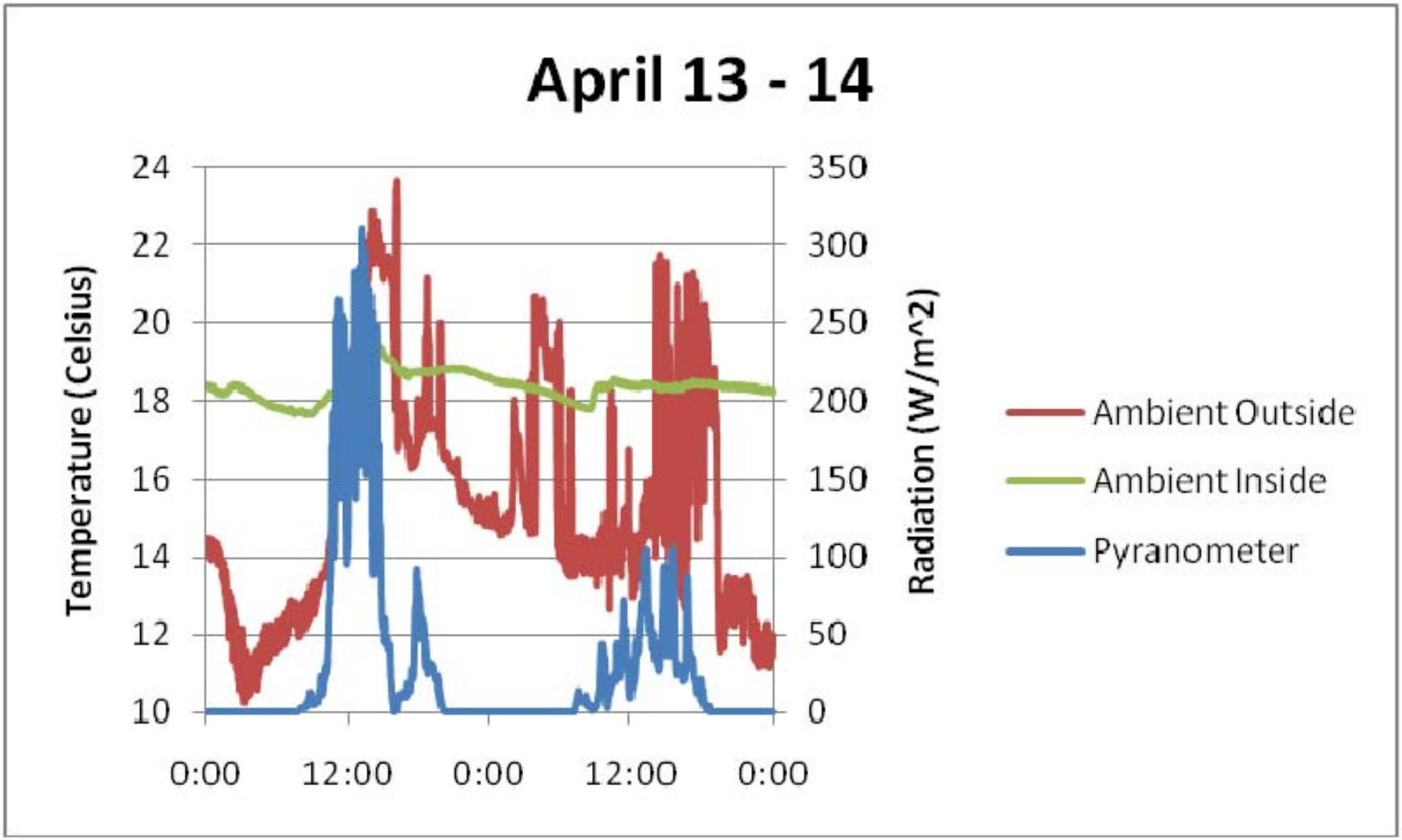
April 13 - 14
Temperature (Celsius)
24
22
20
18
16
14
12
10
0:00
12:00
0:00
12:00
0:00
350
300
250
200
150
100
50
0
Radiation (W/m^2)
Ambient Outside
Ambient Inside
Pyranometer

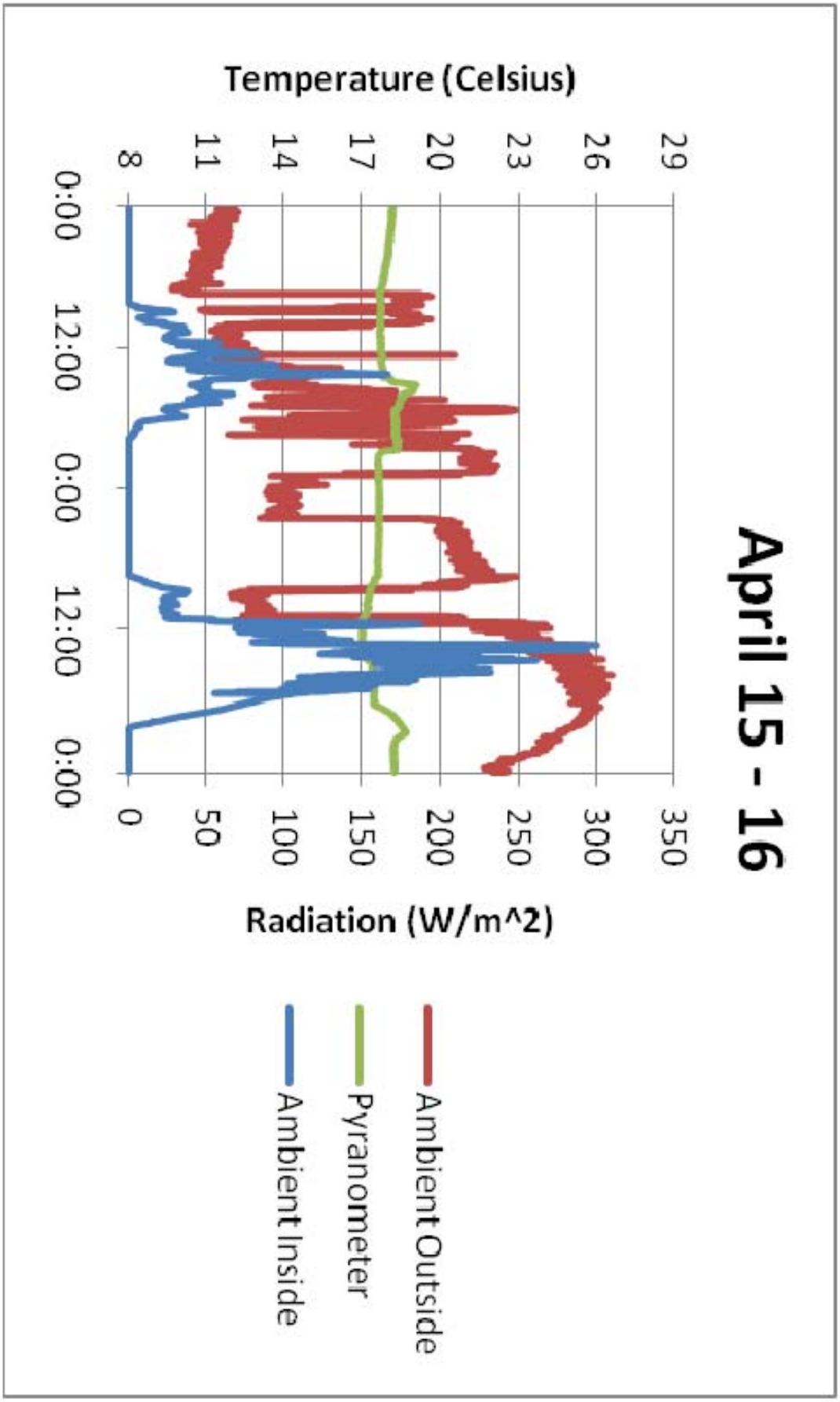
April 15 - 16
Temperature (Celsius)
29
26
23
20
17
14
11
8
0:00
12:00
0:00
12:00
0:00
0
50
100
150
200
250
300
350
Radiation (W/m^2)
Ambient Outside
Pyranometer
Ambient Inside

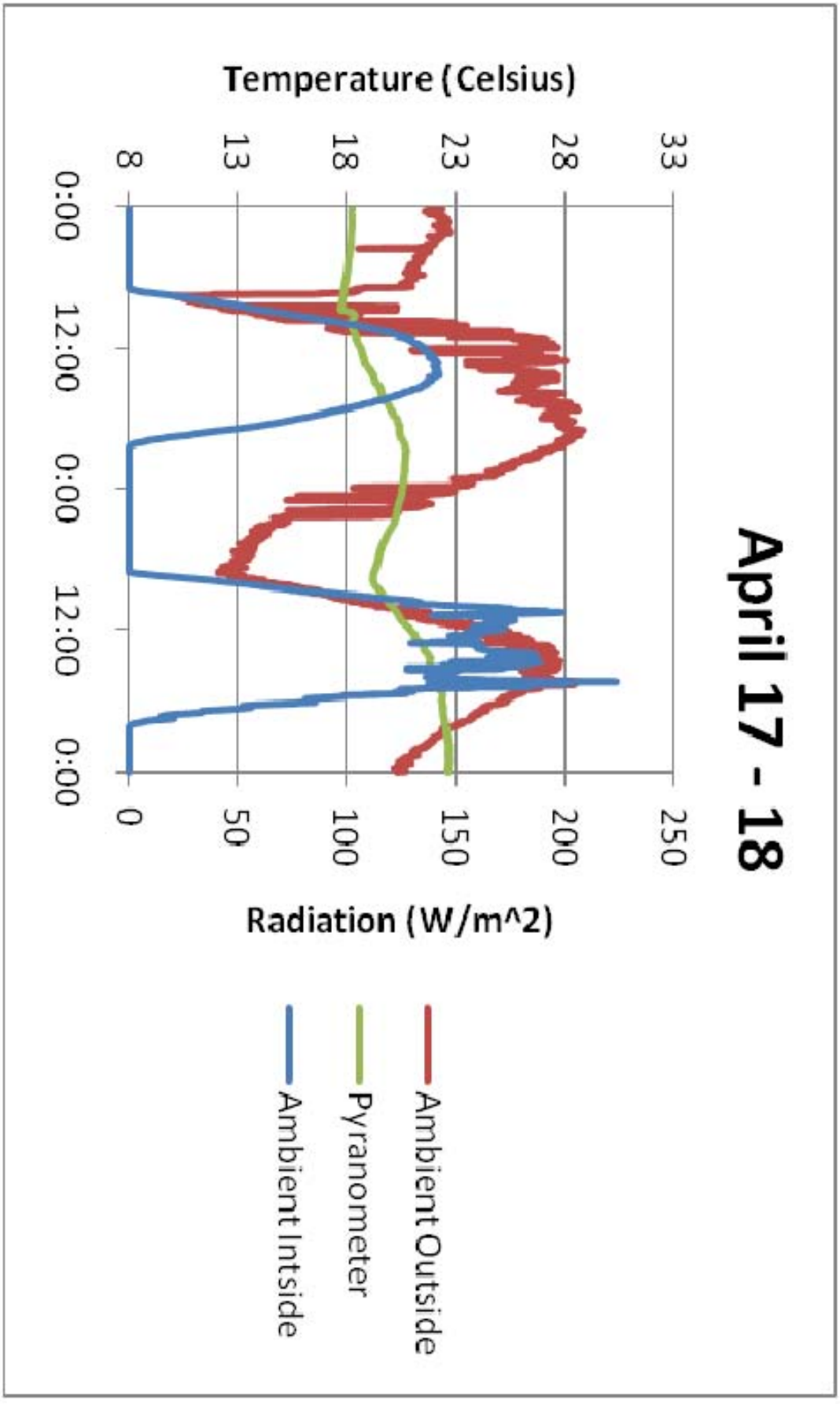
April 17 - 18
Temperature (Celsius)
8
13
18
23
28
33
0:00
12:00
0:00
12:00
0:00
0
50
100
150
200
250
Radiation (W/m^2)
Ambient Outside
Pyranometer
Ambient Intside

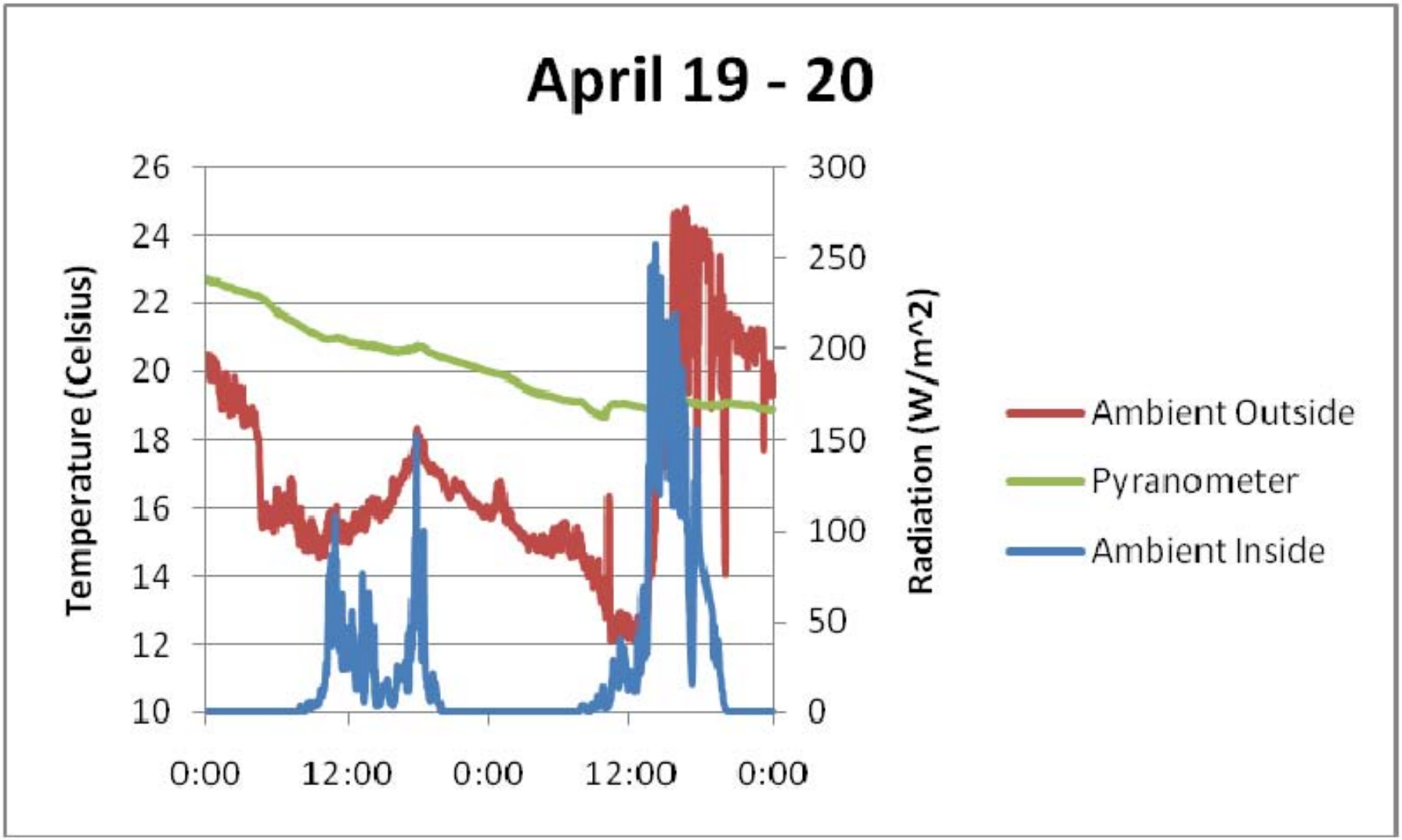
April 19 - 20
Temperature (Celsius)
26
24
22
20
18
16
14
12
10
300
250
200
150
100
50
0
Radiation (W/m^2)
0:00
12:00
0:00
12:00
0:00
Ambient Outside
Pyranometer
Ambient Inside

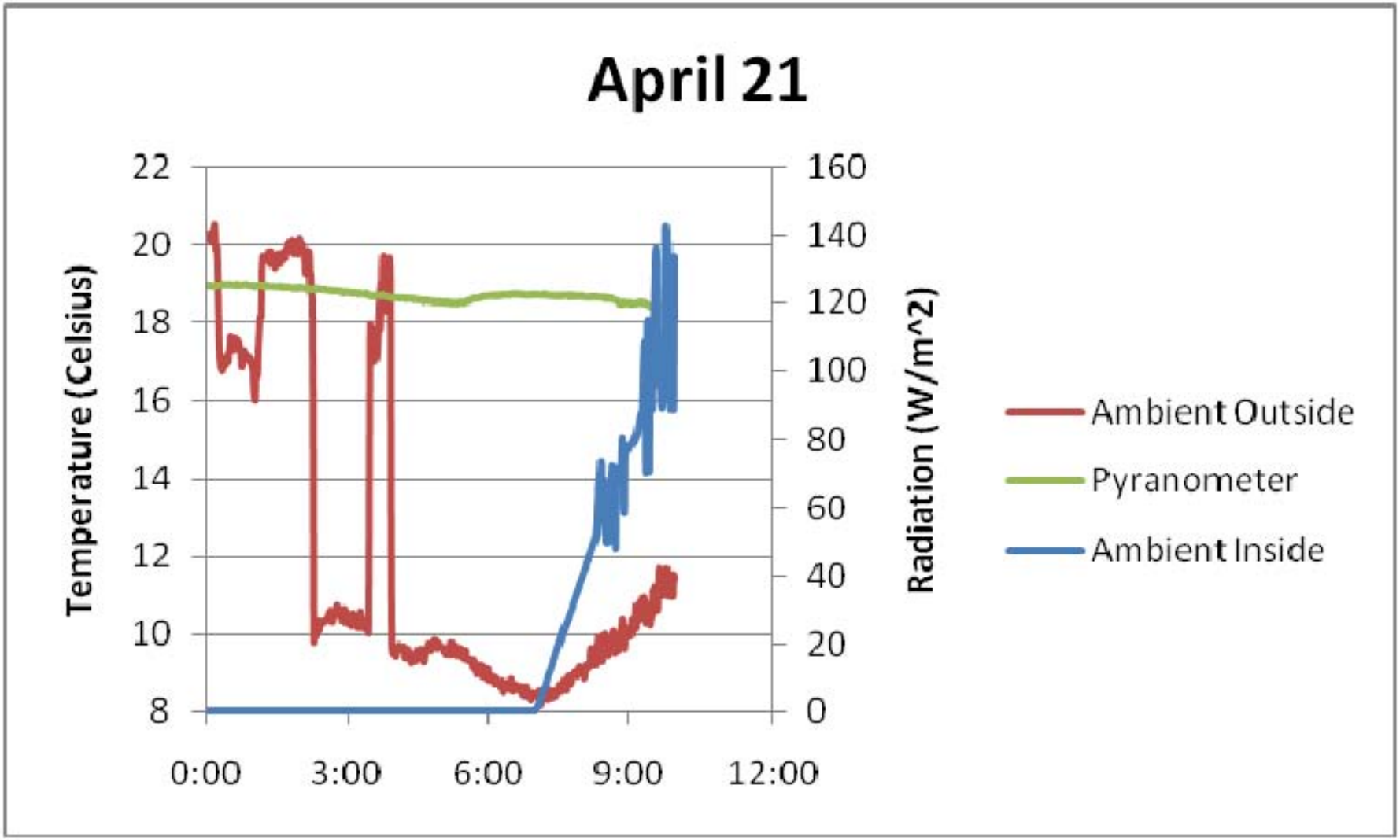
April 21
Temperature (Celsius)
22
20
18
16
14
12
10
8
0:00
3:00
6:00
9:00
12:00
160
140
120
100
80
60
40
20
0
Radiation (W/m^2)
Ambient Outside
Pyranometer
Ambient Inside

APPENDIX VII

EXPERIMENTAL TEMPERATURE DATA

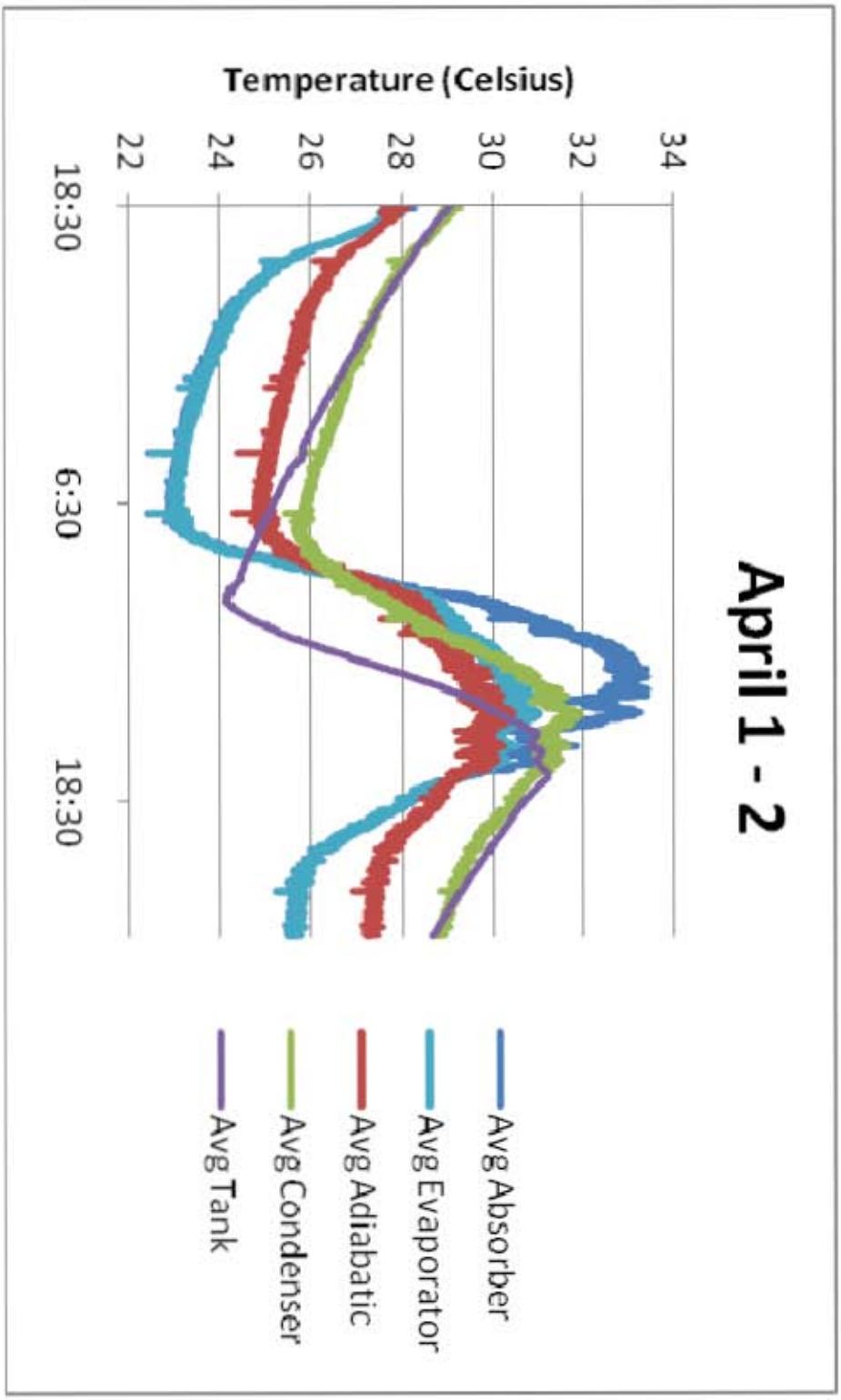

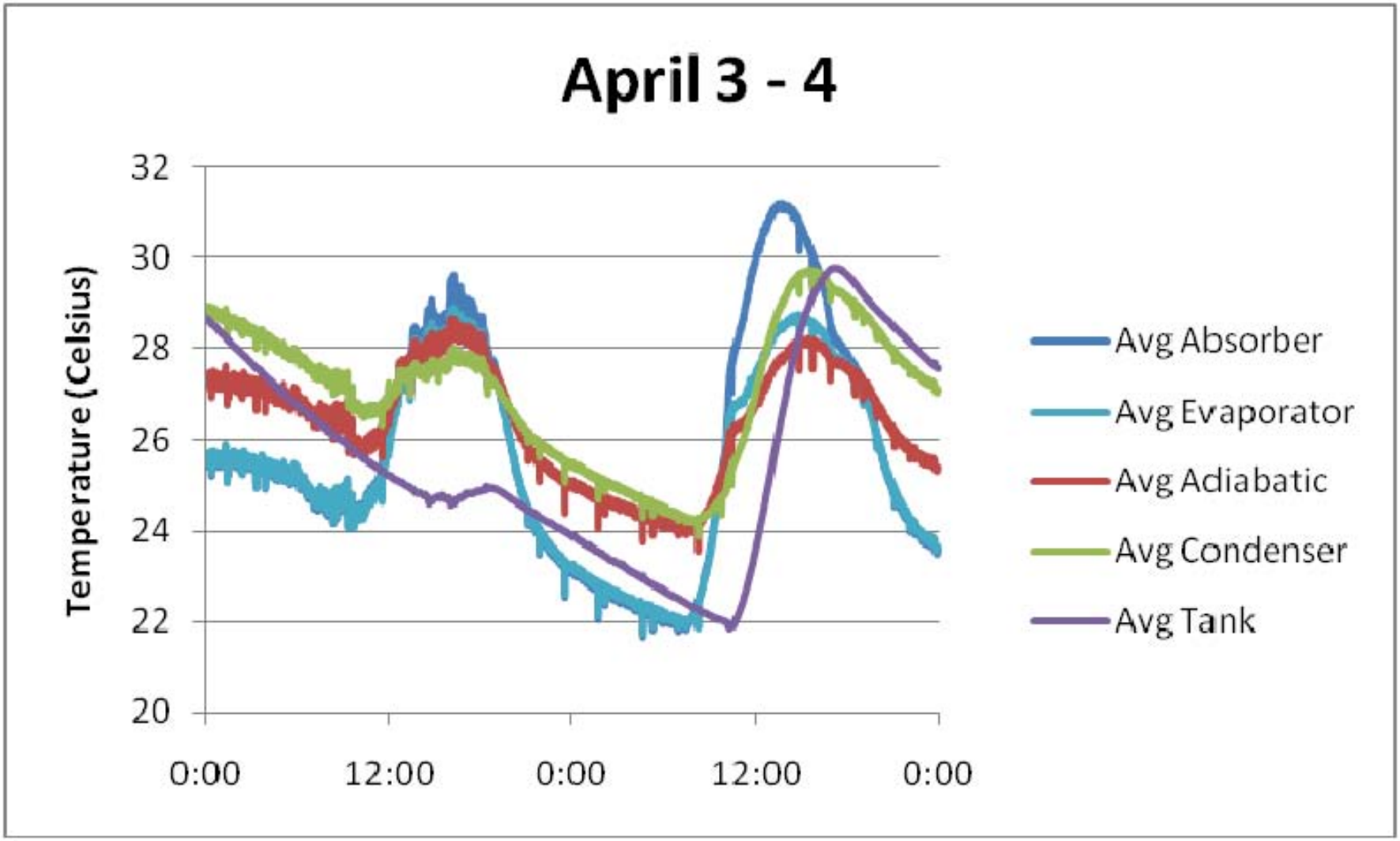
April 3 - 4
Temperature (Celsius)
32
30
28
26
24
22
20
0:00
12:00
0:00
12:00
0:00
Avg Absorber
Avg Evaporator
Avg Adiabatic
Avg Condenser
Avg Tank

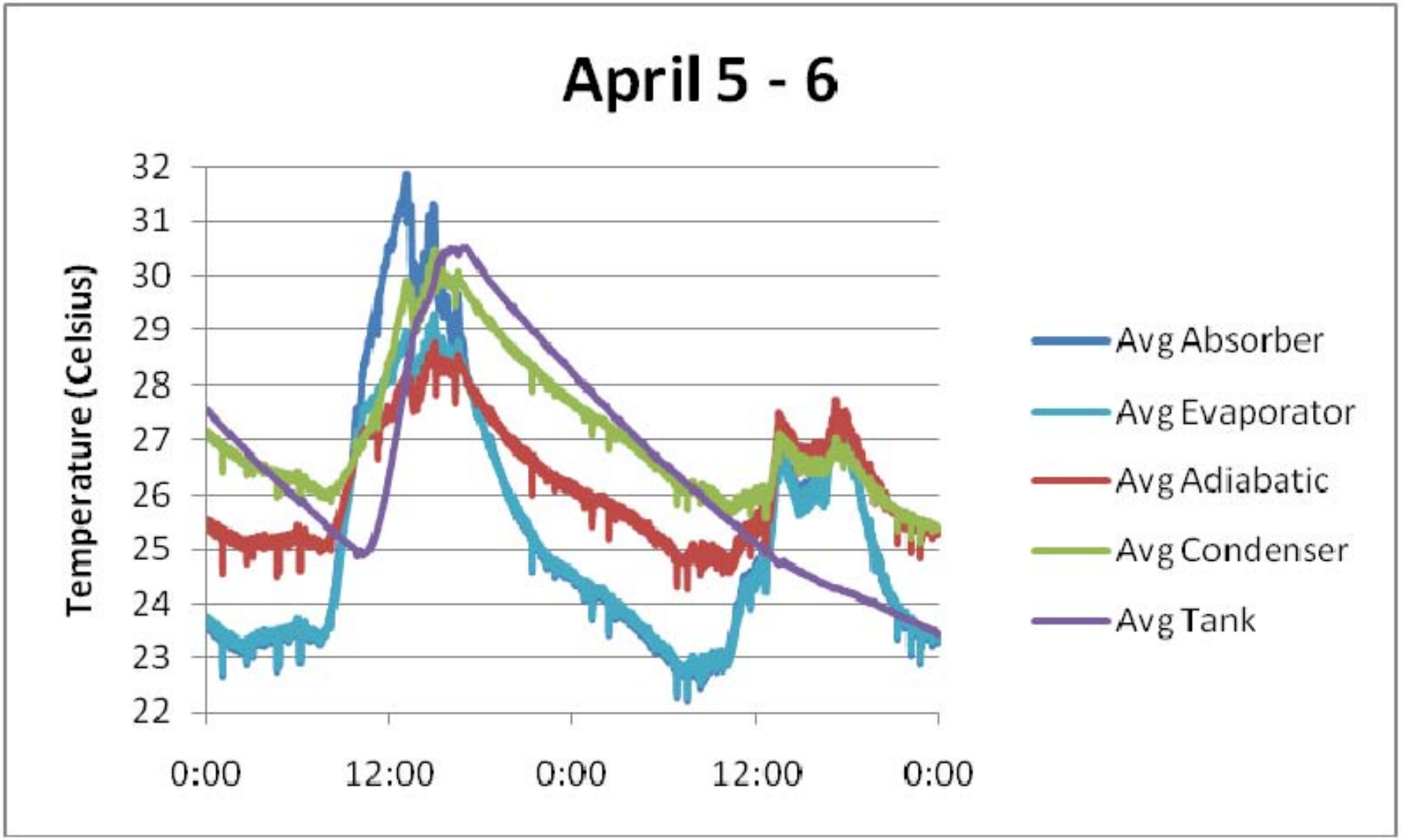
April 5 - 6
Temperature (Celsius)
32
31
30
29
28
27
26
25
24
23
22
0:00
12:00
0:00
12:00
0:00
Avg Absorber
Avg Evaporator
Avg Adiabatic
Avg Condenser
Avg Tank

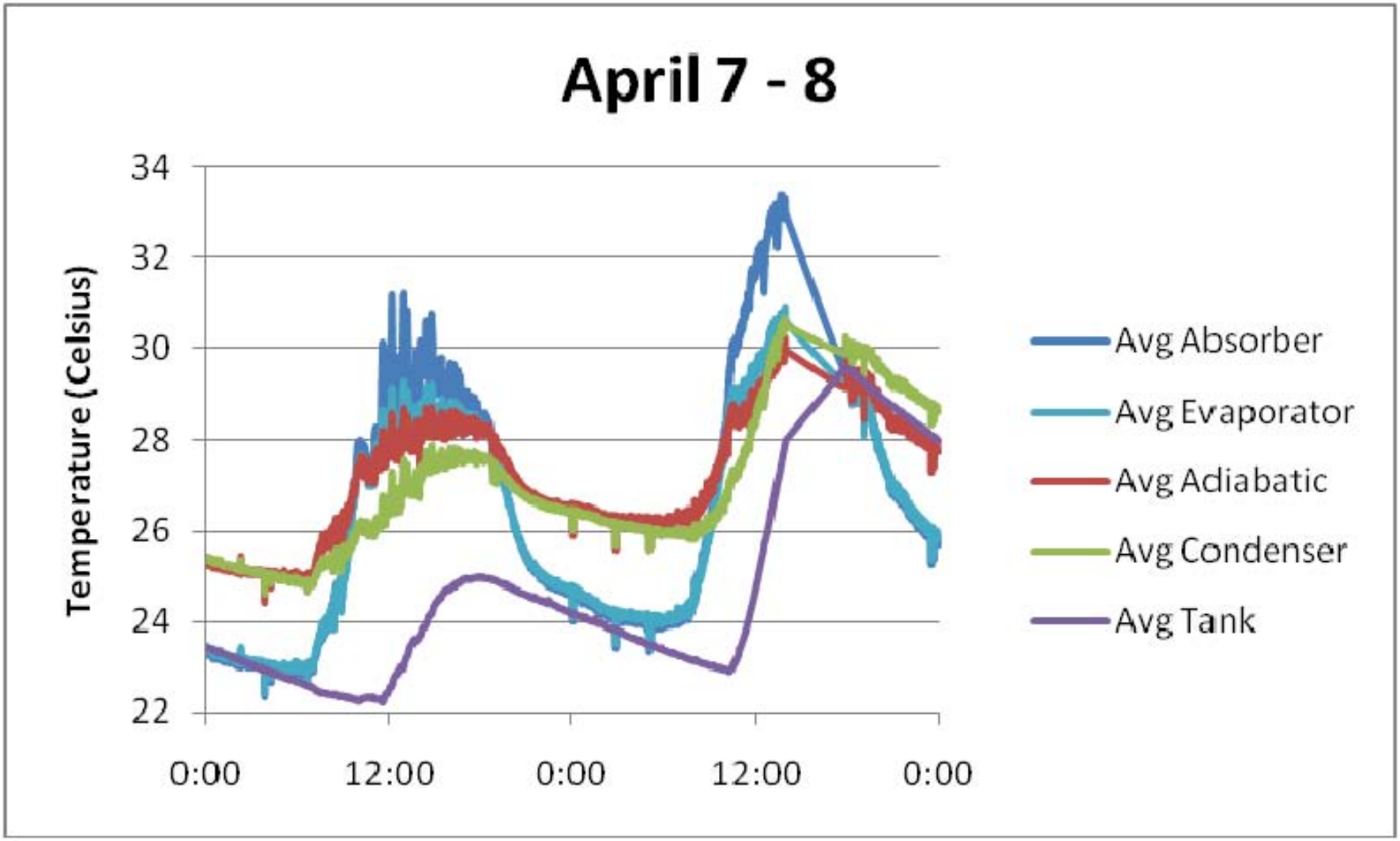
April 7 - 8
Temperature (Celsius)
34
32
30
28
26
24
22
0:00
12:00
0:00
12:00
0:00
Avg Absorber
Avg Evaporator
Avg Adiabatic
Avg Condenser
Avg Tank

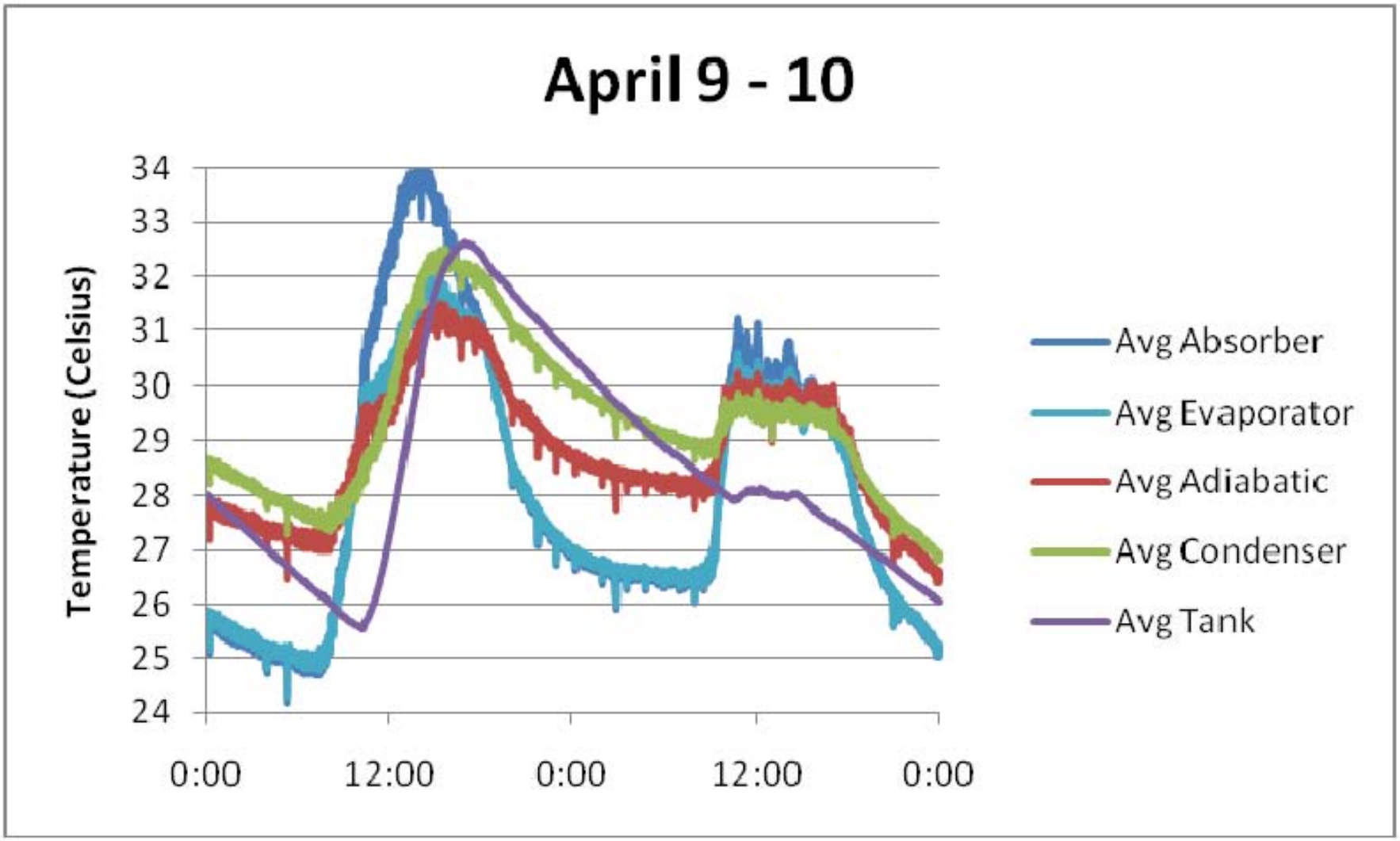
April 9 - 10
Temperature (Celsius)
34
33
32
31
30
29
28
27
26
25
24
0:00
12:00
0:00
12:00
0:00
Avg Absorber
Avg Evaporator
Avg Adiabatic
Avg Condenser
Avg Tank

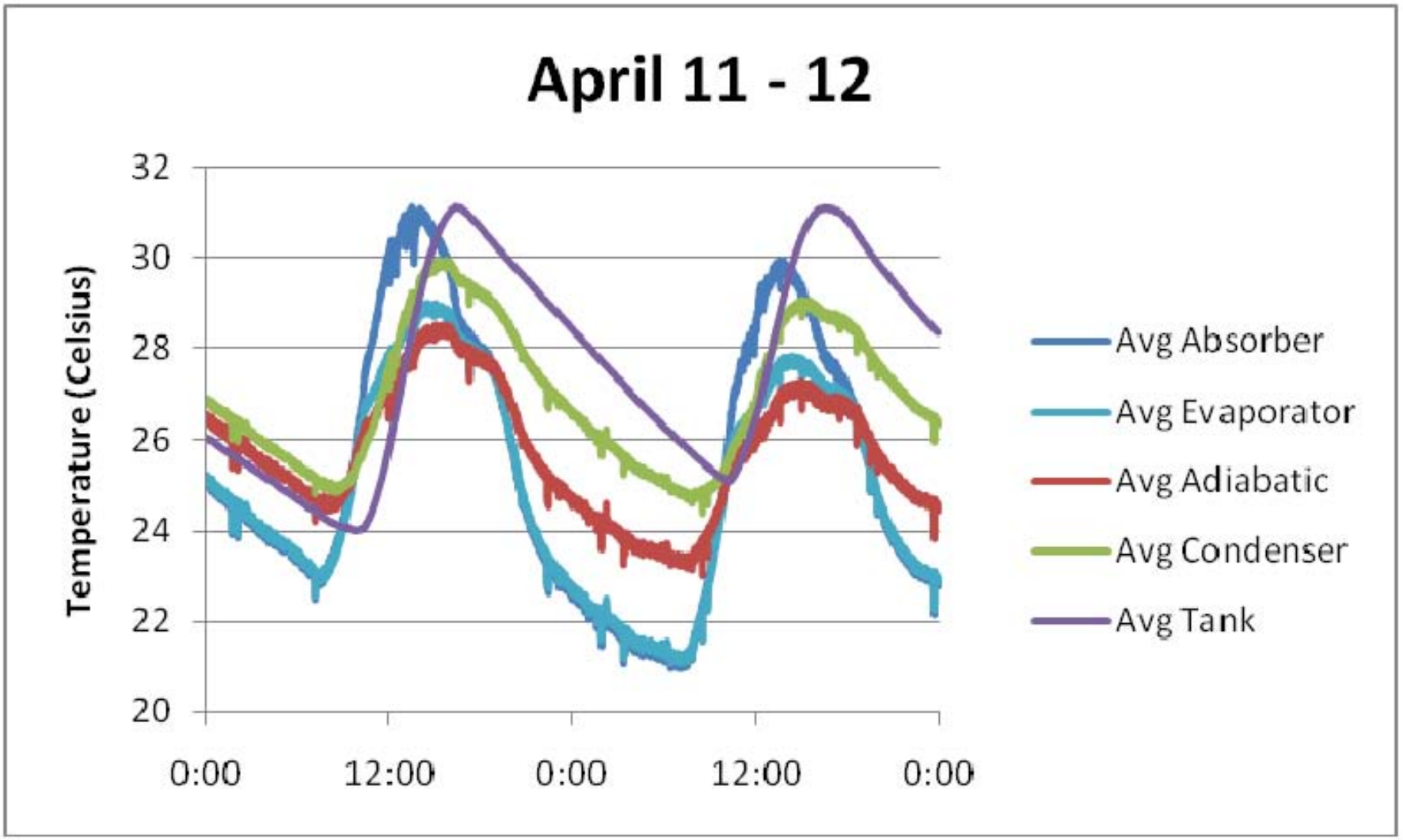
April 11 - 12
Temperature (Celsius)
32
30
28
26
24
22
20
0:00
12:00
0:00
12:00
0:00
Avg Absorber
Avg Evaporator
Avg Adiabatic
Avg Condenser
Avg Tank

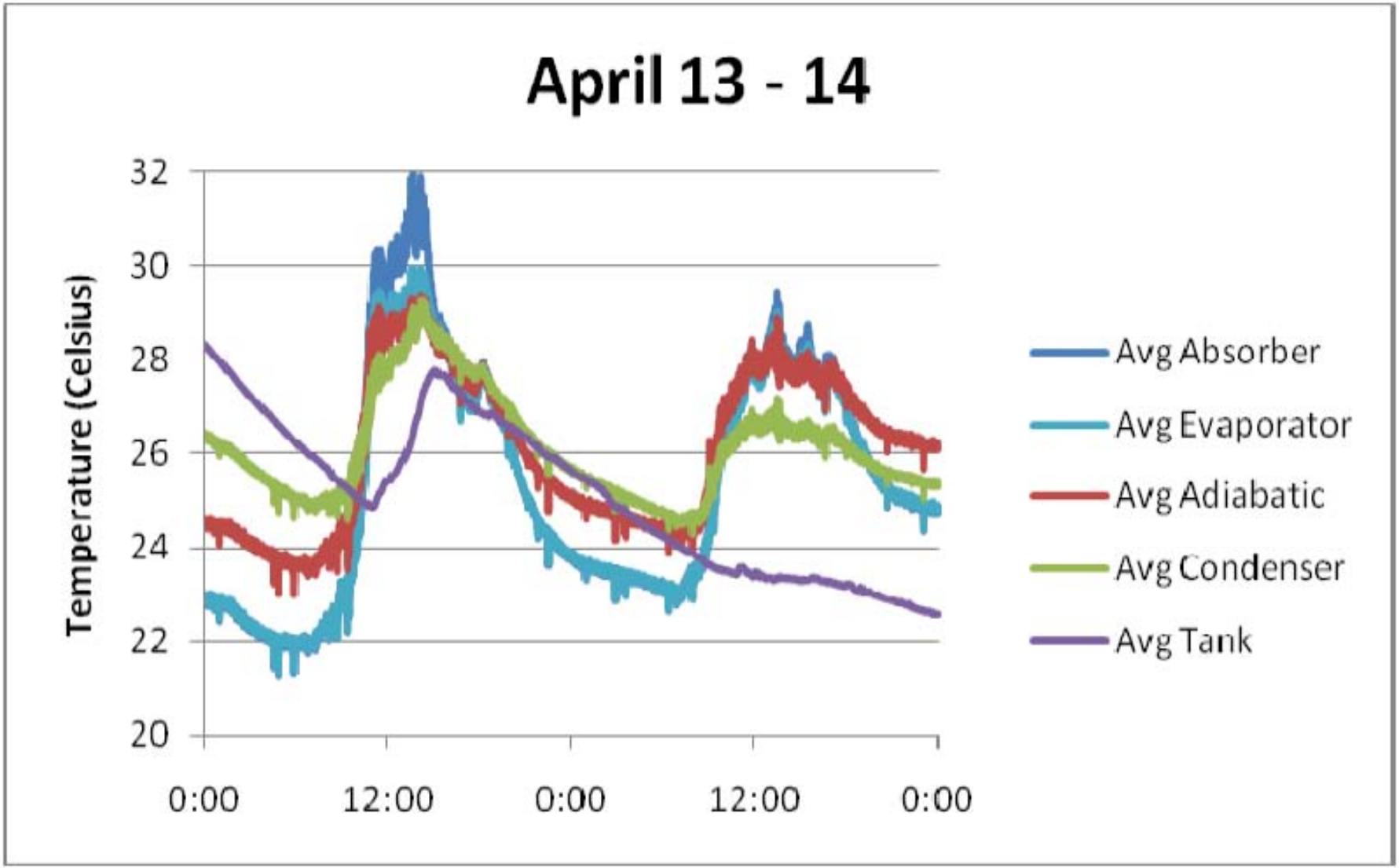
April 13 - 14
Temperature (Celsius)
32
30
28
26
24
22
20
0:00
12:00
0:00
12:00
0:00
Avg Absorber
Avg Evaporator
Avg Adiabatic
Avg Condenser
Avg Tank

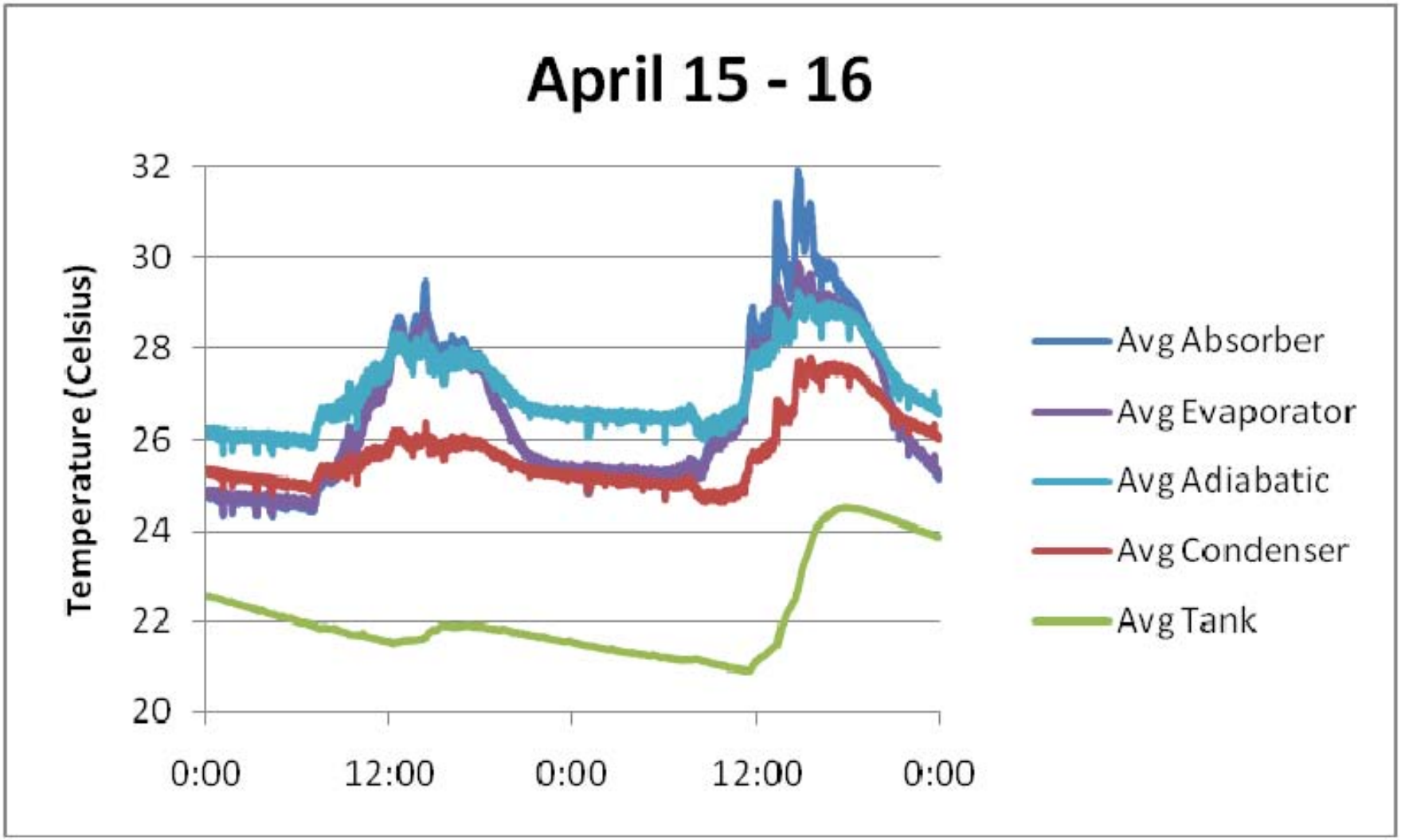
April 15 - 16
Temperature (Celsius)
32
30
28
26
24
22
20
0:00
12:00
0:00
12:00
0:00
Avg Absorber
Avg Evaporator
Avg Adiabatic
Avg Condenser
Avg Tank

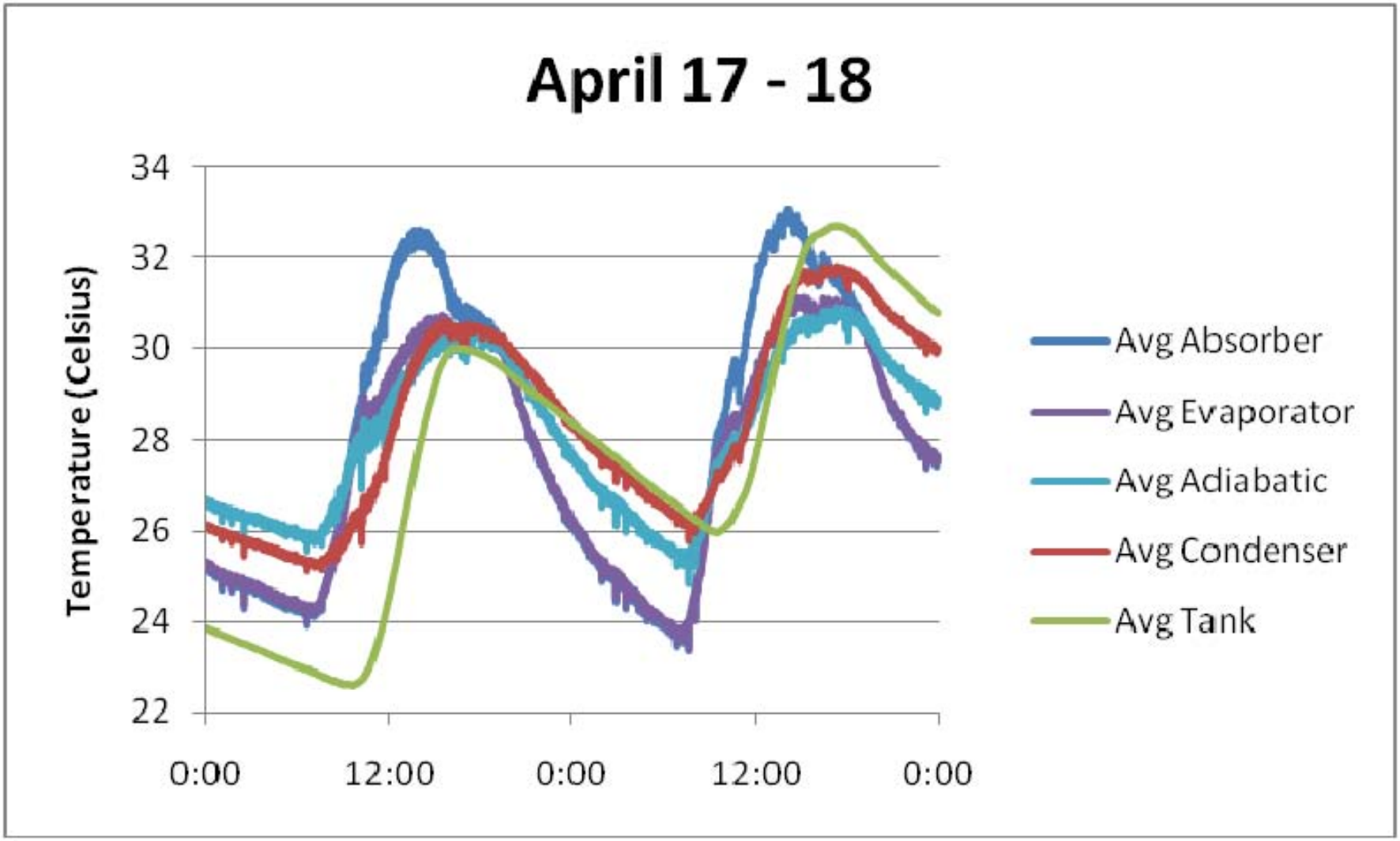
April 17 - 18
Temperature (Celsius)
34
32
30
28
26
24
22
0:00
12:00
0:00
12:00
0:00
Avg Absorber
Avg Evaporator
Avg Adiabatic
Avg Condenser
Avg Tank

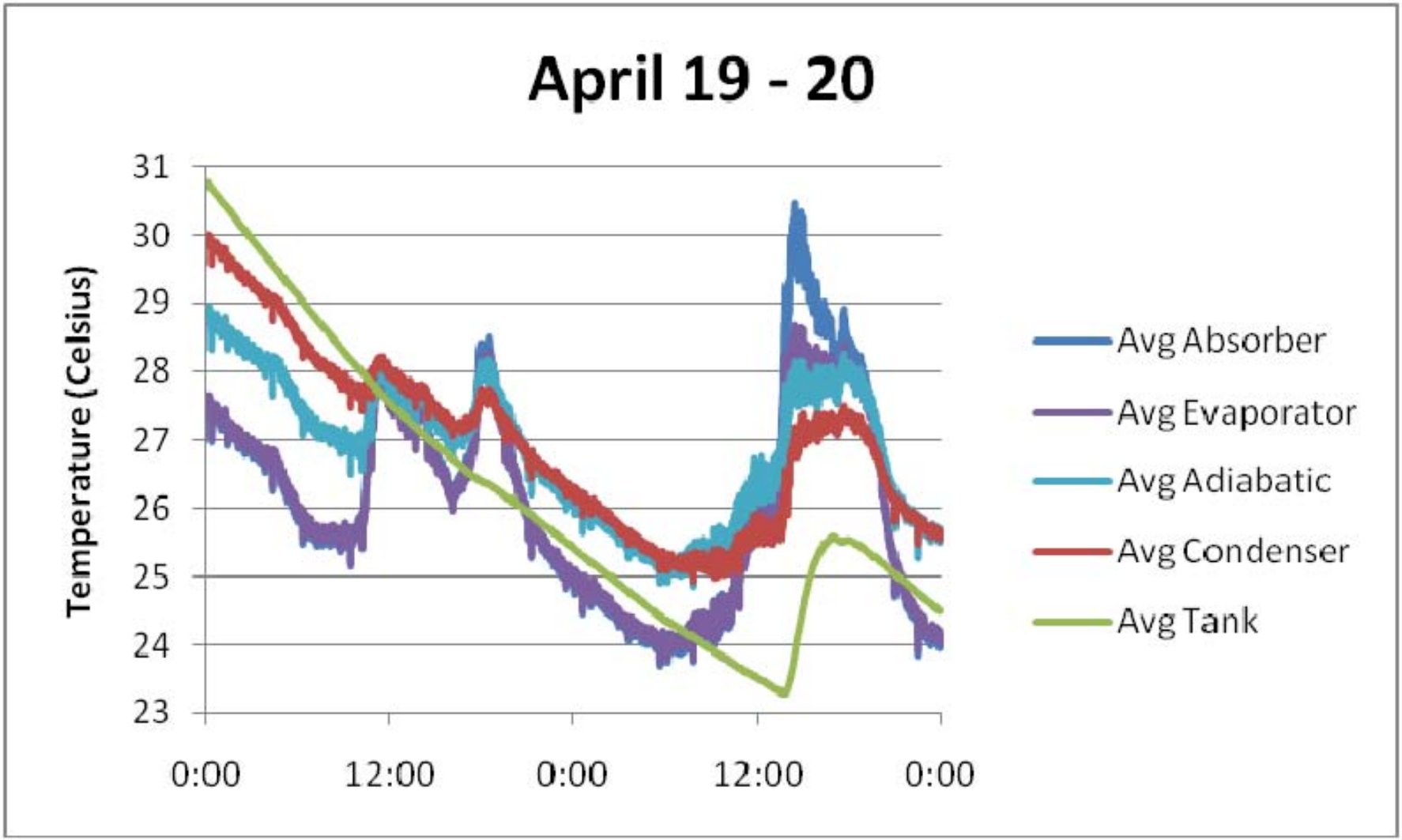
April 19 - 20
Temperature (Celsius)
31
30
29
28
27
26
25
24
23
0:00
12:00
0:00
12:00
0:00
Avg Absorber
Avg Evaporator
Avg Adiabatic
Avg Condenser
Avg Tank

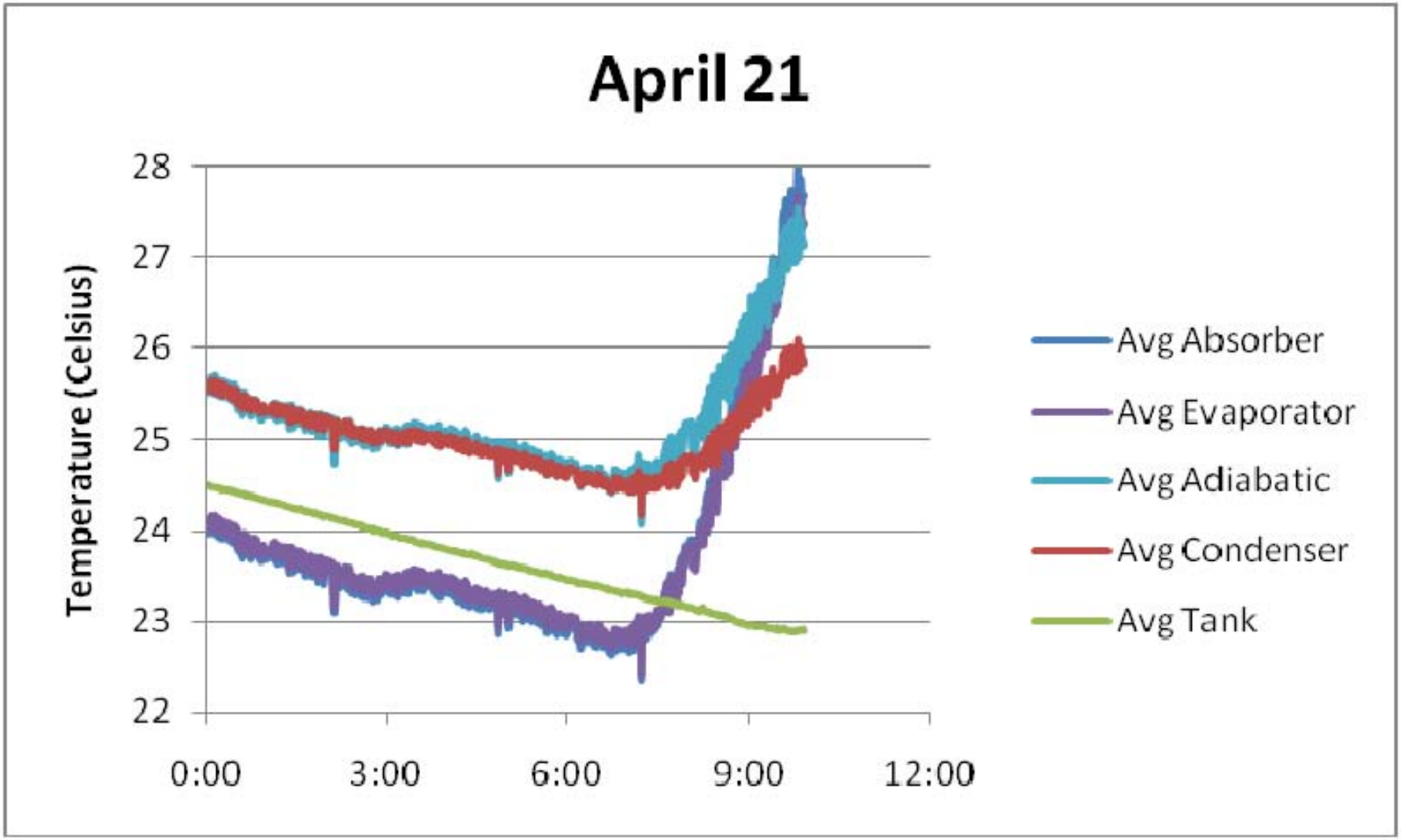
April 21
Temperature (Celsius)
28
27
26
25
24
23
22
0:00
3:00
6:00
9:00
12:00
Avg Absorber
Avg Evaporator
Avg Adiabatic
Avg Condenser
Avg Tank

APPENDIX VIII

REPORTED LOCAL WEATHER CONDITIONS FOR TESTING PERIOD 4/1/09 – 4/21/09

*Table VIII.1 – Local Weather Conditions for Testing Period*

| Date | Clearness Index (0-10) | Max Temp (F) | Min Temp (F) | Average Temp (F) |
|---|---|---|---|---|
| 4/1/2009 | 1 | 64 | 40 | 52 |
| 4/2/2009 | 2 | 76 | 42 | 59 |
| 4/3/2009 | 8 | 60 | 43 | 52 |
| 4/4/2009 | 0 | 64 | 36 | 50 |
| 4/5/2009 | 2 | 76 | 50 | 63 |
| 4/6/2009 | 10 | 53 | 35 | 44 |
| 4/7/2009 | 9 | 48 | 35 | 42 |
| 4/8/2009 | 3 | 60 | 33 | 47 |
| 4/9/2009 | 2 | 67 | 36 | 52 |
| 4/10/2009 | 9 | 63 | 50 | 57 |
| 4/11/2009 | 3 | 60 | 44 | 52 |
| 4/12/2009 | 0 | 61 | 40 | 51 |
| 4/13/2009 | 9 | 71 | 47 | 59 |
| 4/14/2009 | 10 | 55 | 45 | 50 |
| 4/15/2009 | 10 | 50 | 44 | 47 |
| 4/16/2009 | 7 | 64 | 47 | 56 |
| 4/17/2009 | 0 | 74 | 42 | 58 |
| 4/18/2009 | 0 | 77 | 47 | 62 |
| 4/19/2009 | 9 | 64 | 55 | 60 |
| 4/20/2009 | 7 | 62 | 50 | 56 |
| 4/21/2009 | 6 | 53 | 43 | 48 |

Note : Clearness Index scaled at

Clear = 0 – 3 ; Partly Cloudy = 4 – 7 ; Cloudy = 8 – 10

[National Climatic Data Center, Bowman Field, Louisville, KY]

APPENDIX IX

THERMOCOUPLE ERROR READING

Temperatures measured across the evaporator section of the heat pipe for a four-day heating cyclic period are shown in Figure IX.1

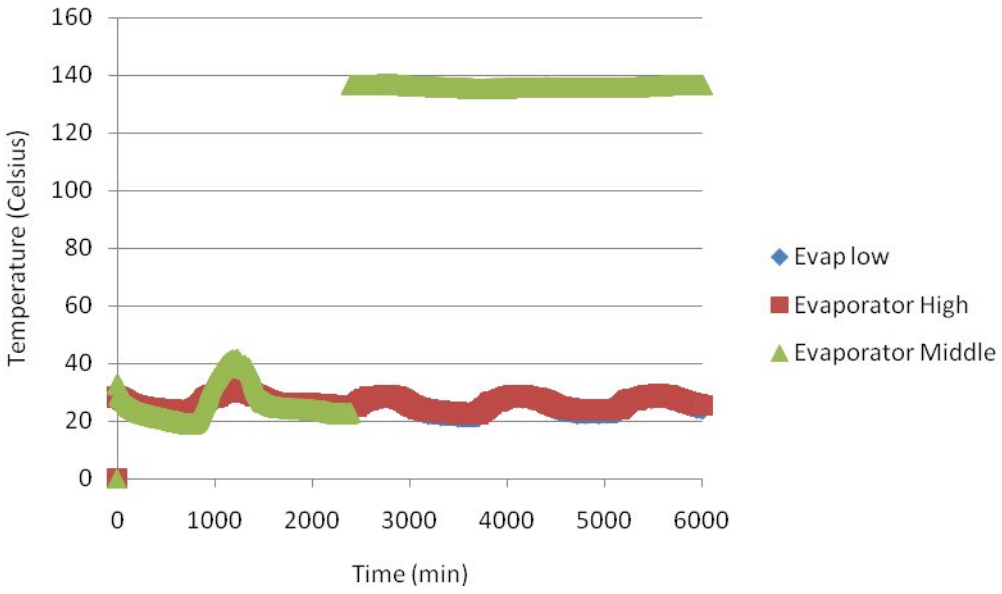


*Figure IX.1 – Evaporator section Temperatures for a Four Day Cyclical Test*

The temperature measurement by the thermocouple on the middle of the evaporator section has a very high step output change. The data from the middle of the evaporator section cannot be accurate because the temperature is significantly higher than the expected temperature range of the system components. The data also cannot be accurate because the heat input necessary for a change in temperature reading of around 100 °C between the sampling time of one minute would require a very high heat input source,

which does not exist around the unit. This corruption of data could be caused by improper shielding of wires and contact with any metal which would change the voltage read across the wires. An alternative possible source of error is a break of the weld joint at the tip of the two wires.

Temperatures measured across the absorber plates are shown in Figure IX.2, and absorber thermocouple placement is shown in Figure IX.3.

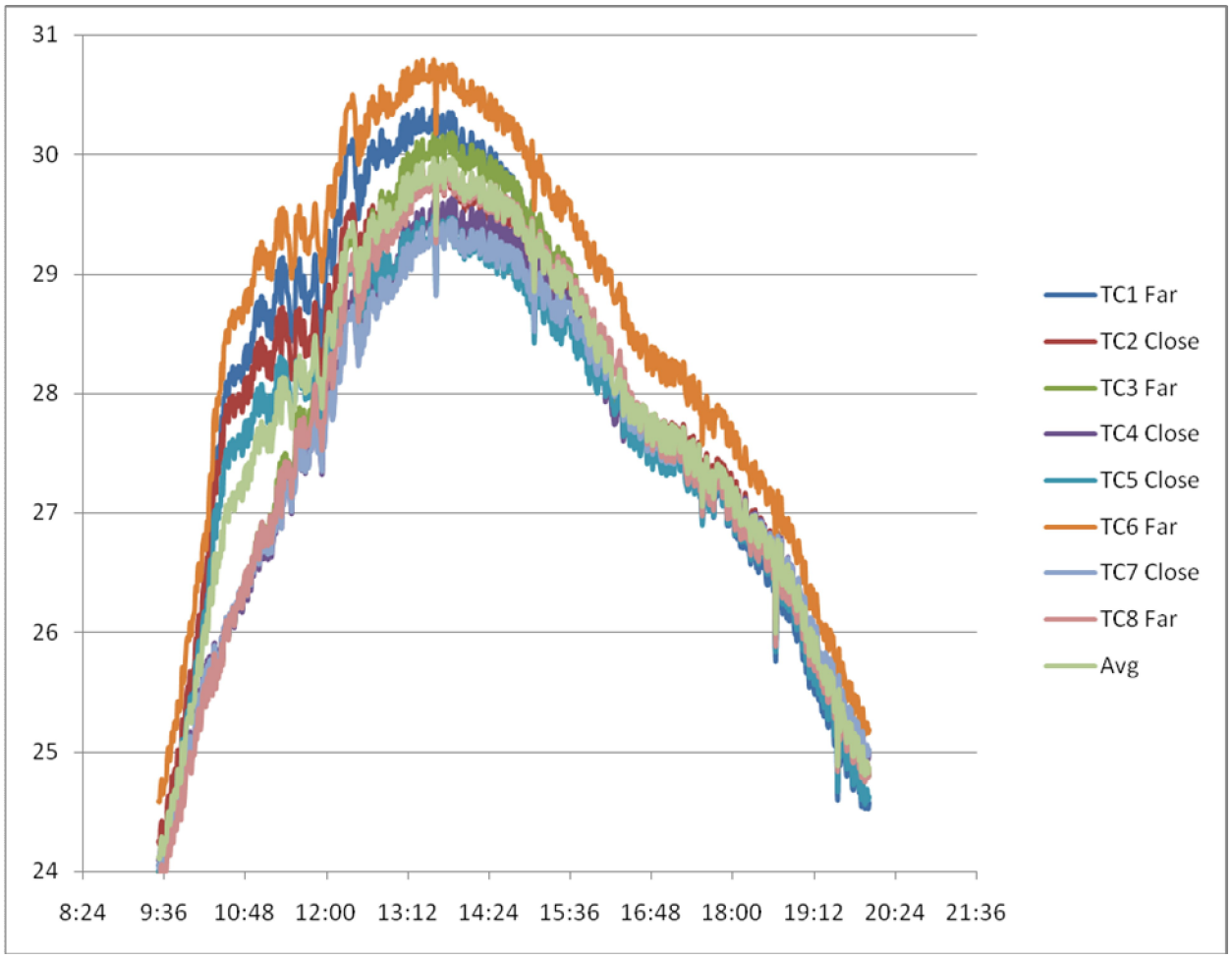


*Figure IX.2 – Absorber Plate Temperature Readings*

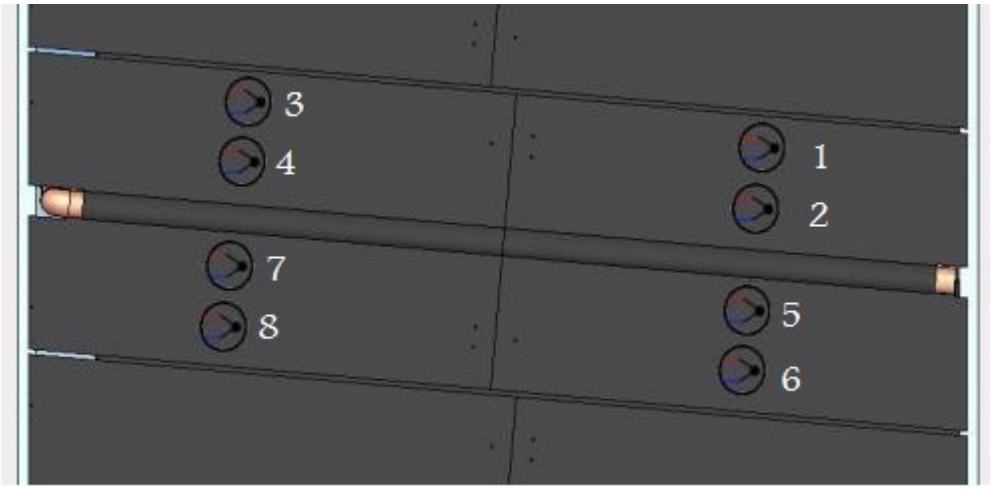


*Figure IX.3 – Thermocouple Placement on the Absorber Plates*

Temperatures measured across the heat pipe for a heating cycle are shown in Figure IX.4.

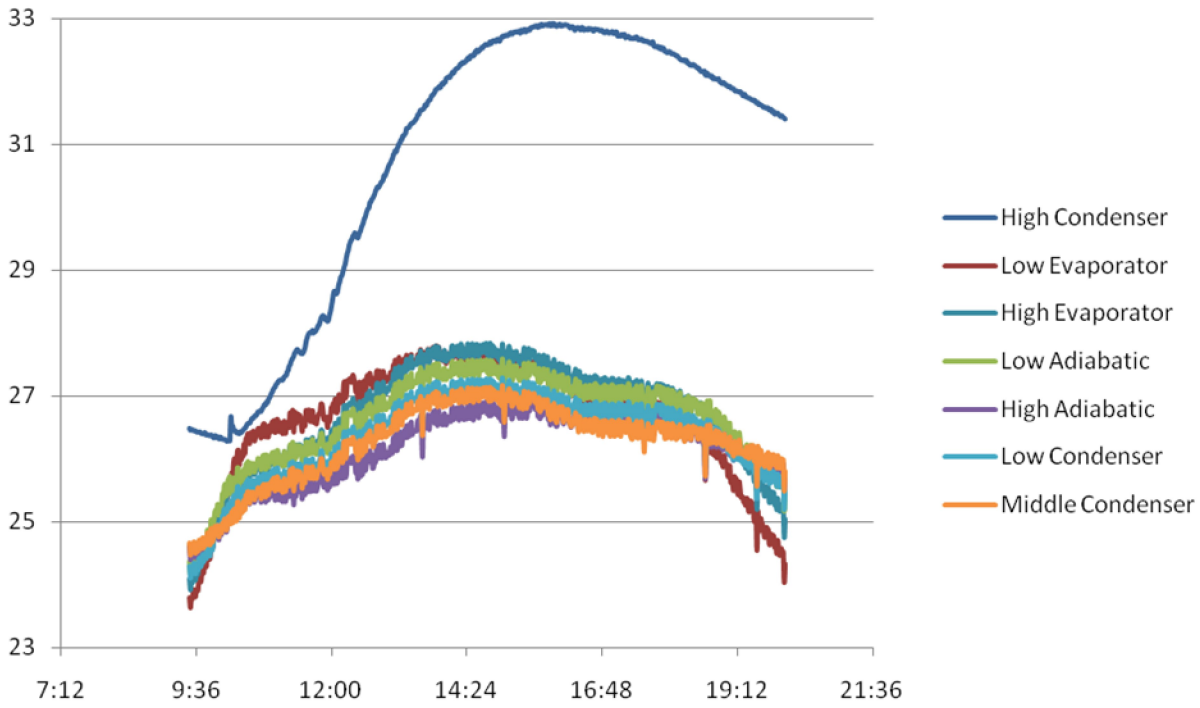


*Figure IX.4 – Heat Pipe Temperature Distribution*

Although temperature distribution of the the absorber plate seems to be as expected, the upper condenser section shows temperatures higher than these during heating conditions. There are two main reasons which suggest the high condenser reading in Figure IX.4 cannot be the temperature at the upper end of the condenser. The first is that it violates a basic law of thermodynamics – that is, during heating conditions, when heat is traveling up from the evaporator section of the heat pipe to the condenser, the condenser is reading a higher temperature than the heat source. The highest temperature the upper condenser reaches in Figure IX.4 is 33°C, and the highest temperature the absorber plate reaches in Figure IX.2 is below 31°C. This would imply that heat is being transferred from the colder absorber plates to the hotter heat pipe. This is a clear violation of fundamental laws, and Figure IX.4 also shows violation of assumed isothermal conditions for an operating heat pipe. The second reason is that the rest of the heat pipe temperatures have noticeable noise in their temperature traces, and the noise corresponds to all data points along the heat pipe except for the upper condenser. The heat pipe experiences these relatively low amounts of noise due to its small thermal mass and the temperature data being recorded once per minute. The upper condenser temperature trend is much more smooth, similar to water tank temperature trends. This elevated temperature, lack of noise, and variation from the isothermal conditions of the heat pipe in violation of basic thermodynamic laws have led to the conclusion that the thermocouples was pulled out of place during assembly and has settled at the upper portion of the water tank. Stratification within the tank would be the only plausible explanation for these elevated temperatures.

# VITA

## Nicholas E. Chmielewski

### Professional Involvement

5/08 – Present — University of Louisville - Graduate Research Assistant
- Design of Heat Pipe Augmented Solar Wall with emphasis on manufacture and production
- Production of full-scale prototype for testing
- Fabrication of data acquisition system and analysis of prototype
- Masters of Engineering thesis and pursuit of journal publications

1/08 – 5/08 — University of Louisville - Student Assistant
- Design and installation of 2-axis tracking solar system
- Design for Photovoltaic and Thermal panels
- Conduct research for University with completed system
- Coordination and drafting of contractual agreements with multiple companies for facility construction
- Prepare Design Report for Department of Energy for Grant Fund Allocation and Justification

5/07 – 8/07, 8/06 – 12/06, 1/06 - 5/06 — Pratt & Whitney - Engineering Co-op
- Military Case, Hollow Fan Blade, and Combustor Cell Lean Process Coordinator: 6S, Standard work, Machine tracking
- Team member of successful implementation of NDT processes including FPI, TAI, Ultrasonic, and Eddy Current
- Create New Repair Process: Military and Commercial
- Update and Create Operation Sheets: Military and Commercial

### Research Promotion and Presentations

- Presentation of Solar Research and Heat Pipe Demonstration to Industrial Board of Advisors
- Presentation of Research Material and lab tour with Dr. Len Peters, Kentucky Secretary of Energy and Environment Cabinet
- Presentation of Heat Pipe Augmented Solar Wall research, Dual axis tracking system, and lab tour with Rocky Adkins, Majority Leader, Kentucky House of Representatives
- Presentation of Thesis Project Research to Senator Robert Stivers
- Research featured in article in *Business First* periodical

- Appeared on WHAS 11 Evening News Project Green segment
- Laboratory tours and Heat Pipe Demonstrations for University of Louisville Campus Preview Day
- Poster Submitted for 2009 National Teach-In on Global Warming
- Poster submitted for 2009 Engineering Exposition at University of Louisville

## Honors and Activities

- Hsing Chuang Award for Excellence in Graduate Study
- Multiple Appreciation Awards at Pratt and Whitney
- Honors Societies: Tau Beta Pi, Phi Eta Sigma, NSCS
- Professional Organizations: ASME (since 2003), ASHRAE
- Local Volunteering: St. John's Center for the Homeless, Habitat for Humanity, Bible study leader, camp counselor, soup kitchen volunteer
- Missions Work: Russia, Honduras, South Africa, Germany, and France